STATE OF THE CLIMATE IN 2003

D. H. LEVINSON[14] AND A. M. WAPLE,[14] EDS.

TABLE OF CONTENTS

Affiliations (alphabetical by author)

1. Lisa V. Alexander and David E. Parker, Hadley Centre for Climate Prediction and Research, Met Office, Bracknell, Berkshire, United Kingdom
2. Peter Ambenje, Drought Monitoring Centre, Nairobi, Kenya
3. Omar Baddour, National Meteorology Direction, Rabat, Morrocco
4. Gennady Belchansky, Institute of Ecology, Moscow, Russia
5. Gerald D. Bell, Muthuvel Chelliah, Timothy Eichler, Michael S. Halpert, Kingtse Mo, and Wassila M. Thiaw, NOAA/NWS/NCEP Climate Prediction Center, Washington D.C.
6. Michael A. Bell, Suzana J. Camargo, Emily K. Grover-Kopec, International Research Institute for Climate Prediction, New York, New York
7. Eric Blake and Richard Pasch, NOAA/NWS National Hurricane Center, Miami, Florida
8. Olga N. Bulygina, All Russian Research Institute of Hydrometeorological Information, Obninsk, Russia
9. John C. Christy, University of Alabama, Huntsville, Alabama
10. Miguel Cortez Vázquez, Servicio Meteorologico Nacionale, Mexico City, Mexico
11. Arthur Douglas, Creighton University, Omaha, Nebraska
12. David C. Douglas, USGS Alaska Science Center, Juneau, Alaska
13. Sheldon Drobot, The National Academies, Washington, D.C.
14. Karin L. Gleason, Jay H. Lawrimore, David H. Levinson, Matthew Menne, Anne M. Waple, (STG, Inc.), and Connie Woodhouse, NOAA/NESDIS National Climatic Data Center, Asheville, North Carolina
15. Brad Garanganga, Drought Monitoring Centre, Harare, Zimbabwe
16. Stanley Goldenberg and Christopher Landsea, NOAA/OAR/AOML Hurricane Research Division, Miami, Florida
17. James Hansen, NASA Goddard Institute for Space Studies (GISS), Columbia University, New York, New York
18. Rupa Kumar Kolli, Indian Institute for Tropical Meteorology, Pune, India
19. Charlotte McBride, South African Weather Service, Pretoria, South Africa
20. David Phillips, Environment Canada, Ottawa, Ontario, Canada
21. David A. Robinson, Rutgers University, New Brunswick, New Jersey
22. Jim Salinger, National Institute of Water and Atmospheric Research, Newmarket, Auckland, New Zealand
23. Russell C. Schnell and Robert S. Stone, NOAA/ERL Climate Monitoring and Diagnostics Laboratory, Boulder, Colorado
24. Andrew Watkins, Australian Bureau of Meteorology, Melbourne, Australia

CORRESPONDING AUTHOR ADDRESS: Dr. David Levinson, Climate Monitoring Branch, National Climatic Data Center, NOAA-NESDIS, Asheville, NC 28801
E-mail: David.Levinson@noaa.gov
DOI: 10.1175/BAMS-85-6-Levinson

ABSTRACT—D. H. Levinson[14] and A.M. Waple[14] (Eds).

The earth's climate was influenced by a moderate El Niño in the tropical Pacific Ocean at the beginning of 2003. This ENSO warm event developed during October–November of 2002, and eventually dissipated during March–April 2003, giving way to near-neutral ENSO conditions for the remainder of the year. Despite the cessation of El Niño during the boreal spring, the ENSO warm event affected regional precipitation anomalies over a broad area of the Pacific basin, including wet anomalies along the west coast of South America, and dry anomalies in eastern Australia, the southwest Pacific, and Hawaii.

The global mean surface temperature in 2003 was within the highest three annual values observed during the period of regular instrumental records (beginning in approximately 1880), but below the 1998 record-high value. Global surface temperatures in 2003 were 0.46°C (0.83°F) above the 1961–90 mean, according to one U.K. record, which ranked as third highest in this archive. In the U.S. temperature archive, the 2003 anomaly was also 0.46°C (0.83°F), equivalent to the 2002 value, which ranked second over the period of record. Similar to the surface temperature anomalies, satellite retrievals of global midtropospheric temperatures ranked 2003 as third warmest relative to the 1979–98 mean value.

The hurricane season was extremely active in the Atlantic basin, with a total of 16 tropical storms, seven hurricanes, and three major hurricanes in 2003. Five of these tropical cyclones made landfall in the United States, three made landfall in northeastern Mexico, and a tropical storm affected Hispañola. In addition, Nova Scotia and Bermuda experienced devastating impacts from hurricanes in 2003. Another notable aspect of the season in the Atlantic was the formation of five tropical storms over the Gulf of Mexico, which tied the season high observed in 1957. In addition, three tropical storms formed outside of the normal (June–November) hurricane season in 2003—one in April and two in December—which made this the first season since 1887 that two tropical storms have formed during December in the Atlantic basin. Also of note was the below-normal activity in the eastern North Pacific basin. There were no major hurricanes in this basin during the 2003 season, which made this the first year since 1977 with no category 3–5 storms. Despite the below-normal activity, four tropical cyclones made landfall on the Pacific coast of Mexico, two as hurricanes and two as tropical storms, which was twice the long-term mean.

The summer of 2003 was one of the warmest on record across parts of Europe, where a heat wave affected most of Central and Western Europe. Two distinct periods of exceptional heat occurred during the season—the first in June and the second during the latter half of July and the first half of August. The July–August heat wave was the more serious of the two, since it coincided with the normal peak in summer temperatures and was accompanied by an almost complete absence of rainfall. The high temperatures and dry conditions exacerbated forest fires that burned across southern France and Portugal in July and August. The record heat wave spread across most of Western Europe in August, and it was likely the warmest summer since 1540 in parts of Central Europe. In France, 11,000 heat-related deaths were reported between late July and mid-August. In Germany, both June and August were the warmest such months since at least the beginning of the twentieth century. The summer was also the hottest in Germany since 1901, and, with the exception of some stations in northern and northwestern Germany, it was the hottest summer since the beginning of recorded measurements.

Other climatic events of note during 2003 included 1) record wet conditions across parts of the southeast, mid-Atlantic, and eastern coast of the United States; 2) record cold temperatures and anomalous June snowfalls in European Russia; 3) 546 tornadoes during May 2003 in the United States, which was an all-time record of reported tornadoes for any month; 4) continuing drought conditions across the western United States, with some areas experiencing their fourth and fifth years of significant precipitation deficits; 5) severe bushfires in eastern Australia in January, the worst wildfire season on record in British Columbia during August, as well as severe wildfires across southern California in October; 6) above-average rainfall across West Africa and the Sahel, which had its second wettest rainy season since 1990; 7) a return to normal rainfall across the Indian subcontinent during the summer monsoon; and 8) a near-record extent of the Antarctic ozone hole, which was 28.2 million km^2 at its maximum in September 2003.

1. INTRODUCTION—D. H. Levinson[14]

This is the 14th yearly State of the Climate article (formerly known as the Climate Assessment), summarizing the annual global and regional climate conditions, and the eighth year that the article has appeared in *BAMS*. This is also the fourth year that the National Climatic Data Center (NCDC) has taken the lead in the article's development and production, and the first year of formal collaboration with the World Meteorological Organization (WMO) Commission for Climatology. In addition to personnel at NCDC, numerous scientists and institutions from around the world have contributed data, figures, and/or text to this article, and their contributions have been noted through authorship citation of individual sections as well as in the list of contributors in the appendix.

This special section of *BAMS* includes analyses of the global climate system for 2003, and the significant events and their impacts that occurred during this past year. A primary goal of this and past State of the Climate articles has been to put the observed climate and weather events over the previous year into historical perspective, with a focus on long-term trends and variations in the primary climatic elements over the period of instrumental observations (since the late 1800s), and, if possible, to extend back in time through the use of paleoclimate data. Due to the large number of data sources, it was impossible to refer to a standard base period for each climatic element in the article. Therefore, the base period for each dataset varied according to convention, and the base periods noted for each dataset herein were chosen by the contributors and authors based on a number of practical and scientific factors.

The record of the past century illustrates an extremely complex and variable climate system, one that is impossible to completely characterize in an article of this length. However, this special section of *BAMS* attempts to address the primary topics of interest related to the climate of 2003 and convey these to a broad audience—one that includes both climate specialists and nonspecialists alike.

Despite the fact that each chapter was intended to be relatively self-contained, concerted effort has been made to cross-reference text and figures where appropriate. Sidebar boxes were also included again this year, in order to emphasize important topics and climatic perspectives. As mentioned, an appendix was included at the end of the article with all of the names and institutions of people who contributed figures, data, or provided other invaluable assistance with the preparation of this report. In addition, efforts were made to further increase the number of authors who are native to their respective region, and it is the intent of the editorial team at NCDC to continue this trend in next year's article.

The following chapters focus on a wide array of topics and parameters that characterized the earth's climate in 2003, including the following:

Chapter 2: Global climate

Temperature

- The global mean surface temperature in 2003 was among the highest three annual values observed during the period of worldwide instrumental records (beginning in approximately 1880), but below the 1998 record-high value.
- The 10 highest mean annual global temperature rankings have occurred since 1990, and the trend in the global average is at least 0.6°C century^{-1} since 1900 and 0.18°C decade^{-1} since 1976.
- The global annual average temperature of both the lower and middle troposphere was the third warmest on record behind 1998. Midtropospheric temperatures have increased since satellite records began in 1979, and the rate of increase has been reported to be as small as +0.04°C decade^{-1} and as large as +0.24°C decade^{-1}.
- The global lower-stratospheric temperature in 2003 was the coldest since 2000, and it was the 11th consecutive year in which the annual average was below that of the base period (1984–90).

Precipitation

- The worldwide land surface precipitation anomaly was –0.9% below the 1961–90 average in 2003, the third year in a row the global mean was drier than average.

Snow cover

- Annual snow cover extent over Northern Hemisphere land areas averaged 25.8 million km^2 in 2003. This was 0.2 million km^2 above the 3-decade-long average, which ranked snow cover in 2003 as the 13th most extensive in the 34-yr record.
- During the boreal summer of 2003, hemispheric snow cover extent was at a record low in July.

Chapter 3: Trace gases

- Carbon dioxide rose approximately 3 parts per million (ppm) in 2003 to reach a preliminary value of 379 ppm at the National Oceanic and Atmospheric Administration (NOAA)/Climate Modeling and Diagnostics Laboratory (CMDL) Mauna Loa Observatory.
- Ozone-depleting gases in the troposphere continued to decline through 2003 in response to international measures agreed to by the 1987

Montreal Protocol on Substances that Deplete the Ozone Layer.

Chapter 4: The Tropics

- A moderate warm ENSO event dissipated during the boreal spring 2003 and transitioned to near-neutral conditions for the remainder of the year.
- Atlantic tropical storm activity was above average in 2003, with 16 named storms, seven hurricanes, and three major hurricanes. Hurricanes Juan, Isabel, and Fabian caused significant damage in Canada, the United States, and Bermuda, respectively.
- Tropical storm activity was below average in the eastern North Pacific and near average in the western North Pacific.

Chapter 5: The Poles

- The Antarctic ozone hole reached a near-record extent in 2003. No discernable trend in ozone hole "recovery" was evident, though concentrations of chloroflourocarbons (CFCs) continued to decline.
- Arctic sea ice reached a record low extent in the boreal autumn, but annual sea ice extent was greater than in 2002.
- Surface air temperatures were warmer than average in the Arctic in 2003, especially in Baffin Bay and the east Siberian Sea.

Chapter 6: Regional climate

- *North America*: Drought continued across western North America, with impacts in the western United States, Canadian prairies, and northeastern Mexico. The Canadian Arctic was warmer than average in 2003, as was the western United States. Anomalously wet conditions impacted the eastern United States, with record annual precipitation in three mid-Atlantic States.
- *Europe*: A record-breaking summer heat wave over much of western Europe led to thousands of heat-related casualties.
- *Africa:* Sahel rains returned to normal during 2003, yielding record crop harvests. Drought continued in parts of the Greater Horn and southern Africa.
- *Asia:* Monsoonal rains were near normal for the Indian subcontinent in 2003. Near-normal rainfall helped ease the long-running drought in southwest Asia. Russia was warmer than average for the year, but June was anomalously cold in European Russia.
- *Australasia:* Severe drought and bushfires in eastern Australia, coupled with extreme heat for much of the continent during the austral summer, caused devastating impacts in 2003. It was the warmest June on record for New Zealand, and numerous annual sunshine records were exceeded across the South Island.

2. GLOBAL CLIMATE

a. Global surface temperatures—M. Menne[14]

According to surface temperature records maintained independently by institutions in the United Kingdom and in the United States, the global mean surface temperature in 2003 was within the highest three annual values observed during the period of regular instrumental records (dating to the nineteenth century), but below the 1998 record high value. As shown in Fig. 2.1, surface temperatures in 2003 ranked as third highest, calculated according to Jones et al. (2001) and Jones and Moberg (2003), or tied for second highest according to the U.S. (NOAA/NCDC) record (Quayle et al. 1999). In this U.K. record, global surface temperatures in 2003 averaged 0.46°C above the 1961–90 mean value, only slightly (0.02°C) below the 2002 value. In the U.S. surface temperature archive, the global 2003 departure from the same base period was also 0.46°C, equivalent to the 2002 value. According to both surface temperature archives, the 10 highest mean annual global temperature rankings

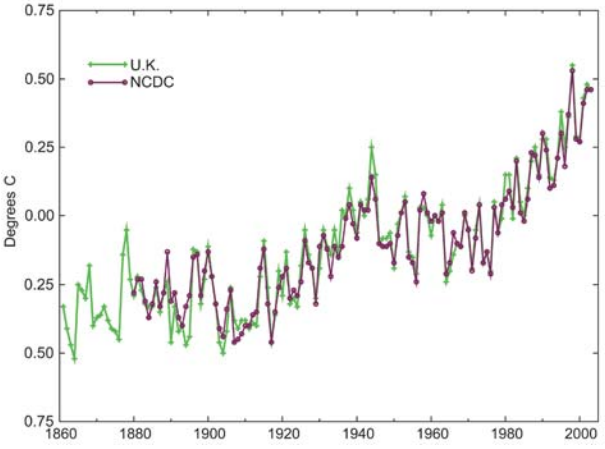

Fig. 2.1. Global annual surface temperature anomalies with respect to a 1961–90 base period. For the United Kingdom record (green line) annual temperature values for the period 1861–2000 were calculated according to Folland et al. (2001b), values in 2001–02 were calculated according to Parker et al. (1995) and Jones (1994), the 2003 values were calculated according to Jones et al. (2001) and Jones and Moberg (2003). For the U.S. (NOAA/NCDC) record (brown line) values were calculated according to Quayle et al. (1999).

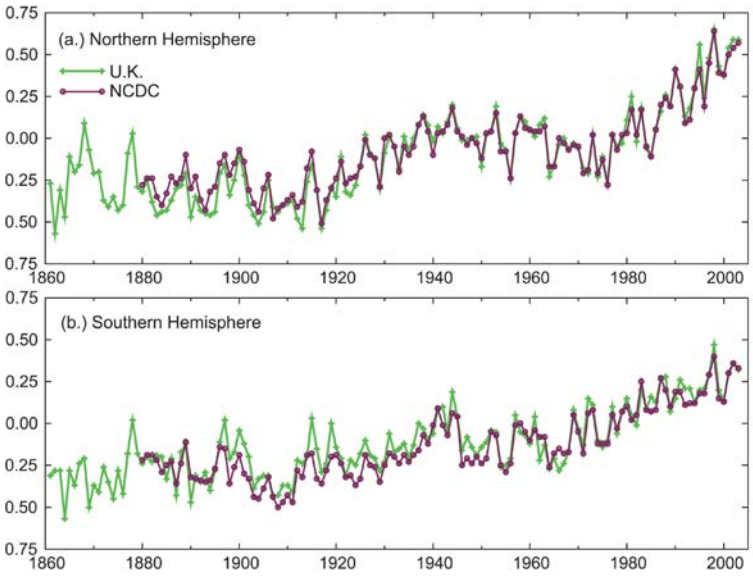

FIG. 2.2. Global annual surface temperature anomalies by hemisphere: (a) Northern Hemisphere (b) Southern Hemisphere. Both were calculated with respect to the 1961–90 base period.

have occurred since 1990. Although by no means monotonic, the rise in global mean surface temperature since 1900 exceeds 0.6°C century^{-1}. Since 1976, the linear trend is about 0.18°C decade^{-1}.

Averaged separately, 2003 surface temperatures ranked as second highest in the Northern Hemisphere and as third highest in the Southern Hemisphere, according to both surface temperature archives (Fig. 2.2). While the top-10 annual temperature rankings in the Northern Hemisphere comprise only years since 1990, the Southern Hemisphere top rankings include 1987 and 1988.

Serial monthly global temperature anomalies since 1961 are shown in Fig. 2.3 using the U.S. surface temperature archive. A calendar-monthly mean record-high value was observed in September 2003, when the global mean surface temperature was calculated to be about 0.05°C higher than the former September record, set in 1997. Worldwide, sea surface temperatures (SSTs) in 2003 ranked as the second highest on record (Fig. 2.4). Large regions of positive sea surface temperature anomalies, some of which exceeded the 90th or 98th percentiles of the mean annual temperature distribution (Horton et al. 2001) can be seen in Fig. 2.5. The positive temperature anomalies across parts of the North Atlantic extended into Western Europe and North Africa (see sections 6d and 6eI, respectively), where extreme summer temperatures were observed during June–July–August. Large positive temperature anomalies were also evident across much of the Northern Hemisphere high latitudes, western North America, and much of eastern Australia (see sections 5b, 6aII and 6gI, respectively). Across parts of these areas, the 2003 mean surface temperature also ranked in the upper-10th percentile of the regional temperature distribution. Conversely, negative temperature departures were observed across eastern North America (see section 6aII).

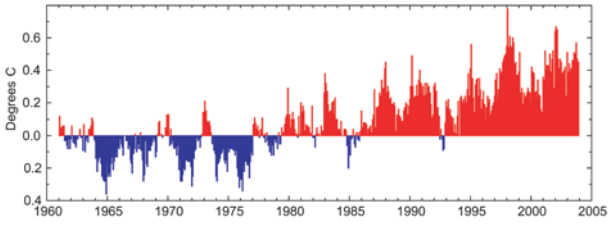

FIG. 2.3. Serial monthly surface temperature anomalies from 1961 to 2003, based on Quayle et al. (1999). Anomalies were calculated with respect to the 1961–90 base period.

b. Upper-air temperature—J. C. Christy[9]

Bulk atmospheric temperatures for three atmospheric layers, the lower troposphere (LT), midtroposphere (MT), and lower stratosphere (LS), were derived from the microwave emissions of atmospheric oxygen. The University of Alabama in Huntsville (UAH) generated these products from measurements made by the microwave sounding units (MSUs) and the advanced MSUs (AMSUs; operational since 1998),

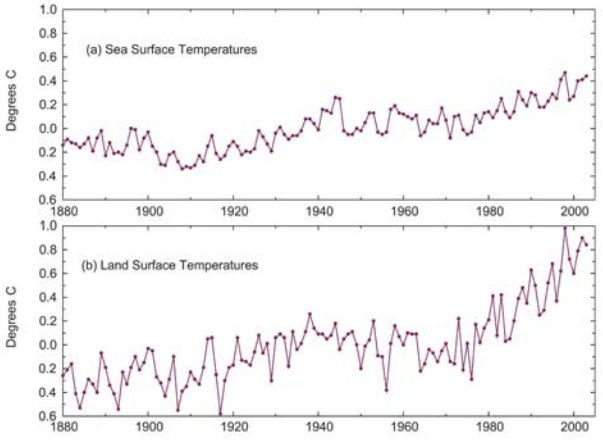

FIG. 2.4. (a) Sea surface and (b) land surface temperature anomalies (in °C) based on Quayle et al. (1999), with respect to the 1961–90 base period.

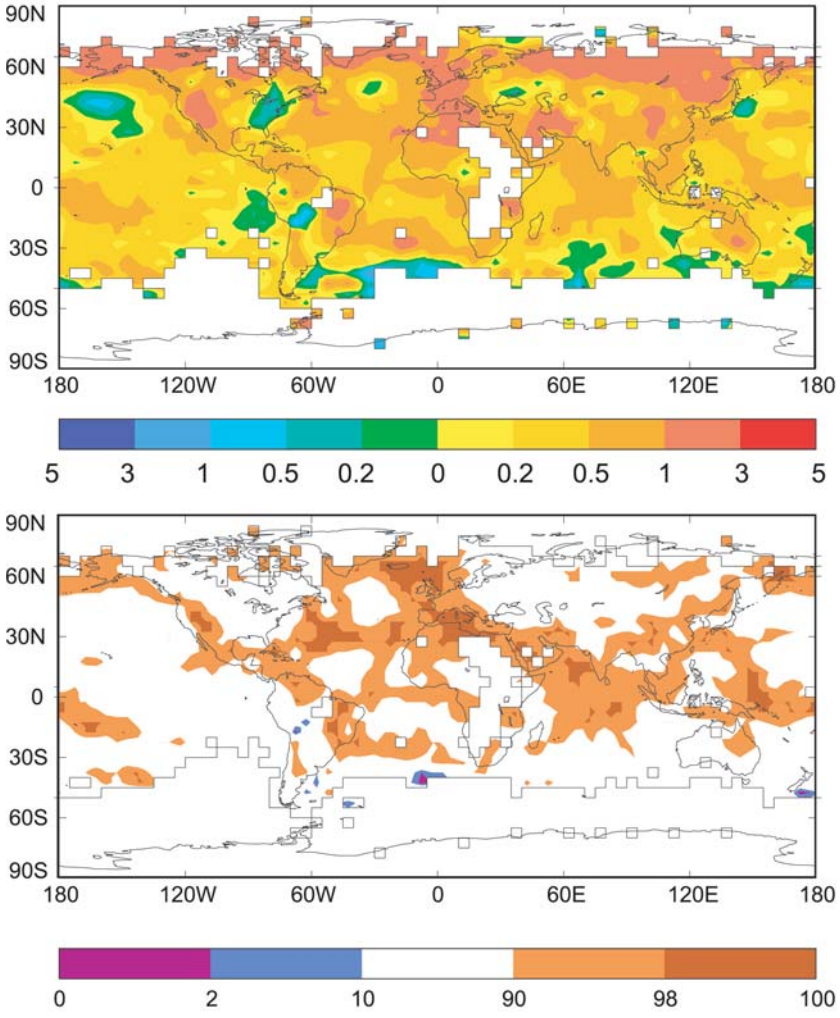

FIG. 2.5. Geographic distribution of temperature anomalies (in °C) in 2003: (a) departure from 1961–90 average (the temperature value of each 5° lat × 5° long pixel was derived from at least 1 month's data in each of four 3-month seasons); (b) same as in (a), but expressed as percentiles of modified two-parameter gamma distributions fitted to annual data for 1961–90, and calculated according to Horton et al. (2001).

which are flown as part of the instrument suite on NOAA polar-orbiting satellites (Christy et al. 2003). Biases and errors due to spacecraft drift (both horizontal and vertical) and on-orbit calibration changes have been identified and removed.

Two new reconstructions of MSU temperatures by Mears et al. (2003) at Remote Sensing Systems (RSS), and by Vinnikov and Grody (2003; hereafter VG03), for the MT (as well as the LS by RSS), have been completed in which differing methods for accounting for east–west drift and instrument calibration have been applied. Briefly, RSS and UAH differ in the magnitude of adjustment for the calibration shift that occurs as a result of differential heating of the instrument components. RSS and UAH use very similar adjustments for diurnal drifting (i.e., the effect of the spacecraft observing the earth at later or earlier local times) and inter-satellite biases. VG03 produced a fundamentally new analysis in which the differences in observed global temperatures, found as two satellites observe the earth at the same time, are eliminated by projecting those differences onto a diurnal cycle. RSS and UAH made separate corrections for the diurnal drift and the calibration shift based on their significant relationships to the diurnal clock and onboard temperature, respectively. Simply, VG03 forced both the diurnal drift and calibration shift to be a single function of the diurnal clock, while RSS and UAH consider them as separate problems. This led to significantly different adjustments to the raw data.

l) Lower troposphere

The annual global average temperature of the LT (surface to about 8 km) developed by UAH was +0.20°C above the 1979–98 mean. Seasonal anomalies are shown in Fig. 2.6. Relative to the past 25 yr, 2003 was the third warmest on record behind 1998 (+0.47°C) and 2002 (+0.24°C). The linear trend since November 1978 is +0.08°C decade^{-1}. Christy et al. (2003) demonstrated that the 95% confidence level (C.L.) precision for UAH annual global LT anomalies was ±0.14°C, and the global trend value was ±0.05°C decade^{-1}. Global averages from the National Centers for Environmental Prediction (NCEP)–National Center for Atmospheric Research (NCAR) reanalyses and the Hadley Centre, both of which are based on radiosonde measurements, also reported similar findings. Regionally, virtually all areas poleward of 45°N were above the 20-yr mean, while elsewhere scattered areas that were slightly warmer or cooler than average temperatures occurred in 2003. The moderate warm phase of ENSO faded by midyear (see section 4a), and near-average to slightly warmer-than-average tropical temperatures persisted for the remainder of the year.

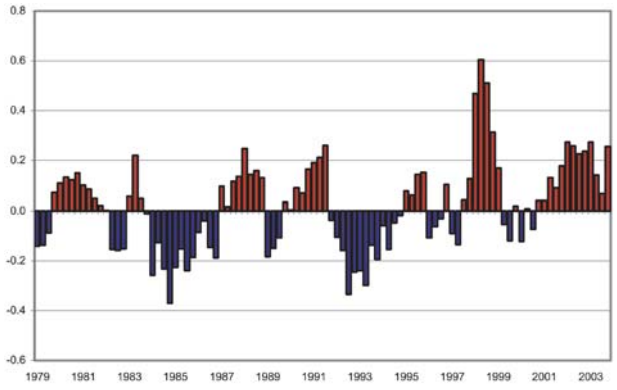

Fig. 2.6. Global seasonal lower tropospheric temperature anomalies (in °C) for 85°S–85°N (UAH). Anomalies were determined with respect to the 1979–98 base period.

Globally, the LT seasonal anomalies in 2003 [beginning with December–January–February (DJF)] were as follows: +0.28°C, +0.16°C, +0.10°C, and +0.21°C.

ii) Midtroposphere

Three realizations of MT global temperatures from microwave emissions give differing results for the past 25 yr. UAH and RSS (VG03 values for 2003 were unavailable at press time) show that 2003 was the third warmest year of the 25-yr period of record (Fig. 2.7). However, the global temperature trend over the 25-yr period is quite different. Linear trend values are +0.04, +0.12, and +0.24°C decade^{-1} for UAH, RSS, and VG03, respectively. The quantity MT is somewhat difficult to interpret because it receives emissions from the troposphere as well as the stratosphere (about 15%), so that variations in MT are a combination of often counter balancing anomalies above and below the tropopause.

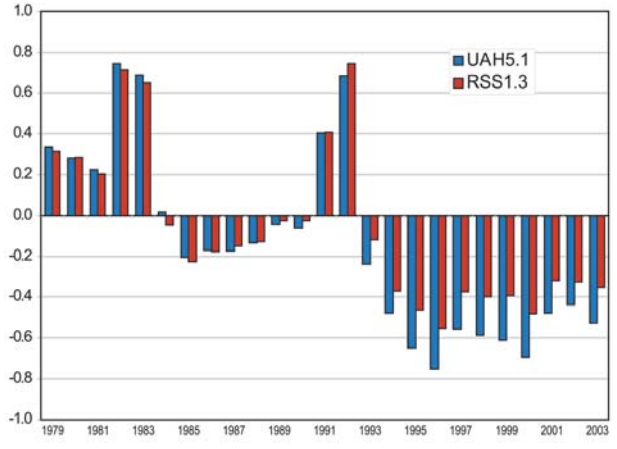

Fig. 2.8. Global seasonal anomalies (in °C) of lower-stratospheric temperature (UAH and RSS). Anomalies were determined with respect to the 1984–90 base period.

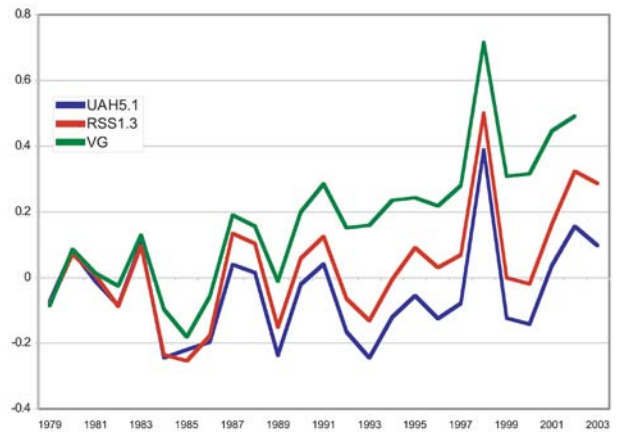

Fig. 2.7. Annual anomalies (in °C) of global mid-tropospheric temperature. Anomalies were determined with respect to the 1979–98 base period.

iii) Lower stratosphere

The global LS temperature was again significantly below the base period (1984–90), with anomalies of –0.41°C (UAH) and –0.35°C (RSS), which were the coldest since 2000, making 2003 the 11th consecutive year in which the annual average was below that of the base period (Fig. 2.8; note the base period was chosen to avoid the impacts of the volcanic eruptions of El Chichon, Mexico, in 1982 and Mt. Pinatubo, Philippines, in 1991). Although the bulk of the layer monitored by these microwave emissions is in the lower stratosphere, a significant portion (~20%) of the tropical signal arises from emissions below the tropopause so that some convolution of upper-tropospheric and lower-stratospheric signals occurs there. Despite this fact, the tropical portion of the globe experienced negative temperature anomalies throughout 2003, consistent with the easterly phase of the quasi-biennial oscillation

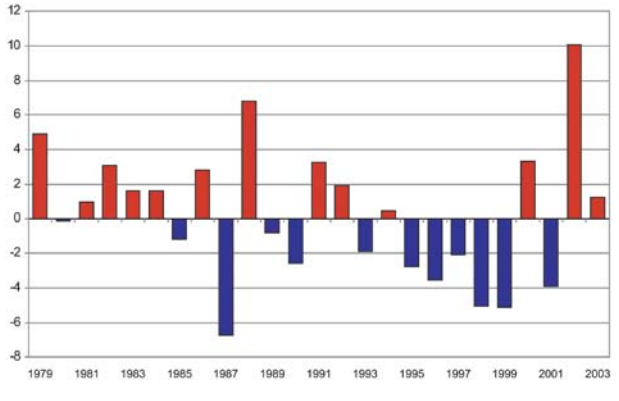

Fig. 2.9. Autumn (SON) anomalies of lower-stratospheric temperature (in °C) over Antarctica (UAH). Anomalies were determined with respect to the 1984–90 base period.

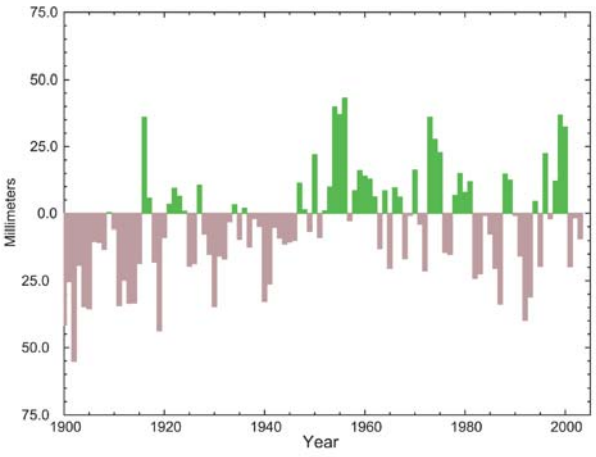

Fig. 2.10. Annual global precipitation anomalies from 1900 to 2003 for land-based stations. Data are from GHCN, and anomalies were determined with respect to the 1961–90 base period.

(QBO). The singular warm anomaly in autumn September–October–November (SON) in 2002 over Antarctica (+10°C) did not reappear in 2003, but the seasonal anomaly was positive (+1.2°C; Fig. 2.9) for the year.

c. Global precipitation—D. H. Levinson[14] and J. H. Lawrimore[14]

For the third consecutive year, global annual precipitation averaged over land areas was below normal in 2003. The graph in Fig. 2.10 shows the annually averaged precipitation from the Global Historical Climatology Network (GHCN), with anomalies determined with respect to the 1961–90 base period (Peterson and Vose 1997; Vose et al. 1992). The global precipitation anomaly was negative (dry) in 2003, reaching approximately −0.90% (−10 mm) from the mean. This was a larger departure from normal than in 2002, when the observed anomaly was slightly negative, but very close to the 1961–90 average. The string of negative global precipitation anomalies began in 2001. Prior to this 3-yr period of negative anomalies and below-normal precipitation, land areas had been dominated by a period of positive anomalies and wetter-than-average conditions as measured by the GHCN. Between 1996 and 2000, the global precipitation anomaly had been positive (wet) for 4 of 5 yr.

The recent drier-than-normal globally averaged precipitation anomalies may be associated with changes in the ENSO in the tropical Pacific Ocean. It has been shown that variability associated with ENSO influences regional precipitation patterns in the Tropics and midlatitudes (Ropelewski and Halpert 1987). For example, the wetter-than-average period from 1998 to 2000 was associated with the development and persistence of La Niña conditions in the tropical Pacific Ocean, while the recent drier-than-average period in global precipitation since 2001 included the 2002–03 El Niño warm event as well as extended periods of near-neutral ENSO conditions. In 2003, the year began with the equatorial Pacific Ocean in the midst of a moderate El Niño warm event (see section 4a). This El Niño weakened during the late winter of 2003, and by April, SSTs in the central and eastern equatorial Pacific basin had cooled to near normal. Despite the cessation of the El Niño warm event and the return to near-neutral conditions in April 2003, precipitation anomalies during the remainder of 2003 continued to reflect an El Niño–like pattern in the tropical Pacific and across parts of North and South America.

Figure 2.11 shows the spatial pattern of precipitation anomalies determined from the GHCN, comparing the boreal winter of 2002–03 (DJF) annual precipitation with the 1961–90 base period. Significant wet and dry regional anomalies were present across the globe during the boreal winter of 2002–03, and traditional El Niño signatures were evident in the observed spatial pattern of these global precipitation anomalies. Wetter-than-normal regions included parts of the eastern United States and the Pacific Northwest, western

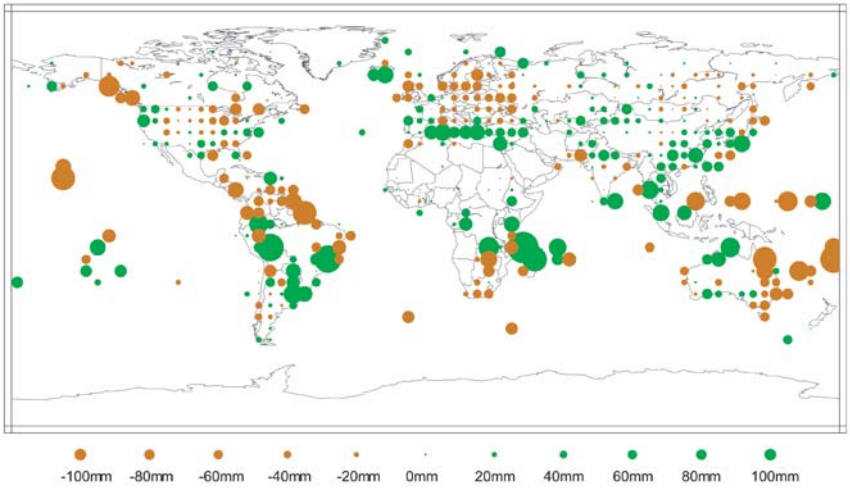

Fig. 2.11. Precipitation anomalies (mm) for Jan–Dec 2003 from GHCN. Positive anomalies (wet conditions) are shown in green, and negative anomalies (dry conditions) are shown in orange. Anomalies were determined with respect to the 1961–90 base period.

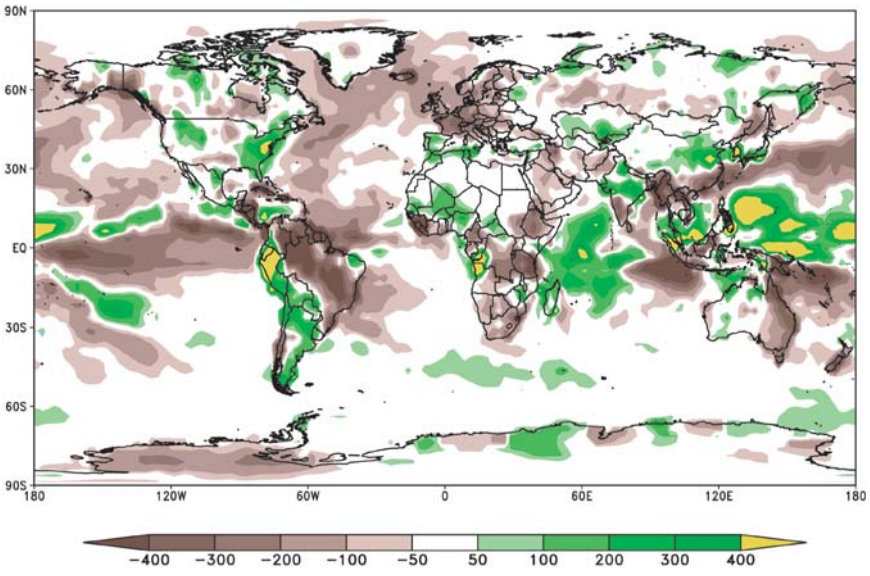

FIG. 2.12. Precipitation anomalies (in mm) for Jan–Dec 2003 from the CAMS–OPI dataset. Anomalies were determined with respect to the 1979–95 base period. Positive anomalies (wet conditions) are shown in green and yellow shading, while negative anomalies (dry conditions) are shown in brown shading.

and central South America, Borneo and Sumatra in Indonesia, Madagascar and the islands of the western Indian Ocean, southern Turkey, as well as islands in the Mediterranean Sea. Negative anomalies and drought conditions, likely enhanced by El Niño and the associated shift in the equatorial Walker circulation, were observed across eastern Australia, the southwest Pacific, and Hawaii (see section 6 for further discussion of regional precipitation anomalies).

Global precipitation over the oceans is often more difficult to quantify than land areas, due to the lack of ground-truth verification of satellite-based retrieval methods. One satellite method that has been widely used is the Climate Anomaly Monitoring System (CAMS) and outgoing longwave radiation (OLR) Precipitation Index (OPI), which uses 1979–95 as its base period. CAMS–OPI is a merged product that utilizes both satellite retrieval estimates and surface rainguage measurements of precipitation (Janowiak and Xie 1999). The CAMS–OPI precipitation anomalies for 2003 are shown in Fig. 2.12. Over land areas, the positive and negative anomalies were generally similar to that measured by GHCN. Qualitative comparison of GHCN with CAMS–OPI shows general agreement between the two products over most areas in the Tropics and midlatitudes where comparable data exist. For example, the exceptionally wet conditions across the south and east coasts of the United States in 2003 were resolved in both the CAMS–OPI and GHCN datasets. These anomalously wet conditions reflected the enhanced subtropical jet and associated

TABLE 2.1. Monthly and annual climatological information on Northern Hemisphere (N. Hem.) continental snow cover extent between Nov 1966 and Dec 2003. Included are the number of years with data used in the calculations (i.e., means, standard deviations), and 2003 values and rankings. Note that areas are in millions of km^2, and North America (N. Am.) includes Greenland. The years 1968, 1969, and 1971 have 1, 5, and 3 missing months, respectively, and, thus, are not included in the annual (Ann) calculations.

	Yrs	Mean	Std dev	2003	2003 N. Hem. rank	2003 Eurasia rank	2003 N. Am. rank
Jan	37	46.9	1.5	48.0	8	4	36
Feb	37	45.9	1.9	48.5	4	3	10
Mar	37	41.1	1.9	41.8	13	9	25
Apr	37	31.5	1.7	31.6	17	13	20
May	37	20.6	1.8	20.6	16	13	22
Jun	36	11.1	2.1	10.5	21	20	24
Jul	34	5.0	1.4	3.1	34	30	34
Aug	35	3.6	1.0	2.4	34	33	33
Sep	35	5.7	1.0	5.1	25	30	15
Oct	36	18.3	2.7	18.5	17	12	28
Nov	38	34.2	2.1	35.7	8	17	4
Dec	38	43.4	1.9	46.3	22	25	12
Ann	33	25.6	1.0	25.8	13	11	22

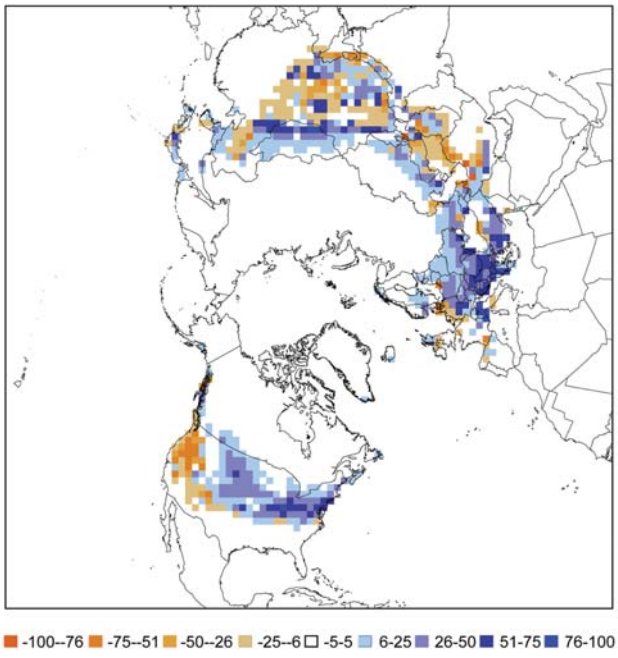

FIG. 2.13. February 2003 monthly snow extent anomalies with respect to climatology maps covering the period from Nov 1966 to May 1999. Departures show differences in the percent frequency of cover between 2003 and the long-term mean.

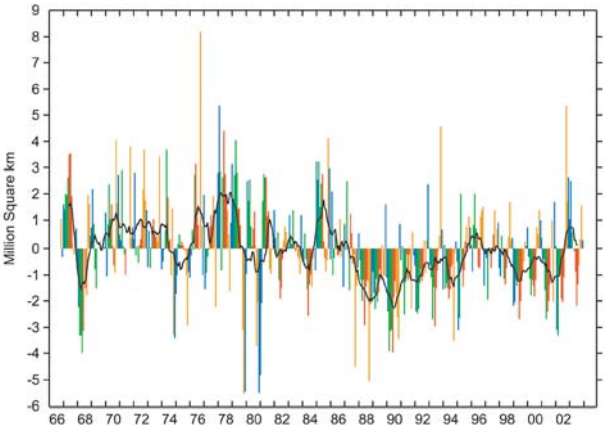

FIG. 2.14. Anomalies of monthly snow cover extent over Northern Hemisphere lands (including Greenland) between Nov 1966 and Dec 2003. Also shown are 12-month running anomalies of hemispheric snow cover extent, plotted on the seventh month of a given interval. Anomalies were calculated from NOAA snow maps. Mean hemispheric snow extent is 25.6 million km² for the full period of record. Note that monthly means for the period of record were used for nine missing months between 1968 and 1971 in order to create a continuous series of running means (the missing months all fell between Jun and Oct).

precipitation enhancement that is typically observed during El Niño events in this region (Ropelewski and Halpert 1987). Despite the general agreement between the two datasets, several regional differences were observed between the CAMS–OPI and GHCN datasets over land areas in 2003, including the northern Rockies area in the United States. The CAMS–OPI technique determined a ~200 mm positive anomaly, and, therefore wetter-than-normal conditions, across a large area of the northern Rockies and Intermountain region in the United States during 2003. In contrast, GHCN reflected drier-than-normal conditions that persisted across these areas in 2003 (see Fig. 6.5a in section 6aii).

Despite these differences between the CAMS–OPI precipitation products with gauge-only measurements, its greatest applicability is over the oceans and those land areas with minimal precipitation-observing sites. Significant positive anomalies (wet conditions) over the oceans as measured by CAMS–OPI in 2003 included a large region of the tropical western Pacific Ocean, as well as the western half of the Indian Ocean. Negative anomalies (dry conditions) in 2003 included the western North Atlantic Ocean and Gulf Stream region, the near-equatorial Pacific basin, the Coral Sea and convection associated with the South Pacific Convergence zone (SPCZ), and portions of the eastern Indian Ocean.

d. Northern Hemisphere snow cover—D. A. Robinson[21]

Annual snow cover extent over Northern Hemisphere land areas averaged 25.8 million km² in 2003. This is 0.2 million km² above the 3-decade-long average, and ranked 2003 as having the 13th-most-extensive snow cover over the past 34 yr (Table 2.1). This evaluation included the Greenland ice sheet, as well as the North American and Eurasian continents. The total land area covered by snow in 2003 ranged from a maximum of 48.5 million km² in February, to a minimum of 2.4 million km² in August. Monthly snow

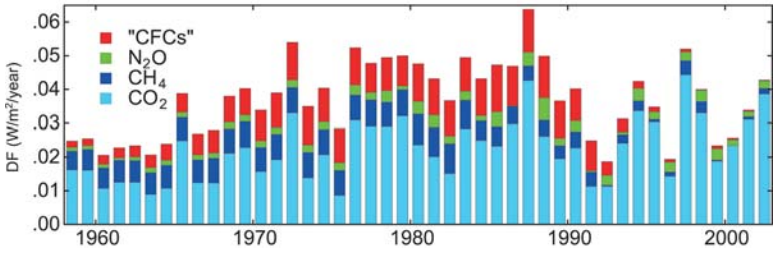

FIG. 3.1. The annual growth rate of global climate forcing by well-mixed greenhouse gases, ΔF (in W m⁻² year⁻¹), over the period 1958–2003. (Courtesy of M. Sato.)

extent values were calculated at Rutgers University from weekly maps of snow cover produced by NOAA meteorologists.

In February 2003, hemispheric snow cover ranked fourth most extensive over the past 37 yr (Fig. 2.13). This included a ranking of the third largest extent over Eurasia. In November, hemispheric extent ranked eighth over the past 38 yr, with the fourth-most-extensive snow cover on record over North America. During summer 2003, hemispheric extent was at a record low in July, and near or within the lowest tercile from June through September. The rankings for each continent were within the same terciles in 6 months during the year, but differed by two terciles in January and October. In both of these cases, Eurasia was in the upper tercile and North America in the lower tercile.

Twelve-month running means of Northern Hemisphere snow cover extent were above the long-term average throughout the year, especially during the first half of 2003 (Fig. 2.14) This is the first such occurrence since the mid-1990s. Eurasian extent was above average for the first time in 5 yr, and the observed anomalies were the largest since the mid-1980s, while the North American extent did not exceed the long-term average in 2003 (not shown). The mid-1990s was the last time that Northern Hemisphere extent exceeded the long-term average, and before that it was in the mid-1980s.

3. TRENDS IN TRACE GASES—R. C. Schnell[23] and J. Hansen[17]

A summary of the annual growth rate of global climate forcing by well-mixed greenhouse gases is shown in Fig. 3.1. Although ozone (O_3) and stratospheric water vapor are additional significant greenhouse gases, they are neither well mixed nor well measured, and consequently were not included in the figure. Historical perspectives and more detailed descriptions of the major greenhouse gases are offered in the following sections (sections 3a–3c). The increase in the climate forcing between 2002 and 2003, just over 0.04 W m^{-2}, was the largest since 1998, and the portion due to carbon dioxide (CO_2) was the third largest in the period of annual data (since 1958). About 90% of the increase of greenhouse gas climate forcing in the past year was caused by CO_2, 5% by nitrous oxide (N_2O), 4% by methane (CH_4), and less than 1% by CFCs and related trace gases, for which increases of some gases were balanced by decreases of others. The increases of CO_2, N_2O, and CH_4, and the associated climate forcing, were all larger in 2003 than in the previous year.

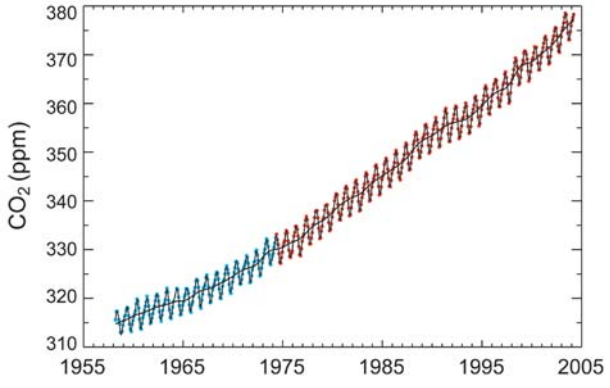

FIG. 3.2. Monthly mean CO_2 mole fractions from the NOAA Mauna Loa Observatory on the Big Island of Hawaii. Prior to May 1974, monthly mean CO_2 data are compliments of C. D. Keeling, Scripps Institution of Oceanography (blue symbols), and since May 1974, data are compliments of K. Thoning, NOAA/CMDL (red symbols).

a. Carbon dioxide

After water vapor, carbon dioxide (CO_2) is the most important atmospheric greenhouse gas. For about 10,000 years prior to the industrial revolution, the atmospheric abundance of CO_2 was nearly constant at ~280 ppm (ppm = parts in 10^6 by dry-air mole fraction). This abundance represented a balance among large seasonal fluxes (on the order of 100 Pg C yr^{-1}, where 1 Pg = 10^{15}g) between the atmosphere and biosphere (photosynthesis and respiration), and between the atmosphere and the ocean (physical exchange of CO_2). Since the late 1800s, atmospheric CO_2 has increased by ~33%, primarily due to emissions from combustion of fossil fuels (currently about 7 Pg C yr^{-1}) and, to a lesser extent, deforestation (0–2 Pg C yr^{-1}).

Monthly mean CO_2 mole fractions from the NOAA/CMDL Mauna Loa Observatory near the summit of the Big Island of Hawaii are plotted in Fig. 3.2. Over the entire time series, the average rate of CO_2 increase is ~1.4 ppm yr^{-1}. During this time, CO_2 emissions from fossil fuel combustion increased from 2.3 Pg C in 1958 to 6.6 Pg C in 2000 (Marland et al. 2003). As a result, the CO_2 growth rate has increased from ~0.8 ppm yr^{-1} averaged over the first decade of measurements to 1.8 ppm yr^{-1} in the most recent decade. During 2003, CO_2 increased by ~3 ppm at the Mauna Loa Observatory site, which was faster than the average increase over the past decade. Overall, the average increase of CO_2 in the atmosphere since 1958 corresponds to ~55% of the CO_2 emitted by fossil fuel combustion (Keeling et al. 1995), but this fraction varies from ~20%–90% (Conway et al. 1994; Ciais et al. 1995). The remaining fossil fuel CO_2 is removed from the atmosphere by the oceans and the terrestrial biosphere.

Variations in the observed atmospheric increase in CO_2 are not due to variations in fossil fuel emissions. Most attempts to explain the interannual variability of the atmospheric CO_2 increase have focused on short-term climate fluctuations (e.g., ENSO and post–Mt. Pinatubo eruption cooling), but the mechanisms, especially the role of the terrestrial biosphere, are not well understood. For example, it has been speculated that the high CO_2 growth rate in 1998 was related to unusually warm temperatures. However, analysis of 1999 CO_2 measurements indicates a return to an average or lower-than-average growth rate in 1999, although 1999 was only slightly cooler than 1998. From 2000 through 2002, the CO_2 growth rate has been ~1.8 ppm yr^{-1}, slightly above the long-term average of 1.5 ppm yr^{-1}.

Understanding the relative contributions of the ocean and biosphere to the net global carbon sink has important environmental policy implications. High-precision measurements of atmospheric CO_2 abundance alone are insufficient to calculate this partitioning. Researchers use measurements of the carbon-isotopic composition of CO_2 and atmospheric O_2 to constrain understanding of this partitioning. The average uptake for the 1990s has been estimated using these methods to be 1.7±0.5 GtC yr^{-1} by the oceans and 1.4±0.7 GtC yr^{-1} by the terrestrial biosphere.

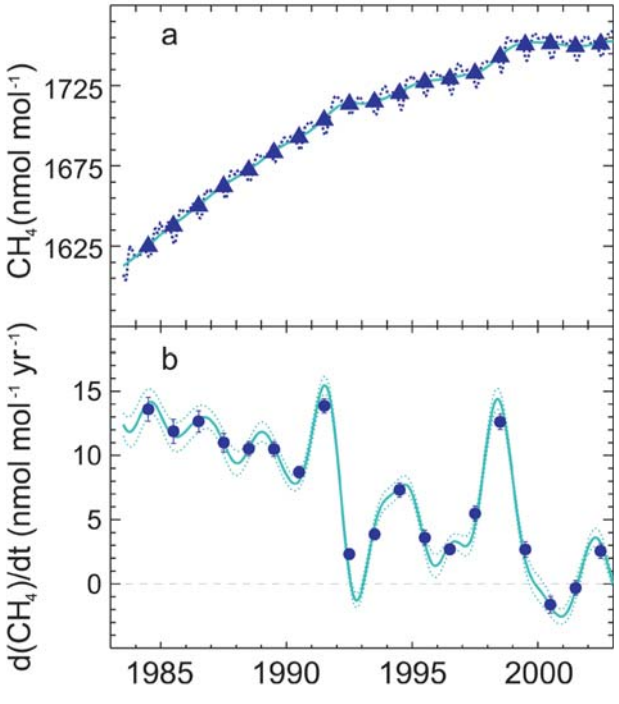

FIG. 3.3. (a) Globally averaged methane mole fractions (dashed line) as a function of time: The solid line is the deseasonalized trend, and symbols are annual averages. (b) Instantaneous rate of increase of globally averaged CH_4 determined as the derivative with respect to time of the solid line above. Dashed lines are ±1σ uncertainties; symbols are annual increase (±1σ). (Courtesy of E. J. Dlugokencky, NOAA CMDL.)

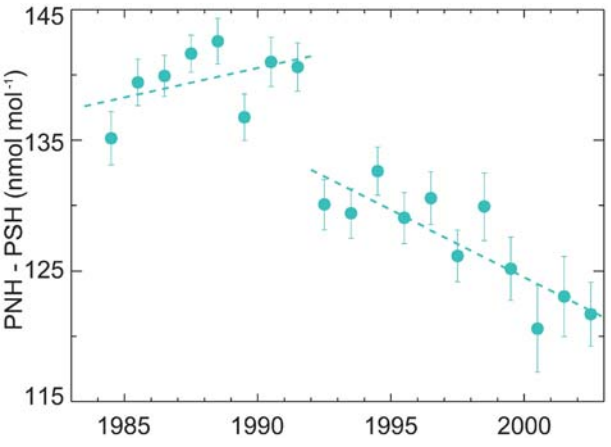

FIG. 3.4. Differences between northern (53°–90°N) and southern (53°–90°S) polar annual CH_4 means plotted as a function of time. (Courtesy of E. J. Dlugokencky, NOAA/CMDL.)

b. Methane

The contribution of methane (CH_4) to anthropogenic radiative forcing, including direct and indirect effects, is about 0.7 W m^{-2}, approximately half that of CO_2. The indirect effects include changes in the burden of CH_4, which feed back into atmospheric chemistry affecting the concentrations of hydroxols (OH) and O_3. The increase in CH_4 since the preindustrial era is responsible for about one-half of the estimated increase in background tropospheric O_3 during that time. Changes in OH concentration affect the lifetimes of other greenhouse gases, such as the replacement refrigerants [halogenated fluorocarbons (HFCs) and halogenated chlorofluorocarbons (HCFCs)].

High-precision measurements of atmospheric methane provide climate modelers with current and past rates of CH_4 increase, and they are also useful in constraining the CH_4 budget and how it is changing with time. In Fig. 3.3a, smoothed, globally averaged CH_4 mole fractions from the NOAA/CMDL air-sampling network are plotted as a function of time. During nearly 20 yr of measurements CH_4 has increased, but the rate of increase has slowed (Fig. 3.3b). In fact, globally averaged CH_4 remained about constant from 1999 to 2002 (Dlugokencky et al. 2003).

It is reasonable to question whether the observed CH_4 trend is temporary or an indication that atmospheric CH_4 has reached a steady state, implying that sources and removal mechanisms are in balance. Based on current knowledge of the global methane budget

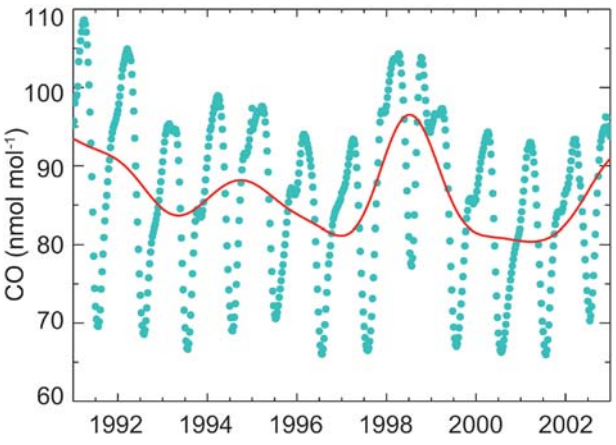

FIG. 3.5. Globally averaged surface tropospheric CO (symbols) determined from the CMDL cooperative air sampling network. Red solid line denotes the de-seasonalized trend. (Courtesy of P. C. Novelli, NOAA/CMDL.)

(and how it has changed with time), it is impossible to tell. However, there is good evidence that, while total global emissions may be changing slowly, emissions are being redistributed. In Fig. 3.4, differences between observed polar northern (53°–90°N) and polar southern (53°–90°S) annual mean CH_4 mole fractions (circles) are plotted as a function of time. This difference increased from 1984 to 1991, dropped abruptly in 1992, and has continued to decrease since then. Using a 3D model of atmospheric transport and chemistry combined with the Emissions Database for Global Atmospheric Research (EDGAR) version 3, we showed that decreased emissions from the former Soviet Union and Eastern Europe, on the order of 12 Tg CH_4 yr^{-1} that occurred after the collapse of the Soviet economy, are consistent with our observations (Dlugokencky et al., 2003). There are now small amounts of methane (2–3 Tg CH_4) captured from landfills and coal-mining operations in developed countries. According to this analysis, these decreases have been offset by increased CH_4 emissions in developing countries. For the future, all emission scenarios in the Intergovernmental Panel on Climate Change (IPCC) Special Report on Emission Scenarios (Nakicenovic et al. 2000) suggest increasing rates of CH_4 emission for, at least, the next three decades.

c. Carbon monoxide

Unlike CO_2 and CH_4, carbon monoxide does not strongly absorb terrestrial IR radiation, but it still impacts climate through its chemistry. The chemistry of CO affects OH (which influences the lifetimes of CH_4 and HFCs) and tropospheric O_3 (itself a greenhouse gas), so emissions of carbon monoxide (CO) can be considered equivalent to emissions of CH_4 (Prather 1996). Current emissions of CO may contribute more to radiative forcing over decadal time scales than emissions of anthropogenic N_2O (Daniel and Solomon 1998).

Globally averaged, CO mole fractions are plotted as a function of time in Fig. 3.5. There is a long-term decrease in globally averaged CO, driven by a decrease in the Northern Hemisphere (Novelli et al. 2003). Superimposed on the decrease was a significant anomaly during the late 1990s. The increased global CO starting in 1997 in the Tropics was likely the result of tropical (Langenfelds et al. 2002) and boreal biomass burning (Bruhwiler et al. 2000; Kasischke et al. 2000). Because the lifetime of CO is relatively short (~several months), the anomaly quickly disappeared and CO returned to pre-1997 levels shortly afterward. Global CO contin-

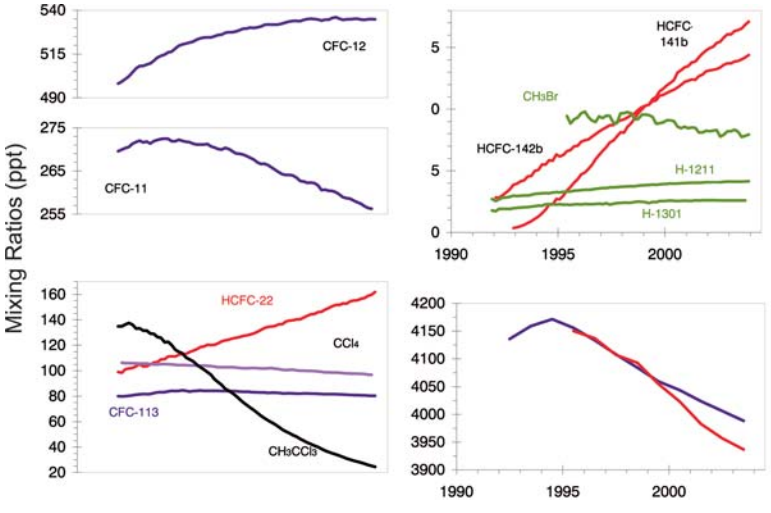

FIG. 3.6. Changes in global tropospheric mixing ratios (in ppt, or pmol mol^{-1}) of the most abundant CFCs (in purple), HCFCs (in red), chlorinated solvents, and brominated gases (in green; halons and CH_3Br). These global changes are estimated from weighted means of measurements from flasks and on-site instruments at 8–10 sites (the NOAA/CMDL cooperative air sampling network). Appearing in the bottom panel are global tropospheric trends for ECl, which is the sum of [chlorine + (45 × bromine)] from all the trace gas measurements displayed in the upper panels (red line) and from those same gases but with the assumption that methyl bromide mixing ratios have remained constant over time (purple line). (Updated from Montzka et al. 1999 and Montzka et al. 2003; courtesy of S. A. Montzka, J. H. Butler, T. Thompson, D. Mondeel, and J. Elkins, NOAA/CMDL.)

ued to decrease slowly, beginning in 1999, until 2002, when more large boreal fires appear to have caused another increase in CO.

d. Decreases in ozone-depleting gases in the troposphere

Atmospheric levels of the most abundant ozone-depleting gases continued to decline in the global troposphere in 2003 (Fig. 3.6), and the observed decreases were the direct result of reduced industrial production as mandated internationally by the 1987 *Montreal Protocol on Substances that Deplete the Ozone Layer*. During the past few years, ground-based measurements suggest that none of the most abundant CFCs are currently increasing in the global troposphere. Although mixing ratios of HCFC-22, a substitute for CFCs, continued to increase steadily in 2003, those for the minor HCFCs did not increase as rapidly in 2003 compared to earlier years. By mid-2003, the chlorine in the three most abundant HCFCs amounted to 205 ppt, or 7.4% of all chlorine carried by long-lived, purely anthropogenic halocarbons. Total chlorine from the HCFCs increased at 8 ppt yr^{-1} over this 2-yr period, which is slightly slower than the mean rate of increase of 9.3 ppt yr^{-1} observed since 1992. Mixing ratios of methyl chloroform continued to decline at an exponential rate; the abundance of this gas has declined nearly sixfold since the early 1990s.

Our understanding of atmospheric trends for ozone-depleting gases improved during 2003 with the publication of recent trends for methyl bromide (CH_3Br; Montzka et al. 2003). Methyl bromide is a gas with substantial natural and anthropogenic sources. The global mean of 8.1 (±0.1) ppt estimated from measurements at 10 sites during 2002 was about 1.2 (±0.3) ppt (or about 10%) lower than the mean during 1995–97. The global mean rate of change from mid-1999 to mid-2002 was –0.35 (±0.05) ppt yr^{-1}, which was a sharp contrast to the continuous increases reported for atmospheric CH_3Br throughout most of the twentieth century (Montzka and Fraser 2003). The observed decrease coincided with declines in industrial production, but was substantially faster and larger than expected.

The sum of chlorine and bromine atoms in long-lived trace gases provides an estimate of the ozone-depleting power of atmospheric halocarbons after the enhanced efficiency of bromine to destroy ozone, compared to chlorine, has been considered (a factor of 45 is used here; Daniel et al. 1999). This sum is often expressed as equivalent chlorine (ECl). Until recent trends of methyl bromide became published, assessments of

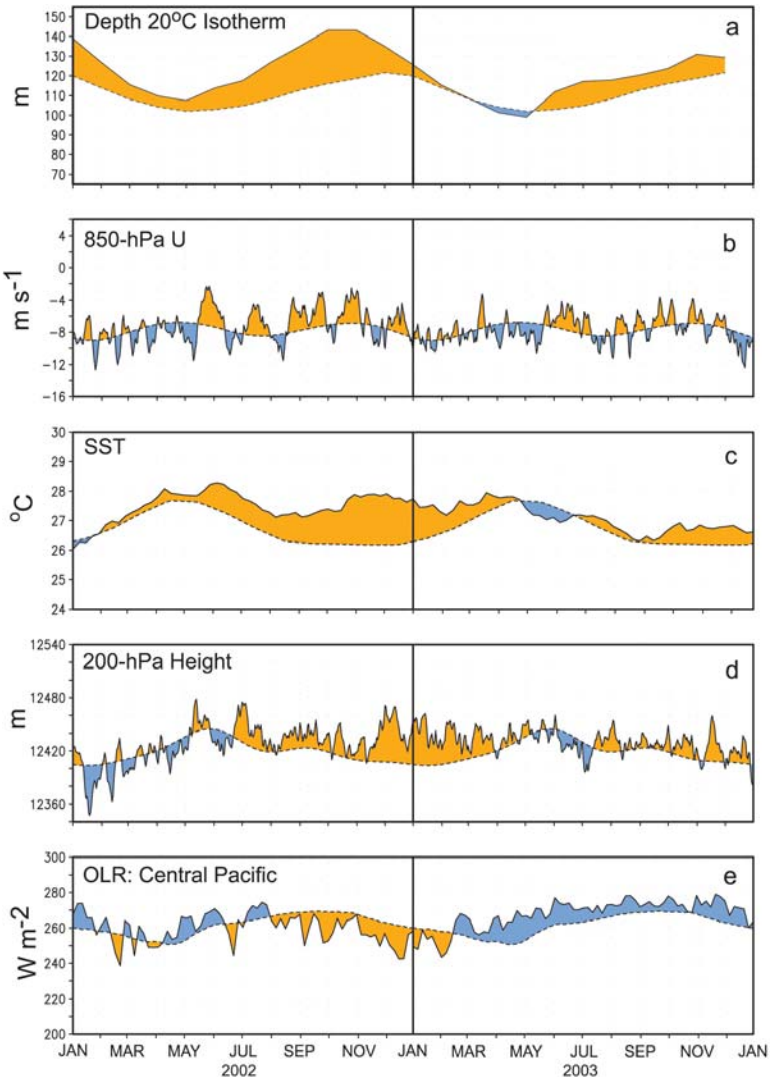

Fig. 4.1. Monthly time series of (a) the depth of the 20°C isotherm (m), (b) 850-hPa zonal wind speed (m s^{-1}), (c) SST (°C), (d) 200-hPa height (m), and (e) OLR (W m^{-2}) over the central equatorial Pacific. Values were determined by averaging over the region bounded by 5°N–5°S and 180°–100°W in (a–d), and 20°N–20°S and 180°–100°W in (e). The solid curve in all panels shows the monthly mean values and the dashed curved shows the climatological mean. The anomalies are shaded, with orange (blue) shading indicating positive (negative) anomalies, except for in (e) where the shading convention is reversed. The climatology and anomalies were computed with respect to the 1979–95 base period.

changes in ECl included the assumption that mixing ratios of this gas were constant over time (Fig. 3.6; blue line). With this assumption, the decline in ECl was estimated at approximately 0.5% yr^{-1} since 1995 (Montzka et al. 1999; Hall et al. 2002). With measurements of methyl bromide now available, however, it becomes clear that ECl has declined 50% faster since 1998 than previously thought (Fig. 3.6, red line).

4. THE TROPICS

a. *ENSO and the tropical Pacific*—G. D. Bell[5] and M. Halpert[5]

i) Overview

An equatorial Pacific warm episode (El Niño) occurred from July 2002 through March 2003 (Fig. 4.1). This event was consistent with past warm episodes in that it featured anomalously warm waters extending to approximately 100–200 m depth across most of the central equatorial Pacific, in association with a deeper-than-average oceanic thermocline. Increased thermocline depths are indicated by positive depth anomalies of the 20°C isotherm, which approximates the center of the thermocline across the eastern equatorial Pacific (Fig. 4.1a). This anomalous warmth was consistent with reduced oceanic upwelling across the central and east-central equatorial Pacific, in response to a weakening of the low-level easterly winds, as indicated by westerly wind anomalies throughout the region (Fig. 4.1b, orange).

The largest area-averaged SST departures (+1.75°C) associated with this event occurred during October 2002–January 2003 (Fig. 4.1c). This warming began during the second half of October in response to strong equatorial westerly wind anomalies associated with the Madden–Julian Oscillation. These westerly anomalies triggered an eastward-propagating oceanic Kelvin wave, which contributed to a further increase in thermocline depths and a sharp increase in SST anomalies in the central and east-central equatorial Pacific (Halpert and Bell 2003; see their section 4a).

The well-known El Niño–related pattern of tropical convection was also prominent during this period, with enhanced convection over the central equatorial Pacific (Fig. 4.1e, orange) and suppressed convection across Indonesia and northeastern Australia. The appearance of above-normal heights at 200-hPa (Fig. 4.1d, orange) reflected the increase in deep tropospheric heating over the central equatorial Pacific in response to the enhanced convection.

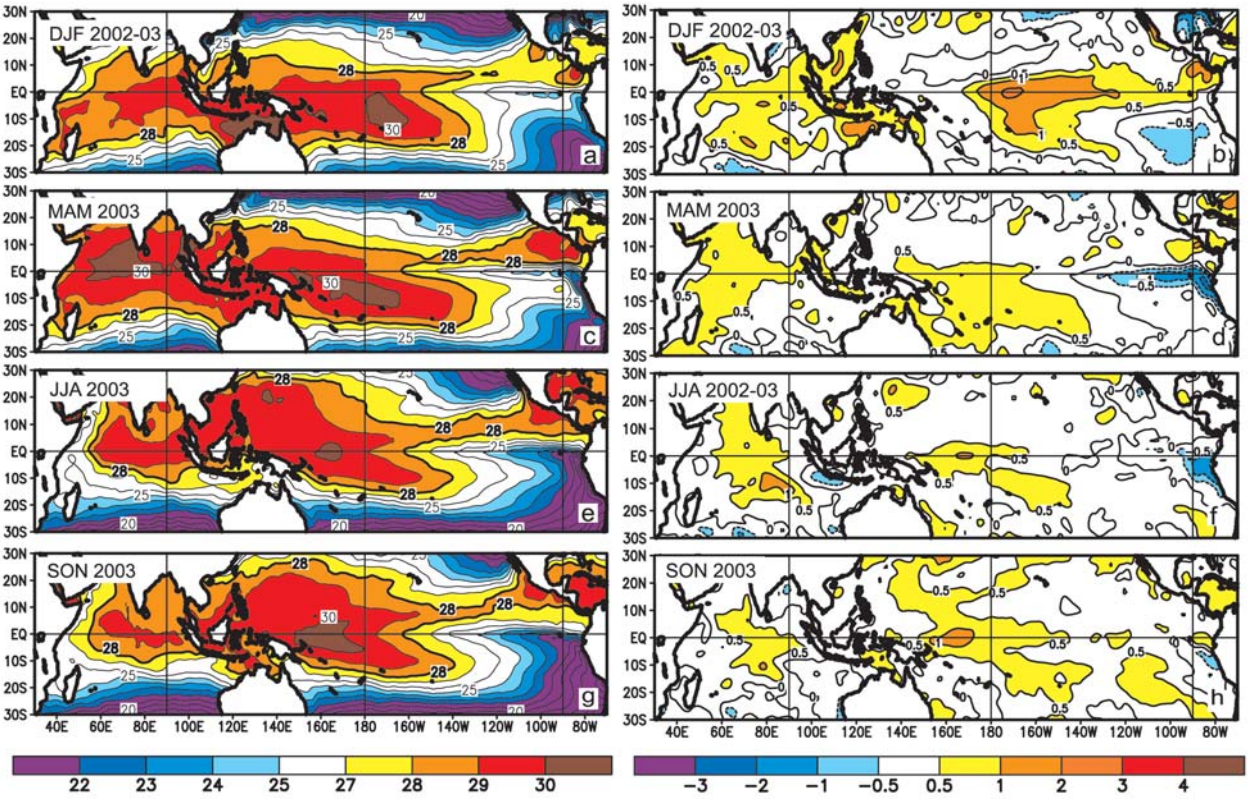

Fig. 4.2. Seasonal SST (left) and anomaly (right) for (a), (b) DJF 2002/03, (c), (d) MAM 2003, (e), (f) JJA 2003, and (g), (h) SON 2003. Contour interval is 1°C, with the 0.5°C anomaly contour included. Anomalies are departures from the 1971–2000 adjusted optimal interpolation (OI) climatology (Smith and Reynolds 1998).

ii) Equatorial Pacific Ocean sea surface and sub-surface temperature evolution

During December 2002–February 2003, anomalously warm SSTs (exceeding 29°C) covered the central equatorial Pacific, with the warmest SSTs in the Pacific basin shifted east of the date line (Fig. 4.2a). The strength of the equatorial cold tongue was also notably weaker than average during this period, because the positive SST departures of +1° to +2°C extended from the date line to 120°W, and departures of 0.5°–1.0°C overspread the eastern equatorial Pacific (Fig. 4.2b).

During DJF, SSTs greater than 28°C normally represent the approximate threshold for deep tropical convection over the central equatorial Pacific (Gadgil et al. 1984). The presence of exceptionally warm SSTs during DJF 2002/03 was consistent with enhanced convective activity and above-average precipitation over the central equatorial Pacific, with a reduced strength of the equatorial easterly winds. This combination of conditions is indicative of mature El Niño conditions.

During March–April–May (MAM) equatorial Pacific SSTs began to cool east of the date line (Fig. 4.2c) and the equatorial cold tongue became stronger than average (Fig. 4.2d), while temperatures west of the date line warmed to more than 0.5°C above average. This evolution marked the end of the El Niño episode. During JJA and SON, the warmest SSTs (Figs. 4.2e,g) and largest positive SST anomalies (Figs. 4.2f,h) became established west of the date line, and near-normal temperatures prevailed across the east-central and eastern equatorial Pacific.

The subsurface thermal structure is a fundamental component of ENSO. During DJF, anomalously warm waters were evident between 100- and 200-m depths across the central and east-central equatorial Pacific (Fig. 4.3a). This warmth was consistent with an increased depth of the oceanic thermocline, and a decreased west-to-east slope of the thermocline across the tropical Pacific. During MAM, this structure changed markedly as the thermocline became shallower than average across the east-central and eastern equatorial Pacific, and anomalously cold water developed over the eastern Pacific between the surface and the 150-m depth (Fig. 4.3b). This cold-episode like structure of the oceanic thermocline did not persist, however, and slightly warmer-than-average waters returned during JJA and SON (Figs. 4.3c,d).

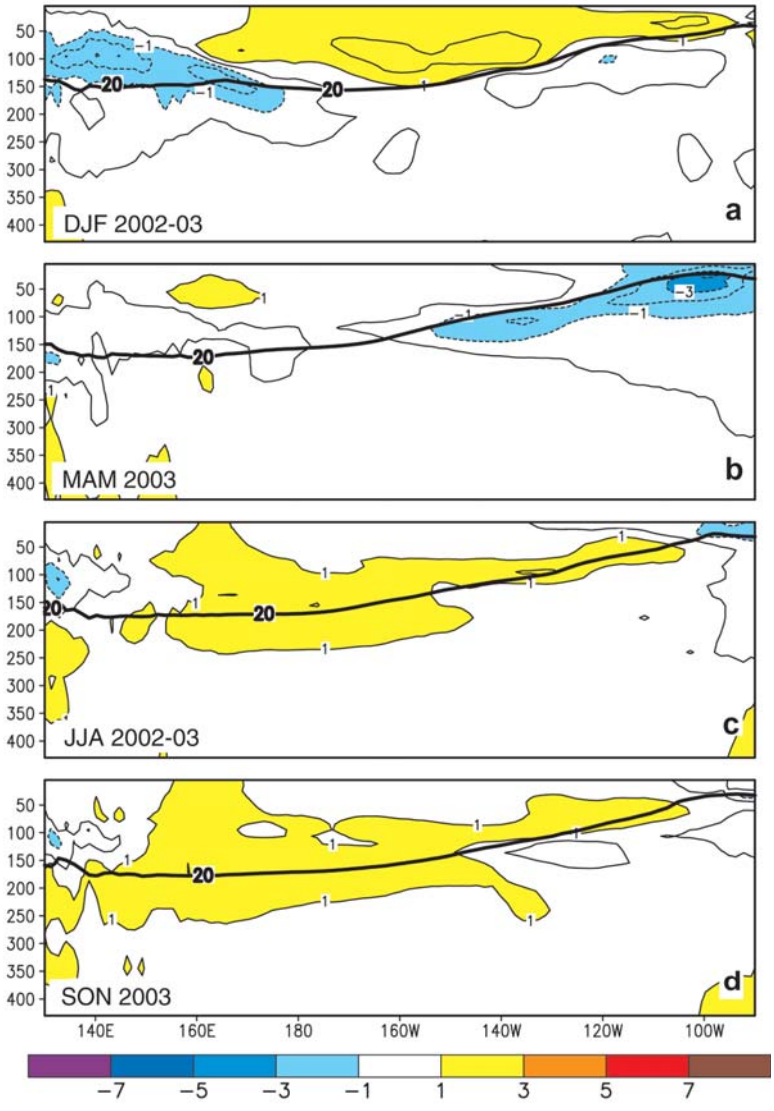

Fig. 4.3. Equatorial depth–longitude sections of ocean temperature anomalies for (a) DJF 2002–03, (b) MAM 2003, (c) JJA 2003, and (d) SON 2003. Shading interval is 1°C, and the dark line is the 20°C isotherm. Data were derived from an analysis system that assimilates oceanic observations into an oceanic GCM (Behringer et al. 1998). Anomalies are departures from the 1981–2000 base period means.

iii) Atmospheric circulation

Many of the prominent atmospheric circulation features typical of past equatorial Pacific warm episodes were observed during DJF 2002/03, reflecting a continuation of conditions

that had become established during SON 2002 (Halpert and Bell 2003; see their Figs. 27 and 28). In the Tropics, the El Niño–related features included 1) lower-level westerly wind anomalies across the eastern equatorial Pacific in association with a reduced strength of the tropical easterlies (Figs. 4.4a), 2) an enhanced ascending motion and convective activity over the central equatorial Pacific, and 3) an anomalous descending motion and suppressed convective activity in the vicinity of northeastern Australia (Ropelewski and Halpert 1987). This reduced strength of the equatorial Walker circulation has been a well-known characteristic of Pacific warm episodes.

In the meridional direction, the circulation during DJF 2002/03 featured anomalous poleward flow in the upper troposphere over the central tropical Pacific extending into the core of the East Asian jet stream (Fig. 4.5a). This enhanced Hadley circulation has been another well-known feature of Pacific warm episodes (Mo and Kousky 1993).

Also typical of past warm episodes, the DJF 2002/03 season featured upper-level anticyclonic streamfunction anomalies in the subtropics of both hemispheres, indicated by positive (negative) anomalies in the Northern (Southern) Hemisphere, which flanked the region of enhanced convection over the central equatorial Pacific (Fig. 4.5b) (Mo and Kousky 1993). These anticyclonic anomalies reflected a strengthening and eastward extension of the subtropical ridges in both hemispheres, and an overall weakening of the mid-Pacific troughs farther east. Enhanced westerlies and anomalous upper-level confluent flow across the

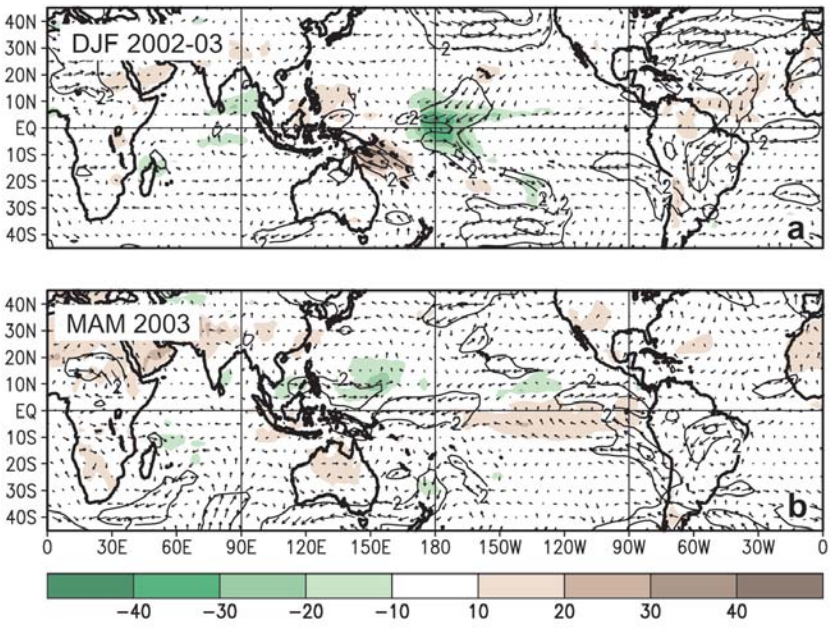

Fig. 4.4. OLR anomalies (shaded) and 850-hPa vector wind anomalies and isotachs for (a) DJF 2002/03 and (b) MAM 2003. Contour interval for isotachs is 2 m s^{-1}. Shading interval for OLR anomalies is 10 W m^{-2}. Anomalies are departures from the 1979–95 base period monthly means.

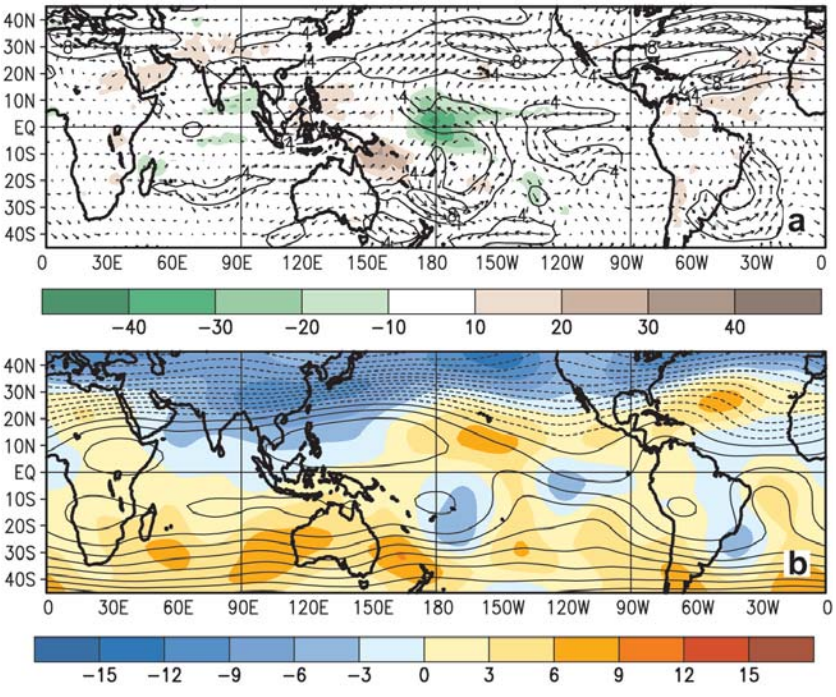

Fig. 4.5. DJF 2002/03: 200-hPa (a) vector wind and isotachs and (b) streamfunction anomalies. Contour interval for isotachs in (a) is 4 m s^{-1}. Shading interval for streamfunction anomalies is 3 × 10^6 m^2 s^{-1}. In the Northern Hemisphere positive (negative) streamfunction anomalies indicate an anticyclonic (cyclonic) circulation. In the Southern Hemisphere, negative (positive) values indicate an anticyclonic (cyclonic) circulation. Anomalies are departures from the 1979–95 base period monthly means.

central extratropical Pacific were evident along the poleward flanks of the anomalous subtropical ridges in both hemispheres (Fig. 4.5a). These anomalies reflected an eastward extension of the midlatitude jet streams in both hemispheres, and an eastward shift in the areas of strong upper-level diffluence that defined the jet exit regions.

These El Niño conditions dissipated during MAM 2003 as anomalous cross-equatorial flow at 850-hPa developed across the Pacific (Fig. 4.4b), and resulted in enhanced oceanic upwelling and a rapid cooling of ocean temperatures across the eastern Pacific.

b. Tropical Storms

i) Atlantic Hurricane Season—G. D. Bell,[5] S. Goldenberg,[16] C. Landsea,[16] E. Blake,[7] R. Pasch,[7] M. Chelliah,[5] and K. Mo[5]

(i) Overview

The North Atlantic hurricane season officially runs from June through November. An average season produces 10 tropical storms (TSs), six hurricanes (Hs), and two major hurricanes [MHs; defined as maximum sustained wind speeds at or above 100 kts, and measured by categories 3–5 on the Saffir–Simpson scale (Simpson 1974)]. In 2003, the Atlantic basin was extremely active, with 16 TSs, seven hurricanes Hs, and three MHs.

Five of these Atlantic storms made landfall in the United States, one as a tropical depression (Henri), two as tropical storms (Bill and Grace), and two as hurricanes (Claudette and Isabel). A sixth system, H Erika, made landfall in northeastern Mexico, and brought tropical storm–force winds and precipitation to southern Texas. Mexico also experienced tropical storm conditions from Claudette and Larry, and TS Odette affected Hispañola. In addition, Nova Scotia and Bermuda experienced devastating impacts from hurricanes Juan and Fabian, respectively.

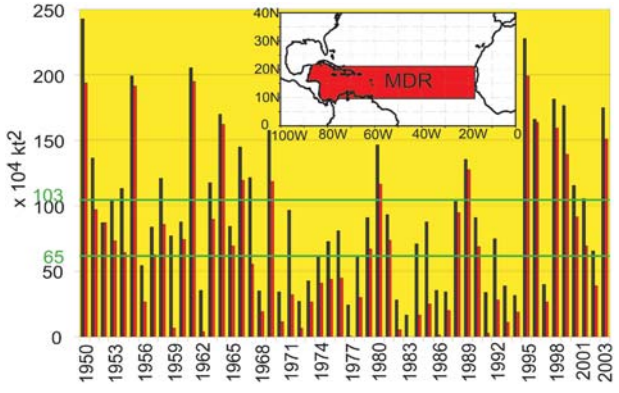

Fig. 4.6. Seasonal values of the ACE index for the entire Atlantic basin (blue) and for the MDR (red). The MDR consists of the tropical Atlantic to 21.5°N and the Caribbean Sea (see inset). The ACE index for the MDR is based on systems that first became tropical storms in that region. NOAA defines near-normal seasons as having a total ACE value in the range of 65–103 × 10^4 kt^2 (green lines).

Most of the activity during Atlantic hurricane seasons occurs during August–October, primarily in response to systems developing from African easterly wave disturbances. During the above-normal 2003 season, 10 tropical storms, of which 4 became hurricanes, developed between mid-August and mid-October. Three of these systems became major hurricanes. Above-normal hurricane seasons also feature a high concentration of activity in the main development region (MDR) (Goldenberg and Shapiro 1996), which consists of the tropical Atlantic and Caribbean Sea beween 9° and 21.5°N (see map inset in Fig. 4.6). Eight tropical storms formed in the MDR during 2003; four of these systems became hurricanes, with three becoming major hurricanes.

Another notable aspect of the season was the formation of five tropical storms over the Gulf of Mexico, which tied the season high observed in 1957. On average, one to two tropical storms form in this region during a given season. Also, three tropical storms formed outside of the normal (June–November) hurricane season in 2003. Tropical Storm Ana formed on 22 April, and TS Odette and TS Peter formed on 4 and 9 December, respectively. This was the first season since 1887 that two tropical storms have formed in December.

Important aspects of the atmospheric circulation during the peak of the 2003 season (Fig. 4.7) can be attributed to the ongoing active Atlantic multidecadal signal (Chelliah and Bell 2004), including 1) an amplified subtropical ridge, 2) reduced vertical wind shear in the MDR resulting from upper-level easterly wind anomalies (green arrows) and lower-level westerly anomalies (light blue arrows), 3) an exceptionally favorable African easterly jet (AEJ; dark blue arrow), 4) an active West African monsoon system, and 5) above-average SSTs in the MDR. During August the exceptionally conducive nature of the total signal was also related to a pre-existing midlatitude circulation pattern known as the positive phase of the East Atlantic teleconnection pattern, and during September–October it was related to an anomalous atmospheric warming across the entire tropical Atlantic in association with a broader warming of the global tropical atmosphere.

(ii) Seasonal activity

NOAA quantifies "total seasonal activity" with the accumulated cyclone energy (ACE) index, which accounts for the combined strength and duration of tropical storms and hurricanes during a given season (Bell et al. 2000). The ACE index is a wind energy in-

dex, calculated by summing the squares of the estimated 6-hourly maximum sustained wind speed in knots ($V\text{max}^2$) for all periods while the system is either a tropical storm or hurricane (Fig. 4.6, blue bars). The total ACE index for the 2003 season was 174.75×10^4 kt^2, or 200% of the 1951–2000 median value (87.5×10^4 kt^2).

NOAA classifies an above-normal Atlantic hurricane season based on two criteria. The seasonal ACE value must exceed 105×10^4 kt^2 (120% of the median), and at least two of the following three must be above average: the number of tropical storms, hurricanes, and major hurricanes. The 2003 Atlantic hurricane season satisfied both criteria, thus marking a continuation of generally above-normal activity that began in 1995.

The eight tropical systems first named in the MDR accounted for most (86.6%) of the total ACE value during 2003 (Fig. 4.6, red bars), with the three major hurricanes (Fabian, Isabel, and Kate) accounting for 74% of the total. Isabel produced one of the largest observed ACE values (63.3×10^4 kt^2) of any Atlantic hurricane on record, lasting 8 days as a major hurricane and 1.75 days at category 5 status (wind speeds at or above 140 kts). Fabian and Kate contributed an additional 43.2×10^4 kt^2 and 21.9×10^4 kt^2 to the ACE index, lasting 7.25 days and 1.5 days as major hurricanes, respectively. The combined duration of these three storms at major hurricane status was 16.75 days, which is fourth largest on record behind 1961 (24.5 MH days), 1950 (18.5 MH days), and 1955 (17.25 MH days).

The ACE index has shown large multidecadal fluctuations in total seasonal activity, characterized by above-normal activity during 1950–69 and 1995–2003, and below-normal activity during 1970–94 (Goldenberg et al. 2001; Bell 2003). During 1995–2003, Atlantic hurricane seasons have averaged 13.6 TSs, 7.7 Hs, and 3.6 MHs. The average numbers of tropical storms and hurricanes were larger than any consecutive 9-yr period in the reliable record dating back to 1944. However, because of continuous improvements in the observational network, including satellite technology, aircraft measurements, and Doppler radar, it is likely that more systems were identified in the latter part of the record than during the above-normal decades of the 1950s and 1960s (Goldenberg et al. 2001). During the below-normal period, Atlantic hurricane seasons averaged only 9 TSs, 5 Hs, and 1.5 MHs. This multidecadal variability primarily reflects changes in activity originating in the MDR (Landsea and Gray 1992, Landsea 1993; Landsea et al. 1999), with the 1995–2003 mean MDR-based ACE index of 114×10^4 kt^2 nearly triple the 1970–94 average of 41×10^4 kt^2.

(iii) Rainfall from landfalling U.S. tropical systems

Five named Atlantic storms made landfall in the United States during 2003, with a sixth system (H Erika) making landfall in northern Mexico and bringing tropical storm–force winds and rain to southern Texas. This compares with seven landfalling U.S. systems during 2002, when six hit as tropical storms and one hit as a hurricane (Bell 2003). For the period 2002–03, 12 named storms have made landfall in the United States, with 9 (4 in 2003 and 5 in 2002) striking the Gulf Coast.

The storm-total precipitation associated with the Gulf Coast landfalling tropical storms and hurricanes during 2003 is shown in Fig. 4.8. The first of these systems (TS Bill) produced more than 150 mm of rain across eastern Louisiana, Mississippi, and western Alabama during 30 June–1 July. Hurricane Claudette then crossed eastern Texas on 15–16 July, generally producing totals of 75–100 mm. One month later Hurricane Erika made landfall in northeastern Mexico on 16–17 August, and brought tropical storm–force winds to extreme southern Texas. Erika produced 75–100 mm of rain in northeastern Mexico and a range of 25–75 mm in southern Texas. Tropical Storm Grace brought 75–100 mm of rain to southeastern Texas on 31 August. This system was followed by TS Henri, which generally brought 100–125 mm of rain to west-central Florida on 6 September.

The sixth Atlantic system to make U.S. landfall was Hurricane Isabel, which came onshore along the Outer Banks of the North Carolina coast as a category 2 hurricane on 18 September. Rainfall totals associated with Isabel averaged 100–200 mm across eastern North Carolina and Virginia, and 50–100 mm across West Virginia and eastern Ohio (Fig. 4.8f). This storm was directly responsible for 17 fatalities and produced mas-

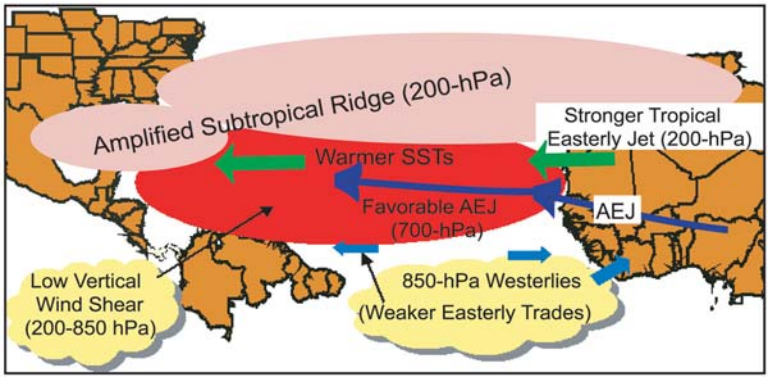

Fig. 4.7. Schematic representation of conditions during the peak (Aug–Oct) of the above-normal 2003 Atlantic hurricane season.

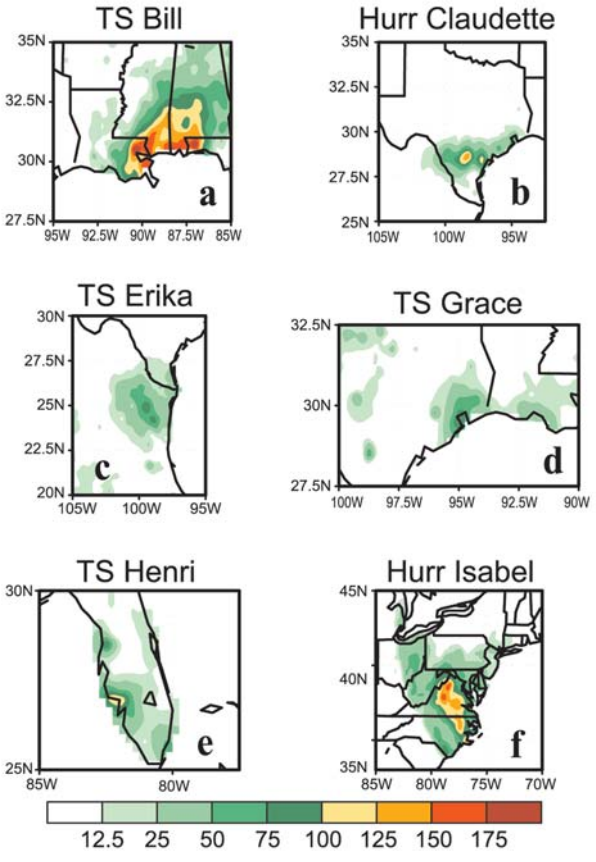

FIG. 4.8. Total rainfall (mm) over land associated with the six U.S. landfalling named storms during 2003: (a) TS Bill during 30 Jun–1 Jul, (b) H Claudette during 15–16 Jul, (c) H Erika during 16–17 Aug, (d) TS Grace on 31 Aug, (e) TS Henri on 6 Sep, and (f) H Isabel during 18–19 Sep.

sive power outages in the mid-Atlantic region, with total damages estimated by NOAA's National Hurricane Center at U.S. $3.4 billion.

(iv) Environmental conditions influencing the 2003 Atlantic hurricane season

(a) 200- AND 850-HPA CIRCULATION AND VERTICAL WIND SHEAR

During August–October 2003, the mean 200-hPa subtropical ridge axis was stronger and farther north of its normal position from the Gulf of Mexico to northern Senegal (Fig. 4.7). South of the ridge axis, upper-level easterly wind anomalies covered the entire MDR in association with an enhanced tropical easterly jet (Fig. 4.7, green arrows). The ongoing multidecadal signal can account for the amplified subtropical ridge and enhanced tropical easterly jet over the eastern North Atlantic and Africa (Chelliah and Bell 2004). These features were not related to the ENSO-neutral conditions observed during the peak of the season.

During August, the extensive area of positive 200-hPa height anomalies across the tropical North Atlantic was also partly related to a continuation of the positive phase of the eastern Atlantic teleconnection pattern (see Fig. 6.21). This pattern has strong links to both the subtropics and extratropics, and during April–August was associated with a marked amplification of the 200-hPa subtropical ridge across the North Atlantic (see Fig. 6.20). During September and October, the amplified subtropical ridge was partly related to an anomalous warming throughout the tropical Atlantic (red in Fig. 4.9), which occurred in association with a warming of the global Tropics (Fig. 4.9, green).

At 850-hPa, westerly zonal wind anomalies across the North Atlantic and western Africa during August–October 2003 (Fig. 4.10a) reflected weaker-than-average tropical easterlies. This anomaly pattern was already evident during the preceding 4 months (Fig. 4.10b), indicating it did not result from the increased hurricane activity (Goldenberg and Shapiro 1996). In both periods these westerly anomalies contributed to anomalous cyclonic relative vorticity at 850 hPa across the heart of the MDR.

The combination of upper- and lower-level zonal wind anomalies resulted in easterly vertical wind shear anomalies between 200 and 850 hPa from the eastern tropical Pacific to western Africa (Fig. 4.11a). The anomalous easterly shear resulted in lower total vertical shear over the heart of the MDR, and higher total shear over both tropical western Africa and portions of the eastern tropical Pacific (Fig. 4.11b). This three-celled anomaly pattern was typical of other above-normal Atlantic hurricane seasons. It was also consistent with the enhanced 2003 West African monsoon system (see section 6eii), and with a below average 2003

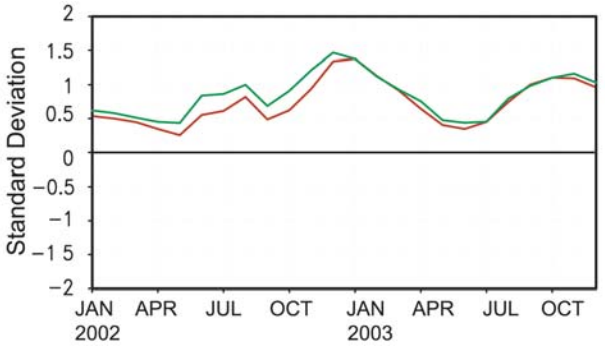

FIG. 4.9. Standardized values of the 3-month running mean area-averaged 200-hPa height anomalies calculated for the entire global Tropics (20°N–20°S) (green curve) and for the region centered on the tropical Atlantic (120°W–40°E, 20°N–20°S) (red curve). Anomalies are departures from the 1971–2000 base period monthly means.

eastern North Pacific hurricane season that featured a record low of no major hurricanes [see section 4bII(ii)].

(b) 700-hPa African easterly jet, convective available potential energy, and SSTs

During August–October, tropical cyclogenesis in the MDR is typically associated with amplifying African easterly wave disturbances (Reed et al. 1977) moving within the region of high cyclonic relative vorticity along the equatorward flank of the 700-hPa AEJ. The AEJ was well defined during 2003, (Fig. 4.12a, contours), with high values of cyclonic relative vorticity extending along its entire equatorward flank (shading). The AEJ was also shifted to almost 20°N over the central MDR, roughly 5° of latitude farther north than its climatological mean position (Bell et al. 2000, see their Fig. 31). This structure was consistent with the weaker-than-average tropical easterlies and enhanced 850-hPa cyclonic relative vorticity previously noted across the heart of the MDR (Fig. 4.10a).

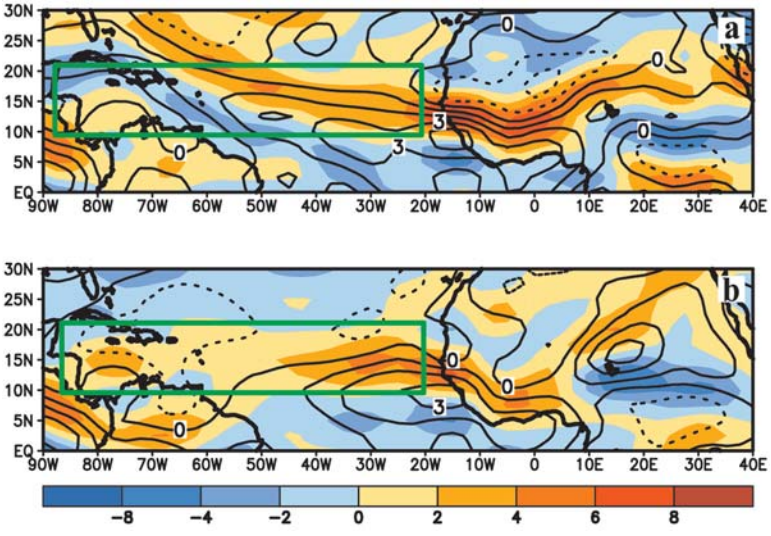

Fig. 4.10. Anomalous 850-hPa zonal winds (contours, interval is 1.0 m s^{-1}) and relative vorticity (shading, x 10^{-6} s^{-1}) during (a) Aug–Sep 2003, and (b) Apr–Jul 2003. Solid (dashed) contours indicate westerly (easterly) wind anomalies. Cyclonic (anticyclonic) relative vorticity anomalies are shaded orange (blue). Green box denotes the MDR. Anomalies are departures from the 1971–2000 base period monthly means.

An enhanced cross-equatorial flow of deep tropical moisture was also evident at low levels, which contributed to high values of convective available potential energy (CAPE) extending well into the central MDR along the equatorward flank of the AEJ (Fig. 4.13a). The high CAPE values were also associated with near-record warm SSTs (0.5°–1°C above average) throughout the MDR (Fig. 4.13b). Area-averaged SSTs in the

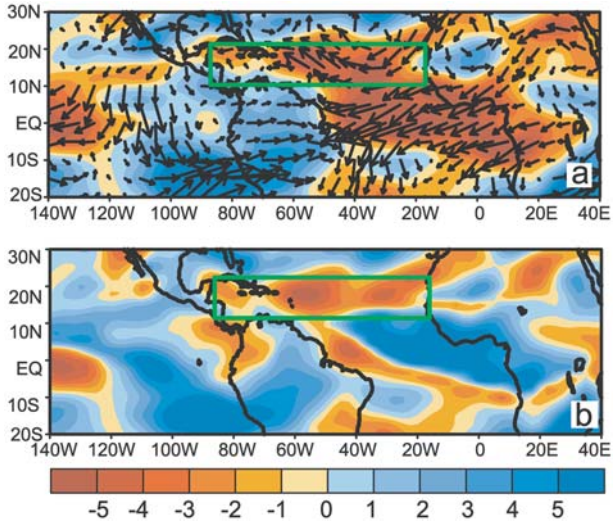

Fig. 4.11. Aug–Sep 2003 (a) anomalous 200–850-hPa vertical shear of zonal wind (shaded, m s^{-1}) and anomalous vertical shear vector, and (b) anomalous strength of the total 200–850-hPa vertical shear. In (a) red indicates anomalous easterly shear and blue indicates anomalous westerly shear. In (b) red indicates lower total shear and blue indicates higher total shear. Green box denotes the MDR. Anomalies are departures from the 1971–2000 base period monthly means.

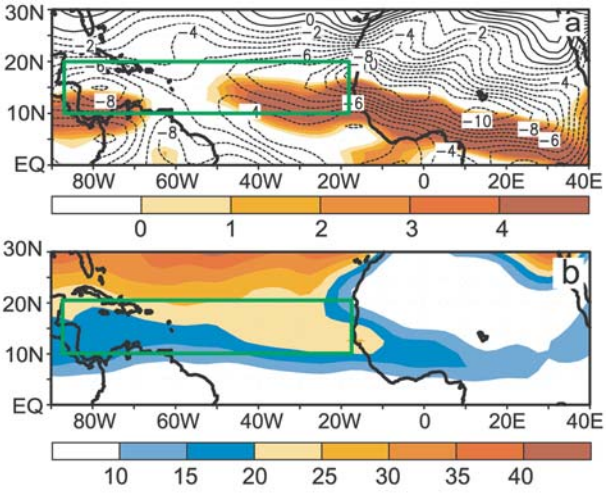

Fig. 4.12. Aug–Sep 2003 mean 700-hPa (a) zonal winds (contours, interval is 1.0 m s^{-1}) and relative vorticity (shading, × 10^{-6} s^{-1}), and (b) potential vorticity [× 10^{-7} K (s hPa)$^{-1}$]. In (a) only cyclonic vorticity values are shaded. Green box denotes the MDR.

MDR were two standard deviations above normal during August–October 2003, which is comparable to the record warmth seen during the extremely active 1998 season (Fig. 4.13c).

These results indicate that the tropical disturbances during the peak of the 2003 season experienced a linearly unstable mean current and an extended region of increased cyclonic vorticity as they propagated westward over very warm SSTs into the low-shear, high CAPE environment in the heart of the MDR. These conditions were exceptionally conducive to tropical cyclogenesis, as has also been described for the above-normal 1998–2000 Atlantic hurricane seasons by Bell et al. (1999, 2000) and Lawrimore et al. (2001). These very prominent circulation anomalies have prevailed throughout the above-normal period of 1995–2003, with the exception of the two El Niño years (1997, 2002) (Fig. 4.14).

These low-frequency fluctuations in key circulation anomalies over the tropical North Atlantic are consistent with the strong relationship between multidecadal variations in the seasonal Atlantic basin activity and the West African monsoon system (Hastenrath 1990; Landsea and Gray 1992; Goldenberg and Shapiro 1996). They are also consistent with the observed transition to the warm phase of the Atlantic multidecadal mode during the early and mid-1990s (Landsea et al. 1999; Mestas-Nuñez and Enfield 1999). Chelliah and Bell (2004) have shown that these multidecadal fluctuations are associated with SST and convective rainfall anomalies spanning the global Tropics. The associated atmospheric circulation anomalies are also Tropics-wide, and are important to seasonal Atlantic hurricane activity because they include key circulation features in the MDR (Fig. 4.14).

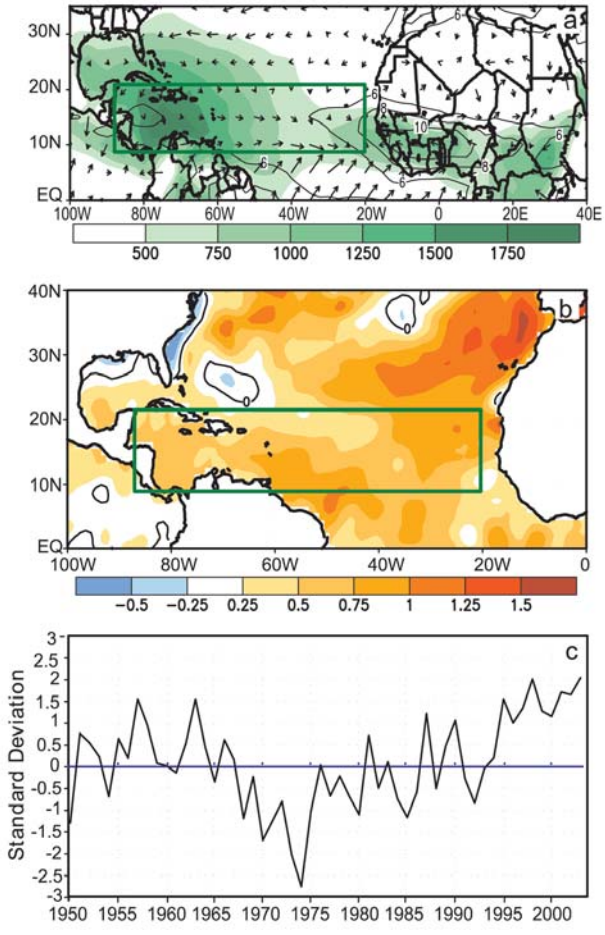

Fig. 4.13. Aug–Oct 2003 (a) CAPE (shaded, in J kg^{-1}), 700-hPa wind speeds (contours, interval is 2.0 m s^{-1}), and anomalous 925-hPa wind vector, and (b) anomalous SST (°C). (c) Standardized, area-averaged SST anomalies (°C) in the MDR (20°–90°W and 9°–21.5°N) for consecutive Aug–Oct periods from 1950 to 2003. Green box in panels (a) and (b) shows the MDR. Anomalies in (a) and (b) are departures from the 1971–2000 base period means. SST anomalies in (c) are departures from the 1951–2000 base period means.

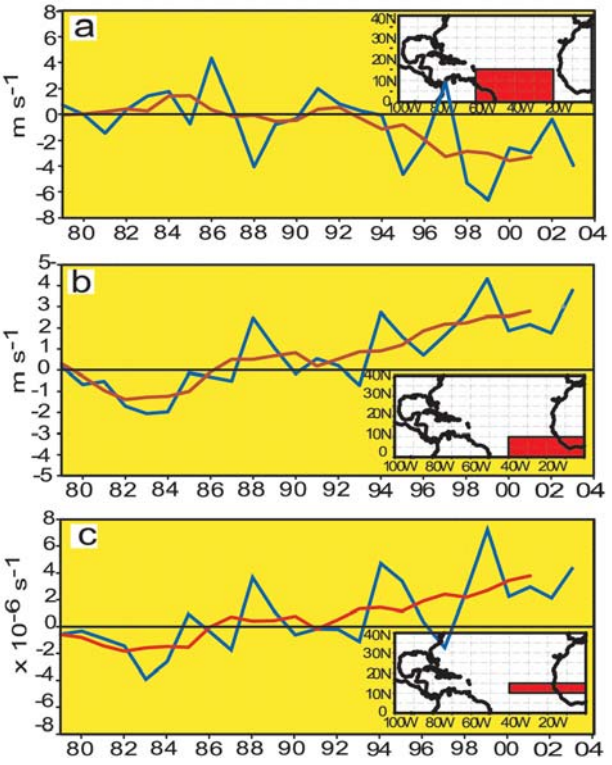

Fig. 4.14. Area-averaged anomaly time series for each Aug–Sep period between 1979 and 2003: (a) 200–850-hPa vertical shear of the zonal wind (m s^{-1}), b) 700-hPa zonal wind (m s^{-1}), and (c) 700-Pa relative vorticity (× 10^{-6} s^{-1}). Blue curve shows unsmoothed 2-month anomalies, and red curve shows a 5-pt running mean smoother applied to the time series. Averaging regions are shown in the insets. Anomalies are departures from the 1979–95 base period monthly means.

ii) Pacific Tropical Storms

(i) Western North Pacific typhoon season—S. J. Camargo[6]

Typhoons can develop throughout the year in the western North Pacific, with peak activity usually between July and November. In 2003, there were 28 tropical cyclones in the western North Pacific basin, including typhoons, tropical storms, and tropical depressions; this was slightly below the 1973–2002 average of 30.3 (median 30.5) [Joint Typhoon Warning Center (JTWC) best-track dataset; JTWC 2004]. One of these (Jimena) developed in the eastern Pacific and entered the western Pacific with tropical depression intensity, while all of the others formed west of the date line (180°). There were 23 tropical cyclones with at least a tropical storm intensity (referred to as "named tropical cyclone"), two of which (03W and 27W) were not named due to their minimal intensity—below the 1973–2002 average of 26.4 (median 26, 25th percentile 24; Fig. 4.15a). The number of tropical cyclones (TCs) reaching typhoon intensity (17) was close to the 1973–2002 average of 16.5 (median 16). Five typhoons (Kora, Imbudo, Maemi, Parma, and Lupit) reached supertyphoon intensity, above the 1973–2002 average of 3.6 (median 3, 75th percentile 5; see Fig. 4.15b). On average, over the last 30 yr 12% of the tropical cyclones reached supertyphoon intensity; in 2003, the percentage was slightly higher (18%). Therefore, while the total number of tropical cyclones that formed in 2003 was slightly below normal in the western North Pacific, the number of tropical cyclones that intensified to typhoon and supertyphoon intensity were normal and slightly above normal, respectively.

Historically, approximately 70% of all western North Pacific tropical cyclones with at least tropical storm strength occur between the months of July and October (Fig. 4.16). During the 2003 season, the contribution of those peak months to the total number of named tropical cyclones was 60%. An above-average number of named tropical cyclones occurred in the previous months (see Fig. 4.16), most notably in May (historical average of one) when two typhoons (Chan-Hom and Linfa) and one tropical storm (03W) were observed. Only twice before has May had more named tropical cyclones, in 1980 and 1971, when four and five named tropical cyclones formed, respectively. Only two named tropical cyclones formed in July, typhoons Imbudo and Koni, which was below the historical average of 4.1. Five named tropical cyclones formed in August and three in September, both months that average five.

The monthly and seasonal values of the ACE index (Bell et al. 2000) for the western North Pacific (Fig. 4.17) show a near normal value for the 2003 June–November season (256.2×10^4 kt^2), corresponding to 116% of the median value (268.3×10^4 kt^2) during the

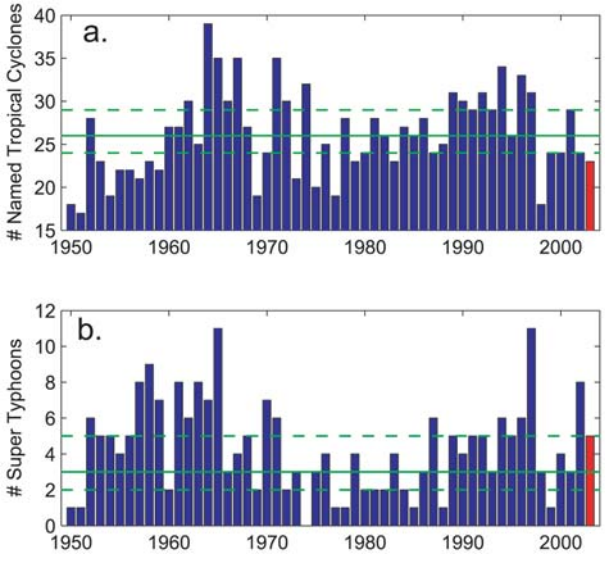

Fig. 4.15. Number of (a) named tropical cyclones and (b) supertyphoons per year in the western North Pacific basin during the period 1950–2003. The solid green line indicates the median for 1973–2002, and the dashed green lines show the 25th and 75th percentiles. (Data courtesy of JTWC.)

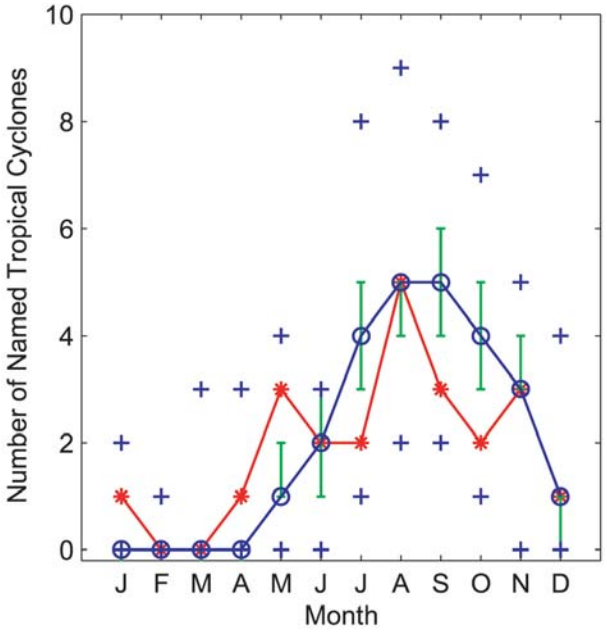

Fig. 4.16. Number of named tropical cyclones per month in the western North Pacific in 2003 (red line) and median for the years 1973–2002 (blue line). The error bars indicate the 75th and 25th percentiles in the years 1973–2002. In the cases with no error bars, the upper and/or lower percentiles coincide with the median. The blue crosses show the maximum and minimum values during 1973–2002. (Data courtesy of JTWC.)

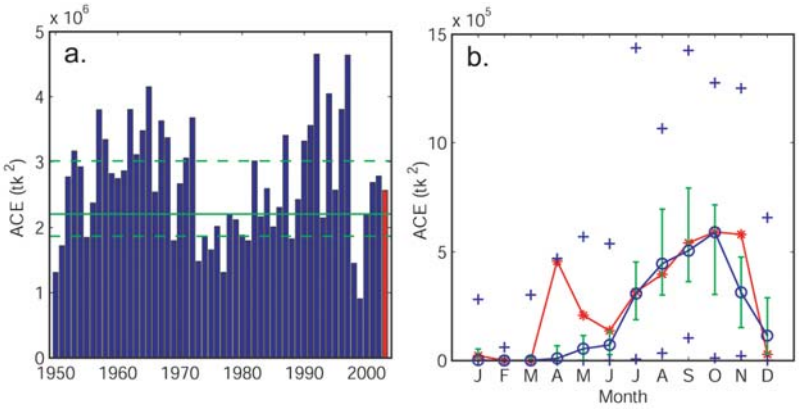

FIG. 4.17. (a) ACE index for the western North Pacific for the years 1950–2003. The solid green line indicates the median for the years 1973–2002 and the dashed green lines show the 25th and 75th percentiles. (b) ACE index per month in the western North Pacific in 2003 (red line) and median in the years 1973–2002 (blue line). The green error bars indicate the 25th and 75th percentiles. In the cases with no error bars, the upper and/or lower percentiles coincide with the median. The blue crosses show the maximum and minimum values during 1973–2002 (JTWC 2004).

period 1973–2002. The ACE index for the whole year was slightly above normal (not shown), with a value 327.6×10^4 kt^2, which corresponds to 122% of the median value (268.3×10^4 kt^2) of the last 30 yr (1973–2002). There was above-average tropical cyclone activity during April 2003 due to supertyphoon Kujira (see Fig. 4.17), which lasted from 9–25 April and reached a maximum sustained wind speed of 130 kt (~67 m s^{-1}). Typhoon Kujira was the fifth supertyphoon on record during the month of April, and one of the longest-lived tropical cyclones on record in the western North Pacific basin. Other months with above-normal activity were May and November. ACE values were near normal during the peak months of July–October. The peak ACE value in 2003 occurred in the latter part of the season during the months of September–November. The five supertyphoons of the 2003 season contributed to 55% of the total ACE. Super typhoons Lupit (19 November–1 December; maximum sustained winds 145 kt, 75 m s^{-1}) and Kujira, with ACE values of 4.60×10^5 kt^2 and 4.56×10^5 kt^2, respectively, represented approximately 28% of the total ACE index in 2003.

Overall, tropical storms and typhoons in the western North Pacific during 2003 had an average tropical cyclogenesis position of 12.8°N, 137.5°E, which was west of the 30-yr historical average (12.8°N, 143.4°E). The average track position of all named tropical cyclones in 2003 was 18.6°N, 131.7°E, which was also west of the historical average position (19.0°N, 134.2°E) observed over the last 30 yr.

The 2003 typhoon season produced significant impacts in many countries of the region (see Table 4.1). Among the typhoons that made landfall, super-typhoon Maemi (5–13 September) caused widespread destruction in South Korea. Maemi formed east of the Philippines and moved northwestward while intensifying, reaching its maximum intensity near Okinawa, Japan, and weakened before making landfall in Korea and finally modifying into an extratopical system in the Sea of Japan.

TABLE 4.1. Western North Pacific tropical cyclones during 2003 with significant impacts in Asia (categories: TS–tropical storm, TY–typhoon, and STY–super-typhoon).

Category	Name	Period	Countries affected
TY	Kujira	9–25 Apr	Taiwan, Japan
TS	Linfa	25–30 May	Philippines, Japan
TY	Soudelor	11–19 Jun	Philippines, Taiwan, Japan
STY	Imbudo	16–24 Jul	Philippines, China
TY	Koni	18–22 Jul	China, Vietnam
TY	Morakot	1–5 Aug	China, Taiwan
TY	Etau	3–9 Aug	Japan
TY	Krovanh	15–25 Aug	Philippines, China
STY	Dujuan	20 Aug–3 Sep	China
STY	Maemi	5–13 Sep	South Korea
TY	Melor	30 Oct–4 Nov	Philippines, Taiwan
TY	Nepartak	13–19 Nov	Philippines, China

High winds and rainfall associated with Maemi were responsible for more than 100 deaths and destroyed more than 1.4 million houses, damaged roads and bridges, and sank at least 82 vessels.

(ii) Eastern North Pacific hurricane season—D. H. Levinson[14]

The hurricane season in the eastern North Pacific Ocean typically begins in mid-May and extends through the end of November. Reliable records for the eastern North Pacific (ENP) basin date to approximately 1951, and currently NOAA's National Hurricane Center uses the 1971–2000 base period for their climatologies. Hurricane detection and tracking has improved greatly during the satellite era, and this is especially true for the ENP basin, where ship reports and other information had been sparse prior to the deployment of geostationary satellites. Therefore, historical records for ENP tropical cyclones are likely incomplete prior to the advent of satellites in the early 1960s.

In 2003, the hurricane season in the ENP basin was below normal in several notable categories. The 2003 season included a total of 16 named storms, seven hurricanes, and no major hurricanes in the ENP basin. The basic statistics of all named storms in 2003 are shown in Table 4.2, while a comparison of 2003 with the 1971–2000 climatology is shown in Table 4.3. The total number of named storms in 2003 equaled the climatological average of 16 for the ENP basin, while the formation of seven hurricanes was below the long-term average of nine, and no major hurricanes formed during the entire season, while on average four typically develop. This was the first year since 1977 where no category 3–5 hurricanes developed during the entire tropical cyclone season in the ENP basin.

The 2003 season was also notable due to the record late development of the season's first hurricane. On 24 August, H Ignacio intensified from a tropical storm to a category 2 hurricane. The average date for the development of the first hurricane of the season in the ENP is 24 June, a full 2 months before Ignacio intensified into a hurricane.

Figure 4.18 illustrates the observed tracks of all tropical storms and hurricanes during 2003. The tracks of tropical storms and hurricanes in the ENP basin (as well as in other basins around the globe) are dominated by cyclones that propagate primarily toward the west-northwest in the Northern Hemisphere (tropical cyclone propagation is typically toward the west-southwest in the Southern Hemisphere), known as β drift. In 2003, most of the named storms and hurricanes that formed in the ENP basin followed a typical west-northwest track, eventually moving over colder waters and weakening. In addition, this west-northwest propagation often brings the cyclone into an unfavorable atmospheric environment for intensification, due to increased vertical wind shear as the cyclone moves away from the near-equatorial region into the trade wind zone and toward higher latitudes.

Recurvature of tropical cyclones in the ENP basin toward the east substantially increases the probability of landfall. In addition to the potential for storm surge, coastal and flash flooding, mudslides, and related natu-

Table 4.2. All named tropical storms and hurricanes during the 2003 season in the eastern North Pacific Ocean. Maximum cyclone intensity: tropical storm = TS, category 1 hurricane = H1, category 2 hurricane = H2; intensity at landfall: tropical depression = LFD, tropical storm = LFTS, hurricane = LFH (LFH1, LFH2). (Data courtesy of NOAA-NHC.)

No.	Name	Dates (cyclogenesis–cyclolysis)	Max 1-min wind (in kt) (intensity, landfall intensity)	Minimum SLP (hPa)	Related deaths
1	Andres	21–26 May	50 (TS)	997	0
2	Blanca	17–22 Jun	55 (TS)	997	0
3	Carlos	25–27 Jun	55 (TS, LFTS)	996	0
4	Dolores	5–7 Jul	35 (TS)	1005	0
5	Enrique	10–13 Jul	55 (TS)	993	0
6	Felicia	17–23 Jul	45 (TS)	1000	0
7	Guillermo	7–12 Aug	50 (TS)	997	0
8	Hilda	9–13 Aug	35 (TS)	1004	0
9	Ignacio	22–27 Aug	90 (H2, LFH1)	970	2
10	Jimena	28–2 Sep	90 (H2)	973	0
11	Kevin	3–6 Sep	35 (TS)	1000	0
12	Linda	14–17 Sep	65 (H1)	987	0
13	Marty	19–24 Sep	85 (H2, LFH2)	973	12
14	Nora	1–9 Oct	90 (H2, LFD)	969	0
15	Olaf	3–8 Oct	65 (H1, LFTS)	987	0
16	Patricia	20–26 Oct	70 (H1)	981	0

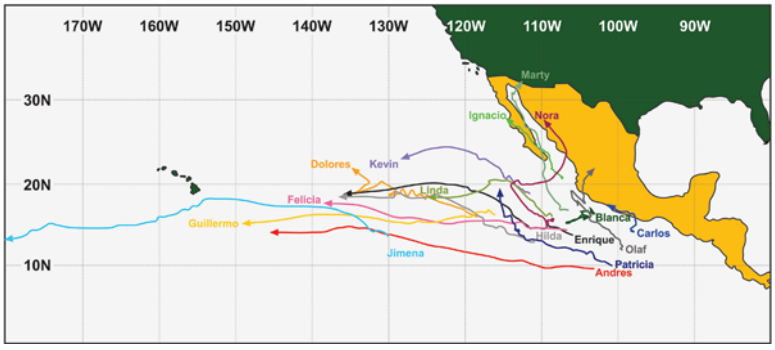

FIG. 4.18. The observed tracks of all named tropical storms and hurricanes in the eastern North Pacific Ocean during the 2003 season. (Data courtesy of the University of Hawaii.)

ral disasters, landfalling tropical storms and hurricanes play an important role in bringing moisture to the coastal areas of Mexico, as well as to inland Mexico and the southwestern United States. Beginning with the formation of TS Andres, which was the only named storm that formed in the ENP in May, most of the tropical storms that developed in June and July did not recurve, but propagated in a typical west-northwest path where the only threat for landfall is the Hawaiian archipelago. The one exception was TS Carlos, which formed on 25 June, 200 miles south-southwest of Acapulco, Mexico, and quickly moved northward, making landfall near Puerto Escondido, Mexico, on 27 June.

In mid-August, there was a significant shift in the observed tracks of tropical cyclones in the ENP. Beginning with development and intensification of H Ignacio, the majority of ENP tropical storms and hurricanes recurved toward the Mexican coast in late August, September, and October. The only exception was H Jimena, which intensified from a tropical storm on 28 August, and moved in a relatively straight path westward. Jimena eventually passed within 100 km of South Point, the southern tip of the Big Island of Hawaii, where tropical storm–force winds and over 250 mm of rain fell on 31 August and 1 September (Fig. 4.19).

During the 2003 season, the last six named tropical cyclones that developed in the ENP basin followed a recurvature path to the north along the coast of Mexico. On average, 1.34 tropical storms and 1.3 hurricanes make landfall during the ENP hurricane season (15 May–30 November) along the Pacific coast of Mexico, with respect to the 1950–2000 mean (Jauregui 2003). Overall, 4 of the 16 named storms made landfall during the 2003 ENP hurricane season. Two of these, Ignacio and Marty, intensified into hurricanes and crossed the Baja Peninsula in Mexico, while TS Carlos and TS Olaf struck the Pacific coast of Mexico. One landfalling storm, TS Nora, was not counted in the total for the season because it made landfall along the central Mexican coast only after it had weakened to a depression in early October. Therefore, despite the below-average number of hurricanes in 2003, the number of landfalling tropical storms and hurricanes were both above average for the season.

Of the landfalling storms and hurricanes in the ENP basin in 2003, by far the most dangerous and destructive was H Marty, which developed into a tropical depression on 19 September. Marty quickly intensified into a tropical storm as it initially moved toward the west-northwest. Marty recurved to the northwest and intensified into a category 1 hurricane on 21 September, turning toward the north and making landfall near Cabo San Lucas, Mexico, on 22 September, with maximum sustained winds of 85 kt (~44 m s^{-1}; a minimal category 2 hurricane). Marty moved up the Baja Peninsula and weakened, although the cyclone generated heavy rains and flooding over much of the region. Twelve deaths were eventually related to Marty, with substantial flooding along the Baja Peninsula and the Mexican coast.

TABLE 4.3. Comparison of the 2003 eastern North Pacific hurricane season with climatology. The climatology is the NOAA/National Hurricane Center 1971–2000 based period, except those statistics with a *, which denotes the 1951–2000 climatology of landfalling tropical storms and hurricanes in Mexico (Jauregui 2003).

	Climatology	2003 season
Named storms	16	16
Hurricanes	9	7
Major hurricanes (category 3–5)	4	0
Landfalling tropical storms*	1.34 (~1 yr^{-1})	2
Landfalling hurricanes*	1.3 (~1 yr^{-1})	2
Intense landfalling hurricanes*	0.3 (< 1 yr^{-1})	0
ACE for the northeast Pacific	129.7 x 10^4 Kt^2	48.67 x 10^4 Kt^2

The lack of any major hurricanes, the development of only one category 2 hurricane, as well as the record late formation of the first hurricane of the season made 2003 a below-normal year in the ENP basin. This was strongly reflected in the ACE index (Bell et al. 2000) for the 2003 ENP hurricane season. The ACE index for the 2003 season was 48.67×10^4 Kt^2 (G.D. Bell 2004, personal communication), which was approximately 37.5% of the mean value of 129.7×10^4 Kt^2 and approximately 43% of the median value of 113×10^4 Kt^2 determined from the 1971–2000 base period climatology. Several environmental factors influenced the observed anomalous conditions, and these included: ENP basin SSTs, higher total vertical wind shear over the ENP (see Figs. 4.11a–b and discussion in section 4bi), the phase of ENSO, and the phase of the QBO in the tropical lower stratosphere.

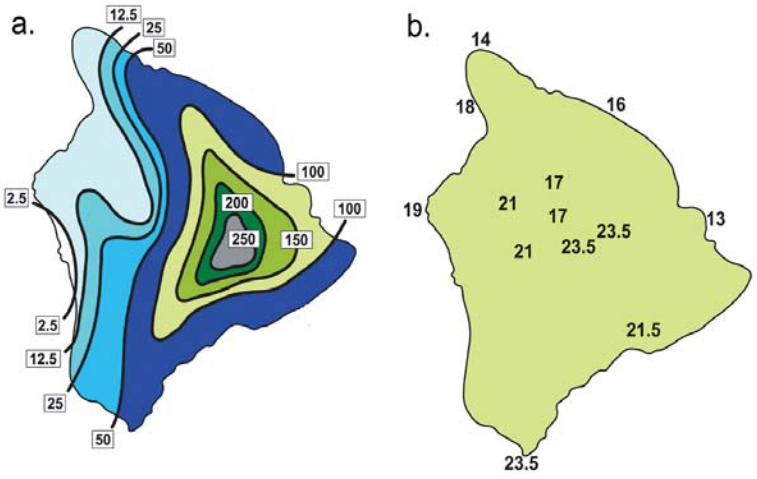

Fig. 4.19. Rainfall totals (mm; panel a) and peak wind gusts (m s^{-1}; panel b) observed on the Big Island of Hawaii during the passage of H Jimena on 31 Aug and 1 Sep. (Courtesy of A. Nash, NOAA/CPHC.)

Whitney and Hobgood (1997) developed an empirical relationship between SSTs and the maximum intensities of tropical cyclones in the ENP basin. They found that only 11% of ENP storms reach 80% of the maximum potential intensity (MPI) in the ENP, while tropical cyclones that formed west of 110°W tended to reach a higher percentage of their MPI than storms that developed farther east. In 2003, a majority of the named storms and hurricanes formed east of 110°W, which would inhibit their ability to intensify to their MPI. This was likely influenced by the presence of enhanced vertical wind shear in the ENP basin during the 2003 season (see section 4bi, Fig. 4.11).

SSTs in the ENP are influenced by the phase of ENSO, which was neutral during the summer and fall of 2003. An equatorial Pacific warm event (i.e., El Niño) typically increases SSTs in the ENP, thereby enhancing the observed intensity of tropical cyclones in the basin. However, the climatological frequency of tropical cyclones in the ENP basin does not necessarily support this physical link. Using tropical cyclone data from 1963 to 1993, Whitney and Hobgood (1997) found that there was very little difference in the frequency of tropical cyclones over the ENP basin between El Niño and non–El Niño years. However, this result may be due to the timing difference between the peak of the ENP hurricane season in September each year and the peak in the warmer-than-normal SST anomalies associated with El Niño events during the Northern Hemisphere winter. In fact, they found that the phase of the QBO was a more important factor than ENSO in influencing the maximum intensity of tropical cyclones in the ENP, mainly by affecting the propagation speed and the outflow circulation from the upper levels of the tropical cyclone. Their 31-yr study of ENP storms showed that tropical cyclones tended to reach a higher percentage of their MPI, as well as a higher maximum intensity, when the QBO was in its westerly phase at 30 mb in the tropical stratosphere. The observed influence of the QBO on tropical cyclone intensities for the ENP basin found by Whitney and Hobgood (1997) was similar to that found in the Atlantic basin by Gray (1984) and Shapiro (1989), among others.

During late 2002, the QBO switched from the westerly to the easterly phase, and the phase remained easterly through the 2003 hurricane season in the ENP. Therefore, a combination of environmental factors inhibited the development and intensification of the tropical storms and hurricanes to reach higher intensities in the ENP, with the presence of the easterly phase of the QBO in the tropical lower stratosphere, as well as the enhanced vertical wind shear in the basin, likely influencing the observed magnitude and frequency of tropical storms and hurricanes during the 2003 season.

5. POLAR CLIMATE—A. M. Waple,[14] R. C., Schnell,[23] and R. S. Stone[23]

a. Antarctic

i) Surface climate

Annual temperature trends over the last 53 yr across the southern high latitudes are shown in Fig. 5.1. Marked seasonal and spatial differences are evident from the stations shown, with eastern Antarctica

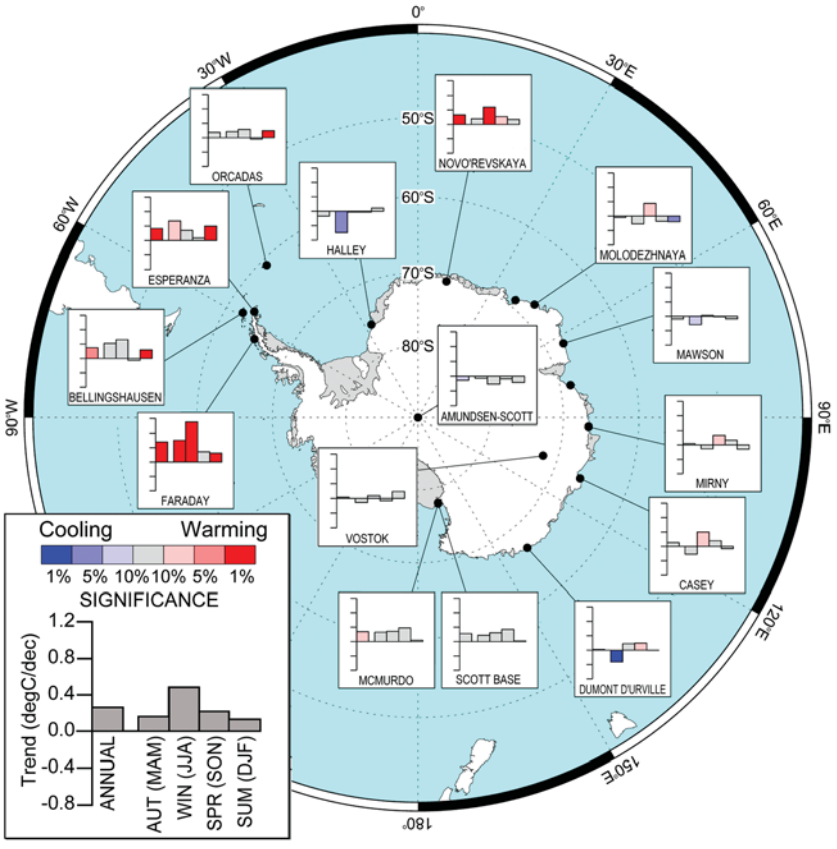

Fig. 5.1. Decadal temperature trends (in °C) for selected Antarctic stations. (Courtesy of G. Marshall, British Antarctic Survey.)

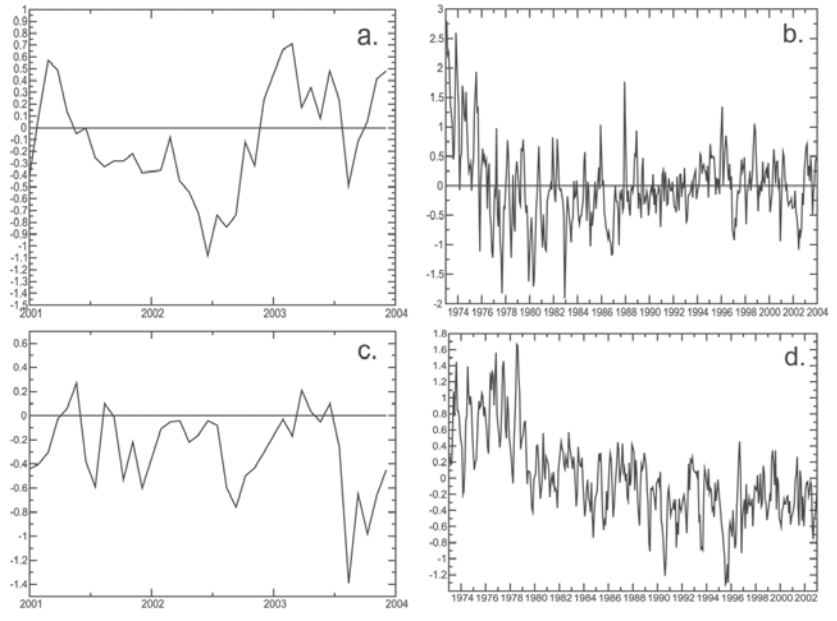

Fig. 5.2 . Monthly sea ice extent anomalies for (a) the NH for 2001–03, (b) the Northern Hemisphere from 1973 to 2003, (c) the SH for 2001–03, and (d) the SH from 1973 to 2003. Anomalies are departures from the 1973–96 base period.

having little or no significant annual temperature trend, while the Antarctic Peninsula has generally warmed over the last 50 yr. Coincident with this warming trend, ice shelves have retreated on the Antarctic Peninsula along with decreases in sea ice extent in the Bellingshausen Sea (e.g., Vaughan and Doake 1996), while sea ice concentration and length of season have increased in the Ross Sea, as well as over much of eastern Antarctica, (e.g., Stammerjohn and Smith 1997). Reliable measurements are difficult to obtain for Antarctica given the harsh conditions and transience of scientific personnel; however, from the limited data available, the last decade has been colder than average in contrast to the general increasing temperature trend from the late 1950s to the early 1990s, averaged across the continent. The June 1991 eruption of Mt. Pinatubo may have had a marked influence on Antarctic temperatures for several subsequent years (Jacka and Budd 1998), likely accounting for some of the decadal cooling. Overall, 2003 was cooler than 2002, but close to the 10-yr mean.

Decreases in sea ice, in response to warmer ocean and surface air temperatures, amplify polar climate change through ice albedo feedback effects. Sea ice extent surrounding Antarctica also regulates the production of Antarctic bottom water formation, which helps to drive global ocean circulation. According to the U.S. National Snow and Ice Data Center (NSIDC), sea ice covers approximately 17–20 million km^2 of the Southern Ocean at its maximum in late winter. The seasonal decrease is larger in the Antarctic, with only about 3–4 million km^2 remaining at

summer's end, compared with approximately 7–9 million km^2 in the Arctic. As shown in Fig. 5.2a, in 2002, sea ice extent in the Antarctic was below average for much of the year. By year's end, sea ice extent had begun to increase in comparison to the 30-yr average, and for the first 6 months of 2003, sea ice extent was above average. A brief decrease relative to the mean was observed in early to mid-winter, and then a recovery to above-average sea ice extent occurred during the remainder of 2003. Sea ice surrounding the Antarctic continent has been increasing from the late 1970s to the mid-1990s (Fig. 5.2b), but this time series belies considerable seasonal and spatial variability. The early part (1973–78) of this sea ice record is determined using different instruments and may reflect data calibration problems. For further discussion on this aspect of the record, see Folland et al. (2001a).

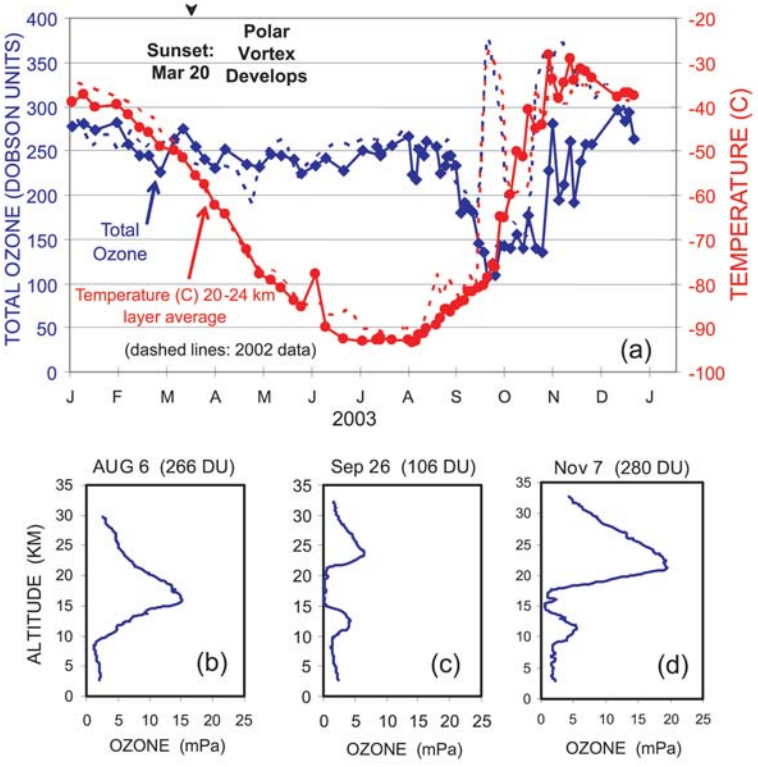

Fig. 5.3. (a) Summary of South Pole total ozone (in DU) and stratospheric temperatures (°C) measured by ozonesondes during 2003. Three selected profiles of altitude vs ozone partial pressure (mPa) are shown in the lower panels: (b) prior to the 2003 ozone hole, (c) the minimum total ozone, and (d) postozone hole. (Courtesy B. Johnson and S. Oltmans, NOAA/CMDL.)

ii) Antarctic stratospheric ozone

The NOAA/CMDL ozonesonde measurements at the South Pole for 2003 are shown in Fig. 5.3. The total column ozone (blue line) in Dobson units (DU) and temperature (red line) in the 20–24-km layer of the stratosphere illustrate the development of an average ozone hole over South Pole station. However, the extent of the ozone hole area (< 220 DU) measured

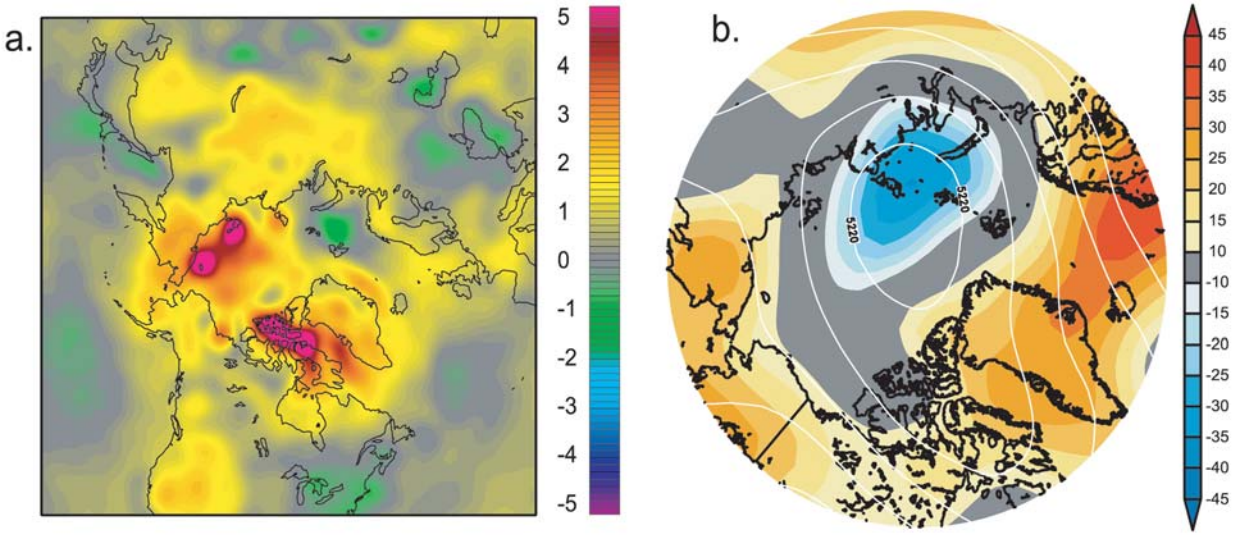

Fig. 5.4. (a) Mean annual surface air temperature anomalies (in °C) for 2003, with respect to the 1954–2003 mean (courtesy of B. Chapman); (b) mean annual 500-hPa height anomalies (m) for 2003, with respect to the 1968–96 mean.

by the National Aeronautics and Space Administration (NASA) Total Ozone Mapping Spectrometer (TOMS) instrument was near record levels at 28.2 million km^2. From June to early August, cold stratospheric temperatures and a stable winter/spring polar vortex provided favorable conditions for the formation of polar stratospheric clouds. These cloud surfaces enable the transformation of chlorine and bromine compounds into species that destroy ozone when sunlight returns to the Antarctic stratosphere.

The selected profiles from 6 August and 26 September show that ozone in the 14–21 km layer was nearly completely destroyed by the time the minimum total ozone column ozone of 106 DU was observed in mid-September. The 60% drop in total column ozone was equal to the 10-yr average loss of 60 ±6%. However, the record minimum total ozone remains at 89 DU measured at South Pole station on 6 October 1993. The ozonesonde measurements in 2002 (dashed lines in Fig. 5.3), show a large increase in stratospheric tempera-

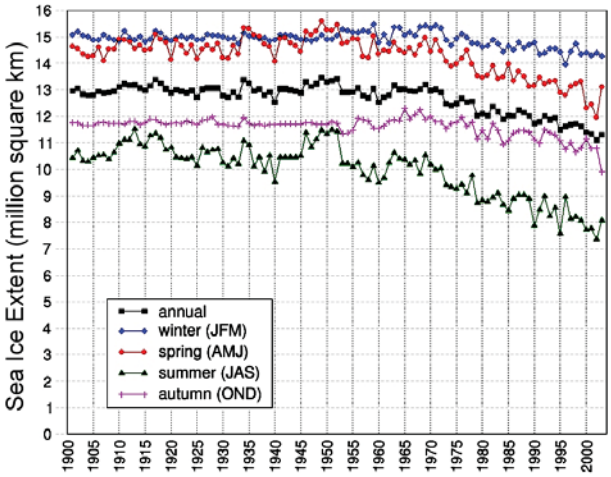

FIG. 5.5. Time series of annual and seasonal sea ice extent in the Northern Hemisphere, 1901–2003 (annual values from Vinnikov et al. 1999; seasonal values courtesy of B. Chapman, updated from Chapman and Walsh 1993).

DIMISHING SEA ICE IN THE WESTERN ARCTIC OCEAN—R. S. Stone,[23] G. Belchansky,[4] S. Drobot,[13] and D. C. Douglas[12]

Since the advent of satellite passive microwave radiometry (1978), variations in sea ice extent and concentration have been carefully monitored from space. An estimated 7.4% decrease in sea ice extent has occurred in the last 25 yr (Johannessen et al. 2004), with recent record minima (e.g., Maslanik et al. 1999; Serreze et al. 2003) accounting for much of the decline. Comparisons between the time series of Arctic sea ice melt dynamics and snowmelt dates at the NOAA–CMDL Barrow Observatory (BRW) reveal intriguing correlations.

Melt-onset dates over sea ice (Drobot and Anderson 2001) were cross correlated with the melt-date time series from BRW, and a prominent region of high correlation between snowmelt onset over sea ice and the BRW record of melt dates was approximately aligned with the climatological center of the Beaufort Sea Anticyclone (BSA). The BSA induces anticyclonic ice motion in the region, effectively forcing the Beaufort gyre. A weak gyre caused by a breakdown of the BSA diminishes transport of multiyear ice into this region (Drobot and Maslanik 2003). Similarly, the annual snow cycle at BRW varies with the position and intensity of the BSA (Stone et al. 2002, their Fig. 6). Thus, variations in the BSA appear to have far-reaching effects on the annual accumulation and subsequent melt of snow over a large region of the western Arctic.

A dramatic increase in melt season duration (Belchansky et al. 2004) was also observed within the same region of high correlation between onset of melt over the ice pack and snowmelt at BRW (Fig. 5.7). By inference, this suggests linkages between factors that modulate the annual cycle of snow on land and processes that influence melting of snow and ice in the western Arctic Ocean.

Causes of a Lengthening Sea Ice Melt Season

Belchansky et al. (2004) found that the duration of the sea ice melt season was correlated with the phase of the previous winter's Arctic Oscillation (AO) index (Thompson and Wallace 1998). Following positive AO index winters, melt onset has tended to be early, and the autumn freeze late, especially in the regional "hot spot" indicated in Fig. 5.7. Serreze et al. (2003) cautioned that while much evidence supports this view, there were notable exceptions. For example, the 2002 record minimum ice extent, which was dominated by a negative anomaly in the western Arctic, followed a winter of alternating AO indices. This anomaly was caused by abnormally warm atmospheric temperatures during spring, followed by a summer during which cyclonic surface winds exported sea ice from the region.

Spring appears to be a critical transition period in the annual cycles of snow and sea ice. A schematic of the synoptic pattern that persisted during March, April, and May of 1996, 1998, and 2002, years when melt onset was early, is shown in Fig. 5.7. During these

ture and ozone over the South Pole on 25 September, when a rare stratospheric warming event in the Southern Hemisphere forced an early breakup of the ozone hole. Therefore, with the return of near-average ozone hole conditions over the South Pole in 2003 there appears to be no immediate signs of long-term recovery, and 2002 remains an anomalous event.

b. The Arctic

i) Sea ice and temperature

Temperature over the Arctic basin for 2003 was warmer than average (Fig. 5.4a), with autumn and winter exhibiting the largest anomalies over the western half of the Arctic Ocean and moderate cool anomalies over the eastern part of the basin. This broadly coincided with the pattern of positive and negative height anomalies at the 500-hPa level in the region (Fig. 5.4b). Spring and summer were moderately warm over most of the basin. Temperature trends over the last 50 yr for the Arctic (not shown) illustrate significant warm-

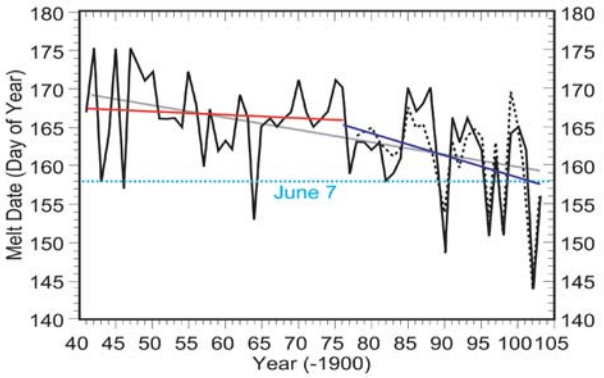

Fig. 5.6. Time series of snowmelt dates constructed for the NOAA/CMDL Barrow Observatory. Three linear regressions are plotted: an overall fit for 1941–2003 (thin black line), for all years prior to 1977 (red), and a third beginning in 1977 (blue). Results of an empirical model are also shown (dashed). The time series was compiled from direct snow depth observations, from proxy estimates using daily temperature records, and (beginning in 1986) on the basis of surface radiometric measurements (updated from Stone et al. 2002).

periods there was a complete breakdown of the BSA. The transport of warm, moist air into the Arctic was greatly enhanced by a persistent synoptic pattern that coupled a high pressure system centered over Alaska with a well-organized AL centered over the western Bering Sea. A mean back trajectory is shown in Fig. 5.7 relative to the region of long duration of sea ice melt.

Warm air advection associated with this synoptic pattern adds moisture to the Arctic atmosphere, increasing cloudiness. Prolonged effects of warm air advection (boundary layer turbulence), augmented by cloud radiative forcing can modify the microphysical structure of the overlying snow. This "ripening" may precondition the snowpack such that the melt is accelerated during May/June when solar insolation reaches its annual peak.

Significant ice melt also cannot occur until the insulating layer of snow atop the sea ice first melts. If snow accumulation on sea ice is low, and conditions favor an earlier ripening of the pack as described above, then the snow cover will melt more rapidly, advancing the onset of ice melt. Thus, reduced snowfall over the western Arctic Ocean in recent years may account, in part, for the decline in sea ice in that region.

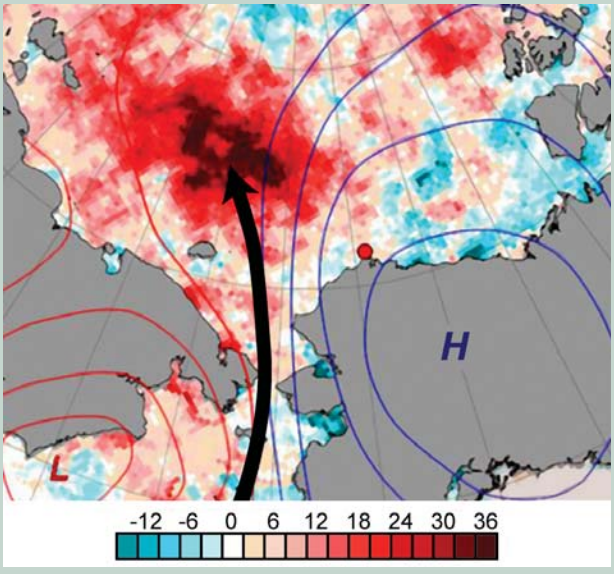

Fig. 5.7. Change in the melt season duration from 1979–88 to 1989–2001 determined from passive microwave-derived melt onset and freeze-onset dates (adapted from Belchansky et al. 2004; Fig. 6). The contours show, schematically, the composite synoptic pattern, and associated prevailing wind (arrow) at 850-hPa during March, April, and May, 1996, 1998, and 2002, preceding periods of extreme ice retreat in this region.

ing across the northern continents. However, it is unclear what trend has occurred across much of the central Arctic Ocean due to a lack of data. Much of the 50-yr trend in the land-based annual temperatures was derived from winter and spring anomalies, which, in the case of winter, exceeded 4°C in broad areas of North America and Russia.

Following the record low sea ice extent in 2002, there was modest recovery in 2003 to annual values similar to those in 2001 (Figs. 5.2b,c). Both spring and summer had large increases over 2002, but further sea ice extent decreases were evident in fall and winter, with fall having its lowest extent during the period of record (Fig. 5.5). Surface air temperature anomalies exceeded 4°C over the majority of the Arctic basin during October, and this aided in delaying freeze up across the sea surface, leading to a record-low sea ice extent for the month. The rate of refreezing remained low throughout November and December, which was reflected in the ice concentrations and extent. Sea ice extent anomalies for October also reached their lowest value for any month since the early 1970s (Fig. 5.2d). The low October sea ice was comparable only to 1995, when the large negative anomaly (over 1 million km^2) was sustained for several months, but did not quite reach the same value as for October 2003 (1.39 million km^2).

ii) Snowmelt

Snow cover for the Northern Hemisphere, including regions extending into the Arctic, is described in section 2d. However, presented here is snowmelt information for northern Alaska as well as an associated discussion of sea ice variability. Previous climate assessments (Lawrimore et al. 2001; Waple et al. 2002; Waple and Lawrimore 2003) documented an advance in the date of snow disappearance (melt date) in spring at the NOAA/CMDL Barrow Observatory (BRW). In this section, the time series of BRW melt date is updated, and the record is examined in the context of sea ice variations in the western Arctic Ocean, defined here as the region from the East Siberian Sea to the Beaufort Sea (see sidebar, p. 32).

Although 1999, 2000, and 2001 were years of moderately late snowmelt at BRW, 2002 was the earliest on record. In 2003, the melt date was again early (Fig. 5.6).

Since 1940, the spring melt at BRW has advanced by about 10 days (±4.8 days, 95% C.L.) and most of the advance has occurred since 1976. The break in the record coincided with shifts in other climatic as well as biological indicators of change (Hare and Mantua 2000). The observed variations in the annual snow cycle of northern Alaska are largely attributable to changes in atmospheric circulation related to intensification of the Aleutian low (AL), in conjunction with fluctuations of the Beaufort Sea anticyclone (BSA). On this basis, an empirical model was developed to predict melt dates at BRW (Fig. 5.6, dashed curve). About 80% of the variance in melt dates at BRW are explained by changes in snowfall during winter, and variations in spring temperatures and cloudiness (Stone et al. 2002).

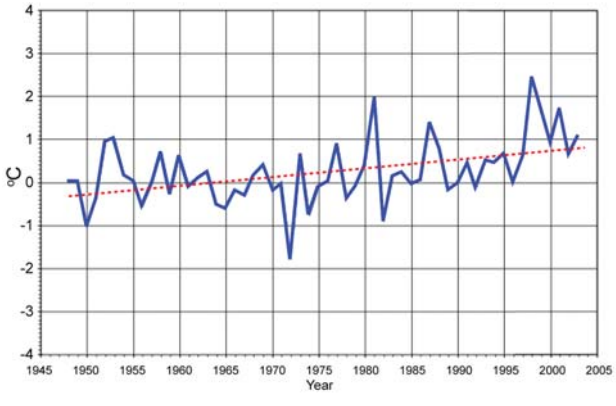

Fig. 6.1. Canadian nationwide annual temperature departures (blue line) and long-term trend (red line) for the period 1948–2003. Anomalies (in °C) were determined with respect to the 1951–80 base period. (Courtesy of the Meteorological Service of Canada, Environment Canada.)

6. REGIONAL CLIMATE

a. North America

i) Canada—D. H. Levinson[14] and D. Phillips[20]

(i) Temperature

The majority of Canadian provinces and territories experienced above-normal temperatures in 2003, and the country as a whole had an annual mean temperature anomaly of 1.1°C above normal for the year (with the respect to the 1951–80 mean). Nationally averaged temperatures have been at or above normal for the last 11 consecutive years, and 2003 ranked as the sixth warmest since nationwide records began in 1948. Canadian temperatures have shown pronounced variability over the 56-yr record of countrywide measurements (Fig. 6.1), but overall there has been a long-term surface warming trend of +1.1°C. The highest annual nationwide temperature anomaly of +2.5°C occurred in 1998, which was by far the warmest year over the period of record. Of the last 6 yr (1998–2003), 5 have been in the top 10 warmest, with the only exception being 2002. On a seasonal basis, the summer of 2003 was the fourth warmest, and the 11th consecutive warmer-than-average summer. In fact, all four seasons had above-normal temperatures in 2003, with warmer-than-average conditions in 25 of the last 26 seasons.

Regionally, all but 1 of 11 climate regions had annual temperatures that were above normal in 2003. Five regions had annual mean temperatures that ranked 2003 among the 10 warmest years on record, and they were the Arctic mountains and fjords (+2.0°C, second warmest), Arctic Tundra (+1.8°C, fifth warmest), southern British Columbia mountains (+1.1°C, seventh warmest), Mackenzie district (+1.4°C, eighth warmest), and Pacific coast (0.9°C, ninth warmest). These rankings illustrate the exceptionally warm conditions experienced across the Canadian Arctic during 2003. Figure 6.2 shows the spatial pattern of observed temperature anomalies in 2003 across Canada. High-latitude areas had by far the largest temperature anomalies for the year. Most of Nunavut, the Northwest Territories, and the Yukon were at least 1.1°C above normal, with some areas exceeding 2.5°C above the long-term annual mean (see section 5b for further discussion of 2003 Arctic temperatures). Western Canada also had above-normal mean temperatures in 2003, with the largest positive temperature departures in the Okanagan River valley in British Columbia.

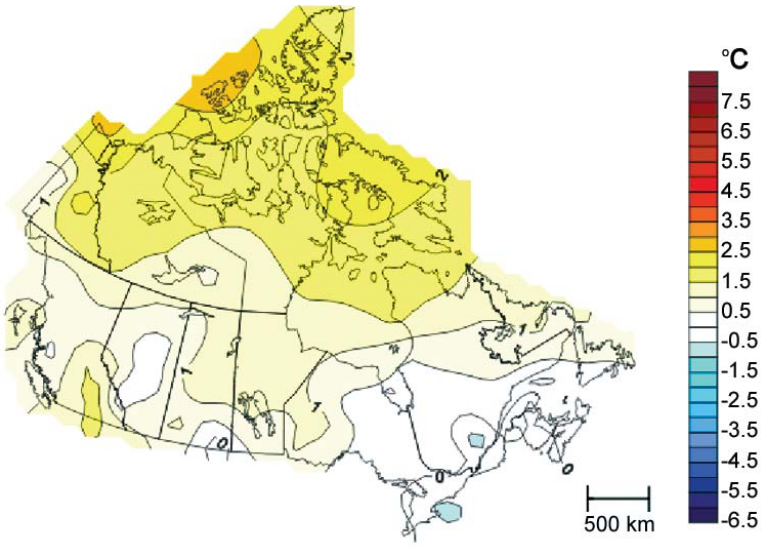

Fig. 6.2. Annual temperature departures (in °C) across Canada in 2003, with respect to the 1951–80 base period.

In contrast, eastern Ontario, southern Quebec, and the Maritime Provinces all had near-normal temperatures for the year, with negative temperature anomalies in the Saint Lawrence River valley of southern Quebec, and a small region in southeast Ontario along the Great Lakes. Overall, the winter of 2002–03 was one of the coldest winters across eastern parts of Canada in 20 yr. The coldest conditions occurred in early March, when an Arctic air mass brought record-low temperatures across most of Canada. The below-normal temperatures produced the most extensive ice conditions since the mid-1990s on the Great Lakes–Saint Lawrence waterways and along the East Coast. In March, the Great Lakes had their greatest ice cover extent since 1996, with the surfaces of Lakes Superior, Erie, and Huron 98% covered at their peak, and in the Gulf of Saint Lawrence the ice extent was 50% above normal.

(ii) Precipitation

Canadian nationwide precipitation was 1.8% above average in 2003 (based on preliminary data, with the respect to the 1951–80 mean), which made it the second consecutive year with wetter-than-normal conditions. Precipitation has been above average in Canada since about 1970, with the wettest year on record in 1996 (+9.1%) and the driest year in 1956 (–7.3%).

The Canadian Arctic was the most anomalously wet region in 2003, which continued a trend of wetter-than-normal conditions across the region for most of the past 3 decades. In 2003, the Arctic tundra region had the largest positive precipitation anomaly (+19.9%, fourth wettest) of any Canadian region (Fig. 6.3), and this region has not had a drier-than-normal year in the last 25 yr.

In contrast to the Arctic, drier-than-normal conditions continued in 2003 in the western provinces, with parts of the Canadian prairies having experienced their fourth year of drought conditions. Annually averaged precipitation was below normal from the coast of British Columbia through the Prairie Provinces (–21%, third driest), with dry conditions extending eastward across northern Ontario to parts of Newfoundland and Labrador. The dry conditions contributed to one of Canada's worst fire seasons in the last 50 yr in the western provinces.

(iii) Significant events–Hurricanes and wildfires

Numerous notable weather events occurred across Canada in 2003, and these included four tropical storms and hurricanes that passed near or made landfall along the Atlantic coast (i.e., Fabian, Isabel, Juan, and Kate; see section 4bi for a thorough discussion of the Atlantic hurricane season). By far the most destructive of these tropical cyclones was hurricane Juan, which struck Halifax, Nova Scotia, on 29–30 September. Juan formed southeast of Bermuda, intensified as it moved directly northward, and made landfall at Halifax as a

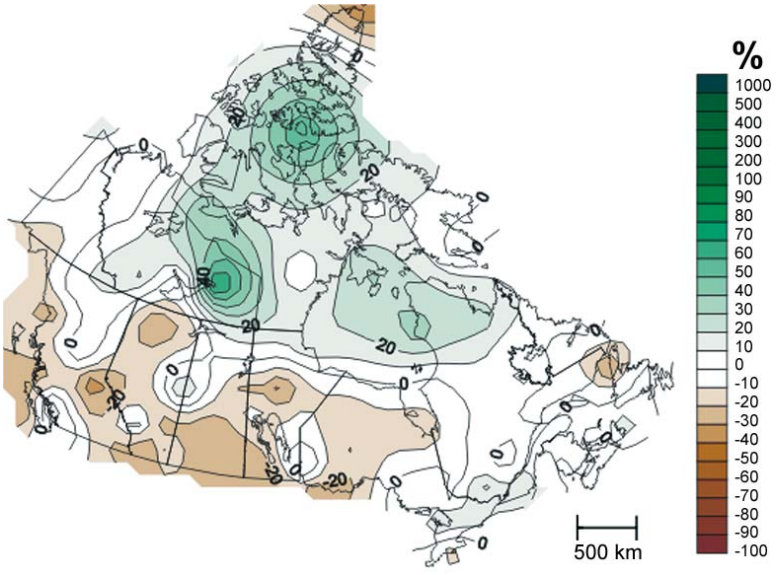

FIG. 6.3. Annual precipitation departures (in %) across Canada in 2003, with respect to the 1951–80 base period.

category 2 hurricane with sustained winds of 158 km h^{-1} and gusts of 185 km h^{-1}. The strong winds generated a storm surge of 1.5 m, and raised the water level of Halifax harbor to a record 2.9 m. The storm weakened as it moved over Nova Scotia, and eventually passed over Prince Edward Island as a marginal category 1 hurricane. Juan was only the fourth category 2 hurricane to strike Nova Scotia since the early 1800s, and only the second hurricane to hit Prince Edward Island since 1930. At its peak, Juan left more than 300,000 homes without power across the two provinces.

Overall, it was a near-average fire year in Canada in terms of number of fires (8226 by the end of November 2003), but only half the total number of hectares consumed (1.6 million ha) when compared to the 10-yr average. While these nationwide statistics imply an "average" year, the severity and extent of the damage from the 2003 fire season made it one of Canada's worst. The most destructive fires occurred in British Columbia in August and September, which experienced its worst fire season as well as the most expensive natural disaster in the province's history. In total, 2500 wildfires burned 2650 mi^2 (6863 km^2 or 686,347 ha) of forests, rangeland, and residential areas across British Columbia, which is 11 times the annual average area burned in the province over the last 10 yr (source: Canadian International Forest Fire Centre). Over the course of the season, more than 50,000 residents of British Columbia were evacuated due to fires and related smoke in 2003, which was the second largest evacuation in Canadian history.

Approximately 1 month after the fires had abated, a week-long autumn rain event in mid-October generated extensive flooding across British Columbia, because the dry rivers and creeks filled quickly with runoff and sediment from the burned areas. The Meteorological Service of Canada estimated that the intense multiday downpour was likely the largest deluge to strike the West Coast of Canada in more than 200 yr.

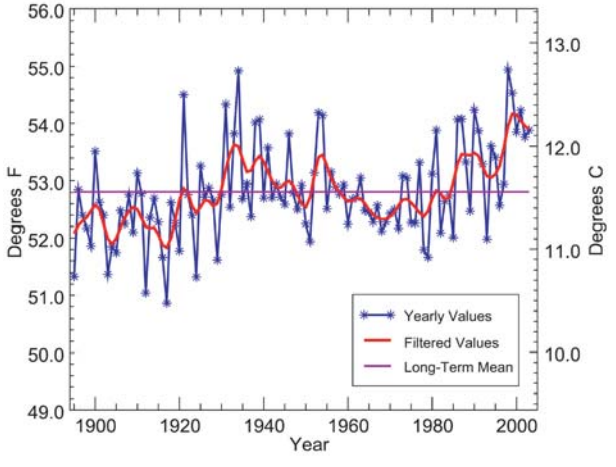

FIG. 6.4. Annual temperature averaged across the contiguous United States from 1895 through 2003. (Data courtesy of the U.S. Historical Climate Network; Karl et al. 1990.)

ii) United States of America—K. L. Gleason,[14] A. M. Waple,[14] T. Eichler,[5] and G. D. Bell[5]

(i) Overview

Reliable monthly, seasonal, and annual weather records for the United States exist from 1895 to the present, enabling the climate of 2003 to be placed in a 109-yr context for the contiguous United States. Annual temperatures in 2003 ranked 14th warmest in the last 109 yr with a nationally averaged temperature of 12.2°C (0.7°C above the 1895–2002 mean). The linear temperature trend averaged across the contiguous United States was 0.1°F $decade^{-1}$ since 1895, with an increase to 0.6°F $decade^{-1}$ since 1976. The last five 5-yr periods (1999–2003, 1998–2002, 1997–2001, 1996–2000, 1995–99) were the warmest five-year periods in the last 109 yr of national records, with the most recent 6- (1998–2003), 7- (1997–2003), 8- (1996–2003), 9- (1995–2003), and 10-yr (1994–2003) periods also the warmest on record for the United States, which illustrates the anomalous warmth of the last decade (Fig. 6.4). Warm

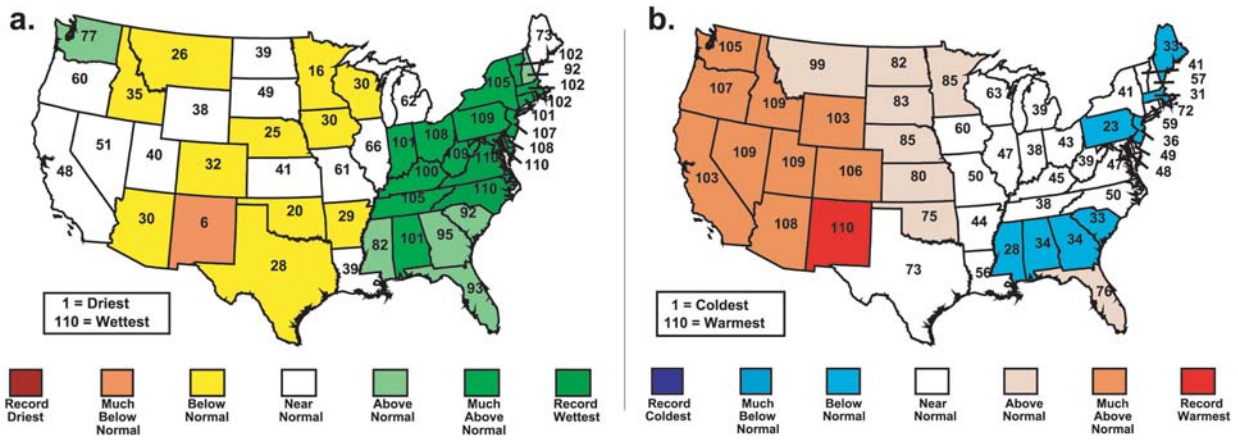

FIG. 6.5. Statewide ranks for (a) temperature and (b) precipitation across the contiguous United States for 2003. A rank of 109 represents the warmest or wettest year since 1895. Much above-normal temperature or precipitation is defined as occurring in the top 10th percentile of the distribution and likewise for a designation of much below average. An above-normal designation for temperature or precipitation is defined as occurring in the warmest or wettest third of the distribution, respectively.

anomalies were not uniformly distributed across the nation. The western half of the United States was persistently warmer than average (Fig. 6.5a) with moderate dry anomalies (Fig. 6.5b) increasing long-term (4–5 yr) western drought extent and severity in some areas. Cooler-than-average temperatures were recorded along the eastern seaboard, with much of the East also experiencing wetter-than-average conditions for the year; three mid-Atlantic states had their wettest calendar year on record.

(ii) Precipitation and temperature

Precipitation across the United States in 2003 was characterized by moderate yet persistent deficits in the West and above average to record wet anomalies in the East (Fig. 6.5a). Averaged across the contiguous United States, precipitation was near the long-term average (1895–2003) of 739 mm at 760 mm. The previous 4 yr had below-average precipitation for the nation, in large part due to a persistent La Niña (1998–2001). As a weak to moderate El Niño developed in 2002, the southeastern United States began to receive more rainfall. Several landfalling hurricanes in September and October 2002 also helped to break the 4-yr drought for much of the Southeast. Apart from January 2003, the remainder of the year was mostly wet for much of the eastern seaboard with Virginia (exceeding the previous annual record by the end of November), North Carolina, and Maryland all breaking their annual precipitation record. September rainfall along the East Coast was also enhanced by the landfall of Hurricane Isabel midmonth along North Carolina's Outer Banks. Heavy rain fell from the North

U.S. TORNADO RECORDS—A. M. Waple[14]

May 2003 had a total of 546 tornadoes, the most reported in any month for the United States, exceeding the previous *month/year* record by 145 tornadoes. Two outbreaks of severe weather, on 3–5 May and on 10–11 May, led to 25 F3–F5 tornadoes (on the Fujita scale*) for the month. A total of 35 F3–F5 tornadoes occurred in 2003, which was near average over the 50 yr of reliable tornado records. A slight negative trend in tornado activity is evident from Fig. 6.6.

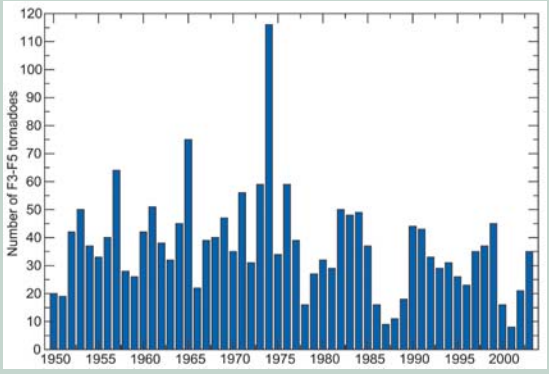

FIG. 6.6. The number of F3–F5 tornadoes between March and August for the contiguous United States from 1950 through 2003.

* The Fujita scale classifies tornadoes based on wind strength, estimated by associated damage (Fujita 1971). The F scale gives each tornado a numerical rating from F0 (weak) to F5 (violent).

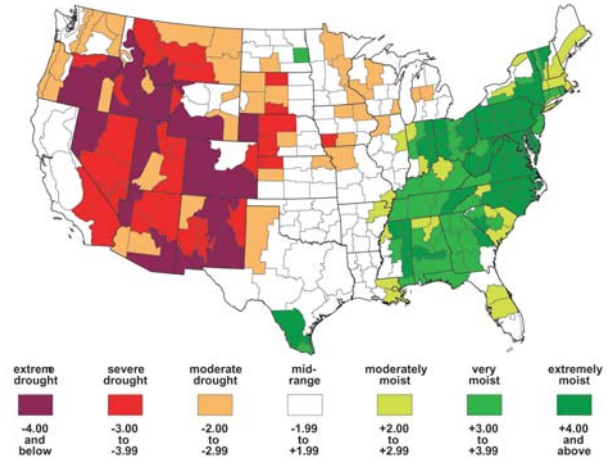

Fig. 6.7. PHDI for Oct 2003, illustrating the maximum drought extent in the West in 2003. The PHDI describes long-term drought conditions (Heim 2002).

Carolina coast northward through Virginia and into West Virginia and Pennsylvania (see Fig. 4.8). Storm-total precipitation exceeding 150 mm was measured in northwestern Virginia. Inland flooding was exacerbated by several months of very wet conditions

The wet conditions in the East coincided with cooler-than-average temperatures, especially in the summer, while record or near-record temperatures were recorded in the West. Significantly above-average heat dominated the weather west of the Rocky Mountains during the summer months (June–August) with both Idaho and Utah having their warmest summer on record, averaged statewide. July was extremely warm in the West, with Idaho, Wyoming, Utah, Colorado, Arizona, and New Mexico each reporting their warmest July in the past 109 yr. Idaho and Wyoming also broke records the following month with their warmest August on record for each state.

Drought continued to be a concern for the United States in 2003. At the beginning of the year, approximately one-third of the contiguous nation was in moderate to extreme drought, [as defined by the Palmer Hydrological Drought Index (PDSI)]. Although improvements were evident in summer months, largely due to beneficial rains in the Plains and Great Lakes, drought extent again increased in the fall, with 42% of the 48 contiguous states in drought in October (Fig. 6.7). At the peak of the 2003 drought in late September/early October, approximately 80% of the western United States, from the Rockies to the Pacific coast, was affected by moderate to extreme drought. This rivals the greatest drought extents of the twentieth century in the West. By the end of 2003, nearly 70% of the western United States remained in moderate to extreme drought.

The prolonged cool/wet conditions in the eastern United States and warmth in the West were related to several persistent circulation features, including an anomalous flow of marine air into the western United States, an enhanced subtropical jet stream, and increased storminess across the South and East. The persistence of these circulation features was linked to three distinct circulation regimes. During October 2002–January 2003, they were linked to a combination of El Niño and the negative phase of the Arctic Oscillation (AO). During April–June they were associated with anomalously zonal flow across the country, combined with major Appalachian cold-air damming events in the East during April–May, and a series of major cold frontal passages in the East during June.

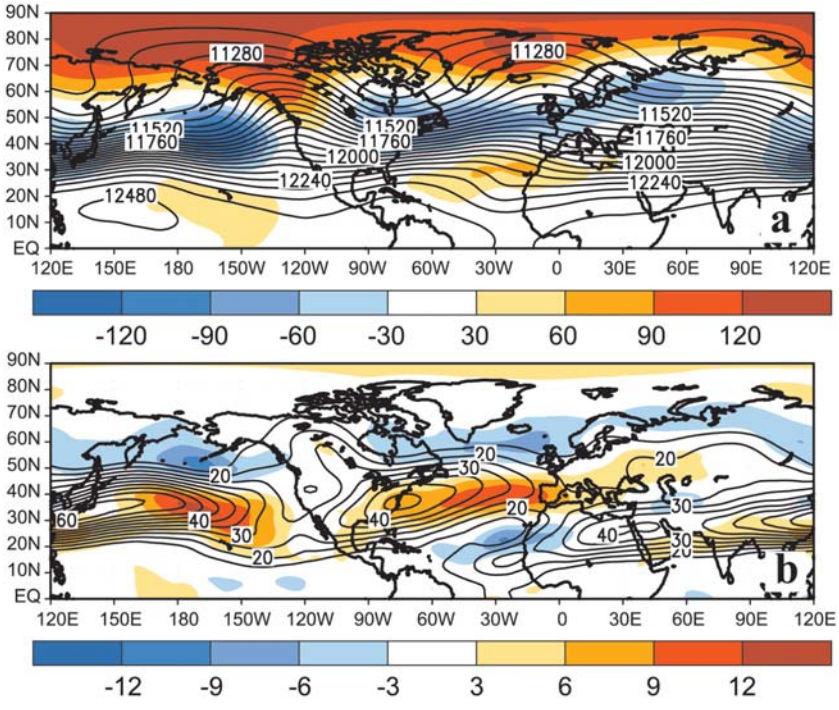

Fig. 6.8. 200-hPa: Oct 2002–Jan 2003 (a) heights and anomalies (m) and (b) wind speeds and anomalies (m s^{-1}). Anomalies (shading) are departures from the 1971–2000 base period monthly means

FIRE HISTORY FROM PALEOENVIRONMENTAL DATA—C. Woodhouse[14]

The frequency and spatial extent of wildfires during the twentieth century in the southwestern United States reflect recent land management practices, including grazing and fire suppression. Both cause a lower incidence of fire, but have also caused an accumulation of biomass, which has lead to catastrophic wildfires. Before such management practices were employed, fires in the southwestern United States were frequent, but were of a low intensity and low severity. These fires often scarred trees without killing them, leaving a record of past fire events contained in the sequence of scars at the base of the tree. By examining and dating scars in numerous trees from ponderosa pine, Douglas fir and pinyon forests throughout Arizona and New Mexico, scientists have been able to reconstruct the amount of area burned and learn more about the spatial and temporal patterns of past fire regimes.

The fire-scar record for the southwestern United States, compiled from several dozen sites across this region, and validated with historical documents, was found to closely correspond to the temporal pattern of ENSO (Swetnam and Betancourt 1990). Greater area burned coincides with La Niña years, which are typically very dry in the American Southwest, while a smaller area burned corresponds to El Niño years, which tend to be wetter. These findings indicate that seasonal climate is a key control on fire at this regional scale. When the fire-scar record is extended back in time, it provides a history of fire occurrence going back three or more centuries. A reconstructed Niño-3 index (Cook 2000) was compared with this record to show that the same relationships between areas burned and El Niño and La Niña events are consistent throughout the full record, and that relationships between fire and climate in the paleoenvironmental records have persisted into the twentieth century (Westerling and Swetnam 2003) (Fig. 6.9, bottom).

It has also been shown that the area burned in the United States can be approximated using a network of tree-ring-reconstructed PDSI grid points (Cook et al. 1999; Westerling and Swetnam 2003). An analysis of the reconstructed area burned indicates an inverse relationship between fire in the northwestern and southwestern United States over the past 300 yr, reflecting the regional ENSO pattern. In general, El Niño years are wet in the Southwest and dry in the Northwest, and vice versa for La Niña (Fig. 6.9). Because of this apparent relationship, and the current forecast skill for ENSO, this information is being used in fire management. In 2003, weak El Niño conditions existed, along with widespread warm and dry conditions across large areas of the western United States. As a result, fire occurred in both the southwestern and northwestern United States, but with near- to below-average acreage burned in both regions (source: National Interagency Fire Center, available online at www.nifc.gov).

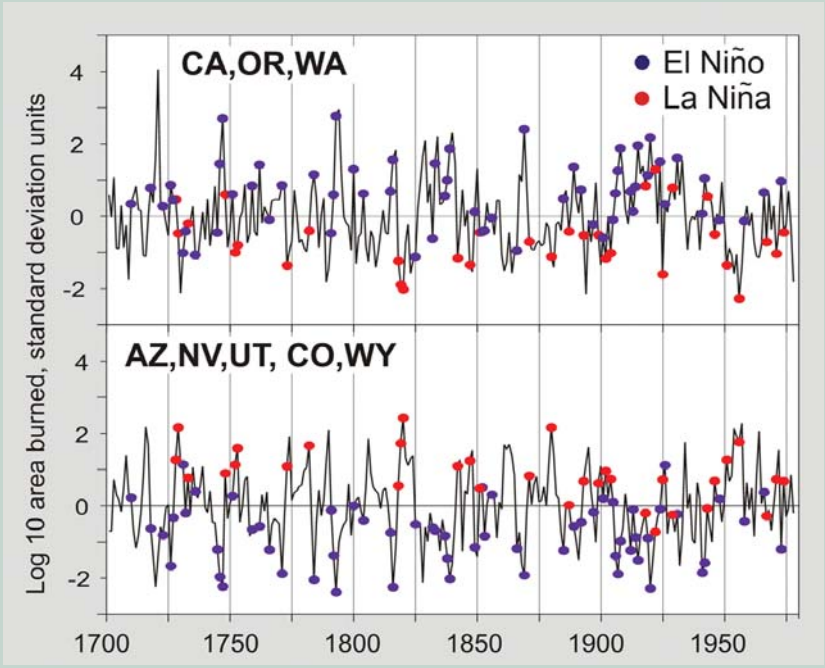

FIG. 6.9. Reconstructions of area burned (shown as the standard deviation of log-10 units) for (top) the northwestern United States (California, Oregon, and Washington), and (bottom)the southwestern United States (Arizona, Nevada, Utah, Colorado, and Wyoming), 1701–1978. El Niño (blue dots) and La Niña (red dots) events from the Cook (2000) Niño-3 index reconstructions are indicated. In general, area burned in the Northwest has been inversely related to area burned in the Southwest. In the northwestern United States, a smaller area burned was associated with La Niña events while a larger area burned was associated with El Niño events. The reverse relationship has been true for the southwestern United States.

During October 2002–January 2003 the upper-level height anomalies exhibited a pronounced zonal symmetry, with positive anomalies over the polar region and at lower latitudes, and negative anomalies in middle latitudes (Fig. 6.8a). These conditions were associated with 1) an eastward extension of the East Asian jet stream (Fig. 6.8b), 2) an enhanced subtropical jet stream across the southern United States, 3) an amplified ridge–trough pattern over North America with anomalous northerly geostrophic flow across the north-central and northeastern United States, and 4) an enhanced North Atlantic jet stream, which was shifted south of its normal position. This combination of conditions contributed to an anomalous flow of mild marine air into the western United States, to an enhanced storm track across the southern United States, and to anomalously cold and wet conditions (including a snowy 2002–03 winter) in the East.

The positive phase of the Pacific North American (PNA) pattern seen during October 2002–January 2003 was also consistent with the weak-to-moderate El Niño conditions (see section 4a) (Horel and Wallace 1981). Therefore, this combination of El Niño and the negative phase of the Arctic Oscillation (AO) is considered a dominant contributing factor to the anomalous temperature and precipitation patterns across the United States during the period. This association of leading modes highlights an important way in which the extratropical climate variability modulates the ENSO teleconnections across North America. For example, El Niño events favor above-average winter temperatures across Canada and below-average temperatures over the southeastern United States (Ropelewski and Halpert 1987). However, this temperature pattern can be modified substantially depending on the phase of the North Atlantic Oscillation (NAO), with the negative phase of the NAO leading to anomalously cold conditions across the southeastern and mid-Atlantic states, and the positive NAO leading to anomalous warmth across the eastern half of the United States (Hurrell 1995).

During April–June 2003, the East Asian jet stream extended southeastward into the base of the mean upper-level trough upstream of California, and an enhanced subtropical jet stream again extended across the southern United States. This circulation pattern again resulted in an enhanced flow of mild air into the western United States, and an enhanced low-latitude storm track across the southern United States. Several of these storms subsequently redeveloped along the East Coast, leading to above-average precipitation across the Southeast and East.

The anomalously cold and wet conditions across the eastern United States during April–May 2003 were also related to an increased frequency of Appalachian cold-air-damming events. Cold-air-damming episodes are often associated with East Coast cyclogenesis events, and can influence the precipitation distribution associated with East Coast storms (Forbes et al. 1987). Cold-air damming was observed on 10 days during both April and May 2003, approximately twice the climatological average (Bell and Bosart 1988; Bailey et al. 2003), and accounted for the main cold-air outbreaks in the mid-Atlantic region during both months.

(iii) Snow

The eastern seaboard had an active 2002–03 snow season beginning in November 2002. Albany, New York, received over 30 cm of snow in November 2002, followed by 53 cm in December. Snowfall totals of 30–60 cm fell across much of central New York and northeast Pennsylvania, and into parts of New England on 2–4 January. Significant snow accumulations occurred over parts of the Southeast in late January when 10–30 cm of snow fell across parts of North Carolina, including the Outer Banks where snow is uncommon. The "President's Day Snowstorm" in mid-February had some of the largest snow accumulations along the mid-Atlantic to New England coasts since the Blizzard of 1996 (Halpert and Bell 1997). As a result of this and other snow events throughout the month of February, several cities along the East Coast set new monthly snowfall records including: Pittsburgh, Pennsylvania, Baltimore, Maryland, Wilmington, Delaware, and Clarksburg, West Virginia. In mid-March, a large winter storm impacted Colorado's Front Range. Snowfall was heaviest just west of Denver where up to 220 cm of snow was reported. Denver received 80 cm over the 17–19 March period. This was the second biggest snowstorm on record for Denver, and the city reported its snowiest March on record. Other cities with significant storm totals were Boulder, Colorado, with 130 cm, Fort Collins, Colorado, with up to 78 cm and Cheyenne, Wyoming, with over 45 cm. Despite the significant snowfall in March, season-to-date snowfall totals in this region were only near or below normal. Nevertheless, this event did help alleviate short-term water supply concerns, which were the result of ongoing drought across the region.

(iv) Wildfires

There were three main centers of action with respect to wildfire activity in 2003: the Southwest, especially New Mexico and Arizona in May–July, the northern Rockies in July–September and southern California in October. For the season, over 1.5 million ha burned in 2003, which is about 80% of the 10-yr national average.

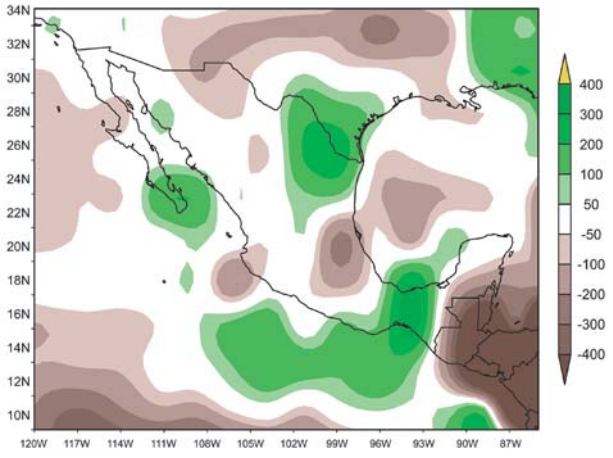

FIG. 6.10. Annual mean precipitation anomalies (mm) over Mexico in 2003. Data are from the CAMS–OPI analysis, with anomalies determined from the 1961–90 base period. (Courtesy of NOAA/CPC.)

The western U.S. wildfire season began later in the year than average as a result of a wet February–April period. By the end of May, a heat wave accompanied by dry conditions affected much of the western United States, which resulted in an increase in fire activity in the Southwest. Persistent hot and dry conditions fueled fires, which continued well into July. Fire danger indices escalated in early July as a result of a persistent ridge of high pressure situated over the western United States. By late July, a series of lightning storms led to an increase in fire activity throughout the Northwest, the eastern Great Basin, and the northern Rockies, including parts of Glacier National Park. Over 280,000 ha were consumed in the northern Rockies wildfire season and wildfire consumption was reported to be about 80% of the 10-yr average at this time.

Large wildfires broke out in southern California in late October as a result of persistent warm and dry conditions, large amounts of available fuel in the form of dead and dormant vegetation, and strong Santa Ana winds. Over 300,000 ha were consumed by 15 large fires during October. Higher humidity, cooler temperatures, and rainfall in early November helped firefighters contain these blazes. The most destructive of these fires, the Cedar Fire in San Diego County, destroyed over 100,000 ha and was the largest fire in California since 1932.

iii) Mexico—D. H. Levinson,[14] M. Cortez Vázquez,[10] and A. Douglas[11]

For 2003, precipitation totals over Mexico were near normal, although significant rainfall anomalies occurred across the country. During the first 5 months of the year, the accumulated rainfall across Mexico as a whole was below normal, with the national weighted precipitation total at 76% of average during the January–May period. In contrast, the latter half of the year was wetter than normal, with the largest positive rainfall anomalies during autumn (September–November). Figure 6.10 shows the annual precipitation anomalies across Mexico from the CAMS–OPI dataset (Janowiak and Xie 1999). The national area-weighted mean precipitation for Mexico in 2003 was 796 mm, which was 103% of the long-term mean of 772 mm. Overall, it was a year of wet and dry contrasts, with significant wet anomalies over the isthmus of Tehuantepec and the northeastern states, as well as in the southern Baja Peninsula, and dry anomalies over central Mexico and the northern Baja Peninsula.

The rainy season, which normally extends from the end of May to mid-October, began with drier than normal conditions during May across approximately 60% of the country. During the June through August period, monthly totals were normal to slightly below normal, with the driest conditions concentrated in the states of Chihuahua and Sinaloa (Fig. 6.11). Heavy precipitation events in September and October across northwestern, northeastern, and central Mexico led a recovery from deficits experienced during the first half of the summer wet season. Several of these heavy rainfall events produced flooding over central Mexico (i.e., Guanajuato, Queretaro, and Hidalgo states). Coun-

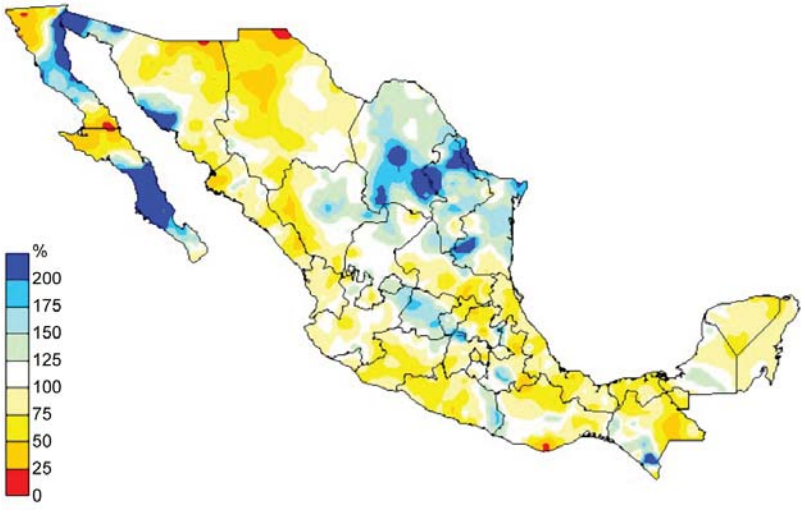

FIG. 6.11. May–Oct 2003 precipitation anomalies (mm) for Mexico, with respect to the 1941–2002 base period. (Courtesy of Servicio Meteorologico Nacionale-SMN Mexico.)

trywide, for the entire summer rainy season (May–October), precipitation averaged 110% of normal, and September and October were 122% and 147% of normal, respectively (Fig. 6.11). The broadest area of below normal precipitation was centered in the large northern Mexican state of Chihuahua, where a significant long-term (> 2 years) moisture deficit continued in 2003.

The heavy rainfall events that occurred during the latter part of the rainy season were related to the influence of tropical storms, and an active period of tropical easterly waves. During the 2003 season, eight tropical cyclones made landfall in Mexico on the Pacific and Atlantic coasts, combined. For the period 1970–2003, this was second only to 1971 when nine TCs made landfall in Mexico. The northeastern Pacific region was particularly active for tropical cyclone impacts, because five TCs made landfall in Mexico. Above-normal rainfall in northeast Mexico was associated with two Gulf of Mexico tropical cyclones that moved westward in July and August (Claudette and Erika) and eastern north Pacific tropical storms that recurved to the northeast in October (Nora and Olaf). In Baja, California, and western Sonora, heavy precipitation was associated with two hurricanes that moved northward through the Gulf of California in August and September (Ignacio and Marty), and two systems that crossed the mouth of the Gulf of California in October (Nora and Olaf). For the season, seven tropical cyclones crossed into northern and western Mexico from July through early October, and rainfall from these systems helped reverse the drought pattern across northern Mexico (see section 4b for a summary of the Atlantic and eastern North Pacific tropical cyclone seasons). During the 5-month rainy season (June–October), the national precipitation index for Mexico averaged 112% of normal, but the majority of this surplus was attributed to tropical cyclone rainfall rather than the normal, more widespread monsoon rainfall.

November–December 2003 were characterized by a return to drier conditions and below-normal precipitation across most of the country. In addition to the dry conditions late in the year, a severe cold outbreak occurred across northwest Mexico at the end of December. This cold snap began with the arrival of an extremely cold and dry air mass from the north on the 27 December. By the next morning, temperatures plunged to –11.7°C in Yecora, Sonora, and –11.4°C in Nuevo Casas Grandes, Chihuahua. On 29 December, Guachochi, Chihuahua, reported a low of –14.7°C, and Basaseachi, Chihuahua, reported a low of –16.1°C. These record-low temperatures were accompanied by dewpoint temperatures of –23°C across the interior northwest, which illustrates the extremely dry air mass during the event.

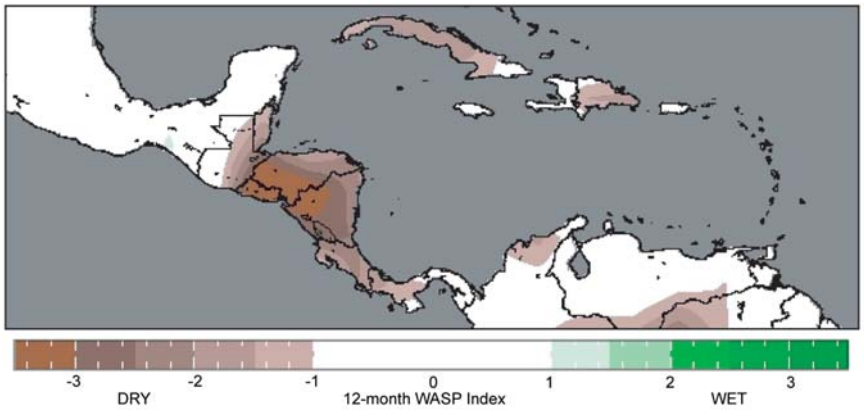

Fig. 6.12. Average of standardized monthly precipitation anomalies for 2003. Data are from the CAMS–OPI analysis for 2003 (courtesy of NOAA/CPC), with anomalies determined from the 1961–90 base period. Note that the "weighted anomaly standardized precipitation" (WASP) index is based soley on monthly precipitation data. The index is computed using monthly precipitation departures from the long-term average, which is standardized by dividing by the standard deviation of monthly precipitation. The standardized monthly anomalies are then weighted by multiplying by the fraction of the average annual precipitation for the given month. These weighted anomalies are then summed over varying time periods—here, 3, 6, 9 and 12 months. On the above plots, the value of the given WASP index has itself been standardized.

b. Central America—E. K. Grover-Kopec[6]

Much of Central America and the Caribbean continued to be relatively dry in 2003, extending the overall dry conditions seen in the region during the past few years (Fig. 6.12). The drought, which settled into the region in 2001 and 2002, was a major contributor to food shortages and malnutrition, especially in rural areas. The vast majority of the region recorded below-normal annual precipitation totals, with those in El Salvador, southern Honduras, and northwestern Nicaragua being the most anomalous relative to the 1961–90 base period (Fig. 6.12). However, the largest absolute precipitation deficits were observed in northeastern Nicaragua and

eastern Honduras, which are typically among the wettest regions in Central America. These areas reported annual precipitation totals that were approximately 1500 mm, or 60% below normal.

Central America generally has a bimodal distribution of precipitation, with relative maxima in May–June and September–October. The largest monthly deficit on the isthmus emerged during this second climatological peak, because the September anomaly accounted for nearly 25% of the annual deficit across the region. Deficits during the wettest part of the year (i.e., June–September) contributed approximately 72% of the annual departure. Because this region typically receives such abundant rainfall, heavy rain events often occur even when monthly and annual precipitation totals are below normal. In May, over 60,000 people were affected by heavy rains and flooding in Costa Rica and Panama as the rainy season first arrived, while drought conditions continued to grip the remainder of the region.

Lingering tropical systems brought heavy rainfall and, consequently, landslides and flooding to El Salvador in October, while heavy rains returned to Costa Rica and Panama in late November and early December. According to the Costa Rica National Meteorological Institute, an entire month's worth of rain (~200 mm) fell in a single day across the southern provinces of the country. Some areas in Honduras also received a break from the dry conditions as heavy rains fell along the northern coast in December. Precipitation totals for December were nearly twice their climatological average in the Honduran departments of Atlantida and Yoro.

The Caribbean region also experienced a mixed rainy season, with heavy precipitation occurring amid overall dry conditions. Northwest Haiti, which has suffered under recurrent drought in recent years, had above-normal spring rainfall, and heavy rains brought flooding to the northeastern part of the country. Heavy rains and flooding inundated the Dominican Republic in late November and early December as well. The floodwaters forced over 47,000 people out of their homes and swamped 200,000 ha of agricultural land at a time when planting for the next harvest would have typically been underway.

Surface temperatures were above average across Central America and the Caribbean during 2003 (not shown). Annual average temperatures were 1.0°–1.5°C above normal in western Honduras, eastern Cuba, and southern Guatemala. Higher-than-average temperatures, which coincided with rainfall in January, contributed to a 30% increase in dengue fever cases in Guatemala, compared with January 2002 (source: Guatemala Ministry of Health; courtesy of the International Society of Infectious Diseases).

c. *South America*—E. K. Grover-Kopec[6]

South America experienced a variety of wet and dry extremes during 2003. Abnormally dry conditions were prevalent across the northeastern half of the continent, with the exception of extreme northeastern Brazil, as well as in southern Chile and western Argentina. Southeastern South America—Peru, Ecuador, northern Argentina and Chile—were among the regions with above-normal annual precipitation totals in 2003.

The South American continent generally receives its largest amounts of precipitation across the Amazon River basin with a secondary maximum stretching to the southeast. The dry conditions of 2003 were most extreme across an area from southeastern to northwestern Brazil and southeastern Columbia (Fig. 6.13). Northwest and extreme southern Brazil generally receive precipitation throughout the year, although most rainfall typically occurs between March and July. In 2003, the below-normal annual precipitation totals were due to precipitation deficits that occurred throughout the year. In contrast, southeastern and central Brazil have a more confined climatological rainy season that generally extends from October to April. The relatively poor start to the 2003–04 rainy season (i.e., OND 2003) accounted for 59% of the annual deficits of 300–700 mm in this region. The exception to these dry conditions came in January, when the South Atlantic convergence zone typically has a strong influence on southeastern Brazil, and heavy rainfall brought flooding and landslides to the region. The states of Rio de Janeiro, Sao Paulo, Espirito Santo, and Minas Gerais, in particular, were most affected.

The relatively wet conditions in northwestern and southern Argentina and portions of northwestern South America, particularly in Peru, are notable in the annual standardized anomalies (Fig. 6.13). The affected regions in Peru and southern Ecuador generally receive precipitation throughout the year, with the maximum occurring between January and March. This is in contrast to the coastal regions of Ecuador and extreme northern Peru, which typically receives less rainfall than the interior areas during a 5- or 6-month-long rainy season, and during 2003 the coastal regions recorded near-normal amounts of precipitation. Above-average precipitation anomalies were observed in Peru and southern Ecuador during most of the year. Although monthly averages during January and February were slightly below normal in some areas, heavy rains were blamed for outbreaks of dengue fever and leptospirosis in Ecuador during that period. In fact, more cases

of dengue fever were reported during the first 2 months of 2003 in Ecuador than during all of 2002 (source: International Society for Infectious Diseases).

Precipitation surpluses were observed throughout the year in the typically arid Patagonia region in southern Argentina. A significant portion of the annual anomaly in this region came during October–December, which are normally the driest months of the year. Southern Patagonia received 42% more than its climatological annual average of 375 mm, with 39% of that anomaly occurring during the last 3 months of the year.

Northeastern Argentina received very heavy rainfall during April, normally the region's wettest part of the year. Most of the region's April precipitation totals exceeded the 90th percentile of the climatological distribution, and some areas received twice their normal amount of precipitation. The rain sparked severe flooding that forced the evacuation of tens of thousands of people, damaged infrastructure, caused localized outbreaks of hepatitis and gastrointestinal diseases, and killed as many as 25 people. Agriculture in the province of Sante Fe was among the worst affected sectors, because one-sixth of its agricultural land was submerged and 200,000 ha of crops were destroyed.

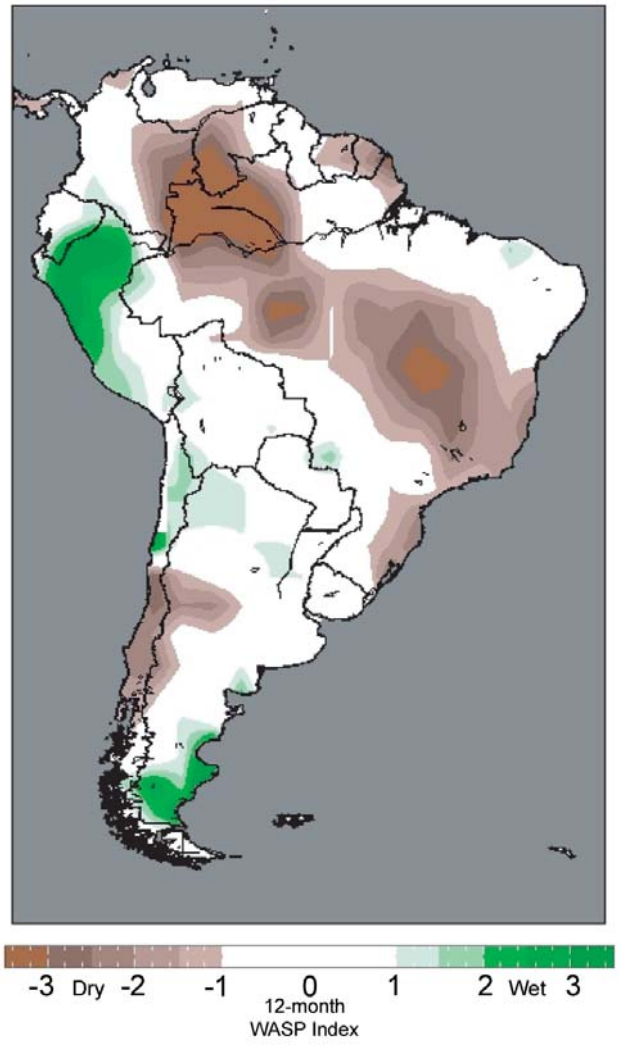

Fig. 6.13. Average of standardized monthly precipitation anomalies for 2003. Data are from the CAMS–OPI analysis for 2003 (courtesy of NOAA/CPC), with anomalies determined from the 1961–90 base period (see Fig. 6.12 for a definition of the WASP index).

Average temperatures for 2003 across the continent were above normal (not shown). The largest departures were observed in Venezuela, northwestern Argentina, and across northern and eastern Brazil. Temperatures in these areas averaged approximately 2°C above normal for the year. Regions with near- to slightly below normal temperatures included southwestern Peru, northern Bolivia, and southwestern Argentina. In contrast, the Peruvian highlands experienced a cold snap in July as temperatures fell to –20°C during the austral winter. Over 200 fatalities, largely from pneumonia, were reported, as well as livestock and crop losses due to the extreme cold across southern areas of Peru.

d. *Europe*—L. V. Alexander[1] and D. E. Parker[1]

i) Overview

Annual temperatures in 2003 were well above average across Europe, especially in western regions. Although cooler than 2002, annual temperature anomalies averaged over land surfaces within the area between 45°–65°N and 25°W–60°E were 0.66°C above the 1961–90 mean. However, there were significant regional and seasonal variations (Fig. 6.14). Temperatures across the Mediterranean, southern Adriatic, and much of the northwestern part of the European continent were above the 98th percentile of the 1961–90 distribution, when averaged over the entire year. In general, it was also a dry year (Fig. 6.15), especially in February–March and for most of the summer, although there were some regional flooding events. Several sunshine records were broken in 2003: De Bilt in the Netherlands recorded the sunniest February in its 103-yr record, and the United Kingdom experienced its sunniest year since readily available records began in 1961.

Anomalous warmth was widespread in all four seasons, particularly in the summer (see section 6dii on the summer European heat wave), with only the three Baltic States and an area around the northwest shore of the Black Sea colder than the 10th percentile in winter and spring (see Figs. 6.14a,b). Western Europe and parts of Eastern Europe were exceptionally warm during summer (Fig. 6.14c) and it was likely the warmest summer since 1540 in parts of Central Europe (Beniston

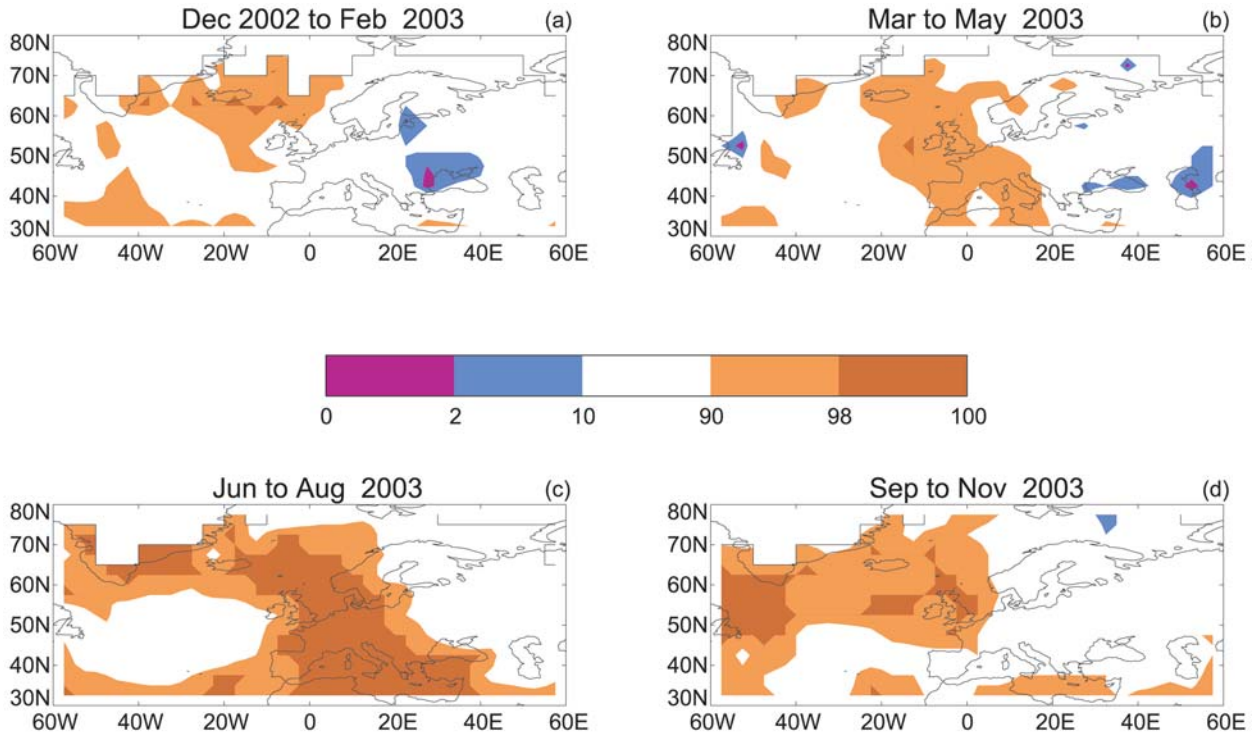

Fig. 6.14. European surface temperature in 2003 expressed as percentiles of 1961–90, using a modified two-parameter gamma distribution for (a) Dec 2002–Feb 2003 (b) Mar–May, (c) Jun–Aug, and (d) Sep–Nov 2003 (sources: Jones et al. 2001; Horton et al. 2001; and Jones and Moberg 2003).

2004). In June, several stations in Switzerland recorded temperatures more than 7°C above the 1961–90 average, making this an unprecedented event in the historical record (Fig. 6.16). Although some station records may have been affected by urban warming, homogenized records from other parts of Europe were consistently 5°C warmer than average for several months. Glaciers in the European Alps lost an average thickness of ice equivalent to ~3 m of water, which was nearly twice as much as during the previous record year of 1998 (1.6 m). The Mediterranean and Near East region (30°–40°N, 20°W–60°E) had their warmest land and SST anomaly on record for both June and July. In contrast to the record heat, regions further east had

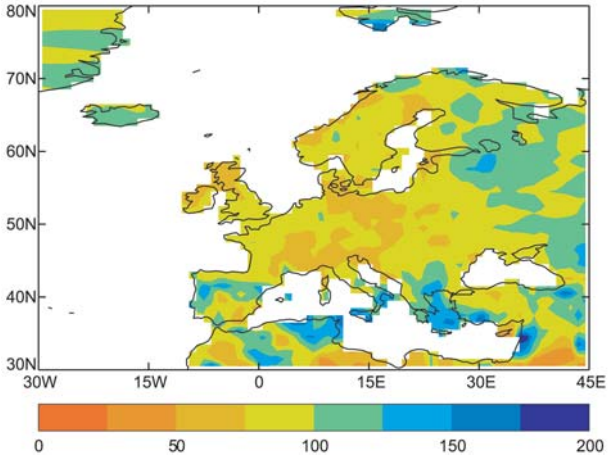

Fig. 6.15. Precipitation anomalies for the European region for the period Dec 2002–Nov 2003, expressed as a percentage with respect to 1961–90 (source: GPCC 1998; Rudolf et al. 1994).

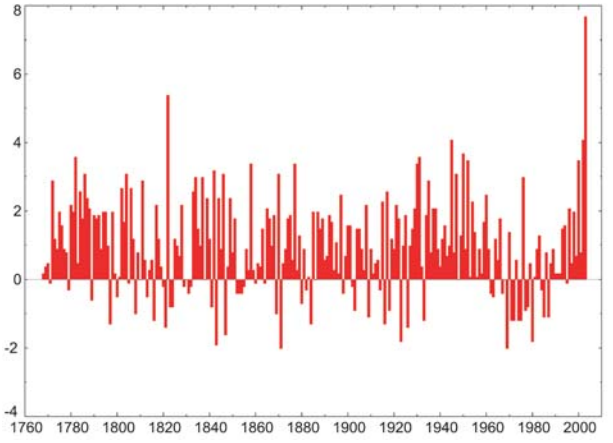

Fig. 6.16. Jun temperature anomalies (°C) for Geneva, Switzerland. (Source: Monthly Climatic Data for the World)

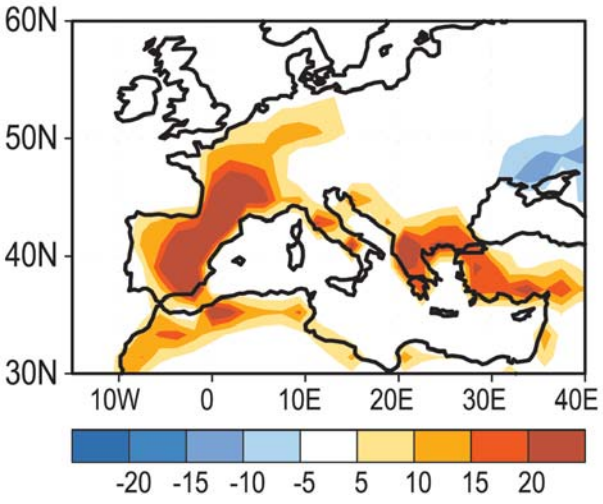

Fig. 6.17. Anomalous number of days with maximum surface temperatures reaching 34°C for JJA 2003. Anomalies are departures from the 1971–2000 base period daily means.

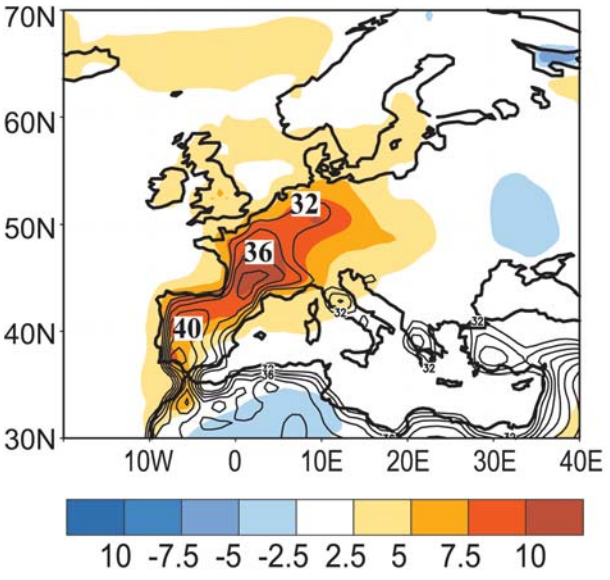

Fig. 6.18. Mean daily maximum surface temperature (contours, interval is 2°C) and anomalies for 1–15 Aug 2003. Anomalies are departures from the 1971–2000 base period daily means.

much cooler temperatures. Moscow, Russia, experienced one of its coldest Junes on record, with its first snowfall in June since 1963 (see section 6f(iii)). When averaged across 45°–65°N, 25°W–60°E as a whole, June temperatures over land areas were close to normal. However, July and August, with land temperature anomalies of 1.42° and 1.95°C, respectively, were much warmer than average. The high temperatures and dry conditions exacerbated forest fires that burned across southern France and Portugal in July. In contrast to the devastating flooding across central Europe in summer 2002, July saw the Danube and Elbe Rivers at their lowest levels for several decades, while Hungary had its worst drought since 1950. The record heat wave spread across most of Western Europe in August. At Paris (Orly), France, temperatures reached or exceeded 35°C on 10 consecutive days, and the United Kingdom recorded its highest-ever daily maximum temperature of 38.5°C.

The warmth persisted into autumn (Fig. 6.14d), with average fall temperatures across the western North Sea region exceeding the 98th percentile. The year ended with more extremes; December temperatures across Europe were greater than 2°C above the long-term average, but also during the month severe regional flooding in southeast France forced 15,000 people from their homes.

ii) Summer heat wave—G. Bell,[5] and T. Eichler[5]

Most of Europe was affected by an extreme heat wave during JJA 2003. In France, 11,000 heat-related deaths were reported between late July and mid-August (source: World Health Organization; Reuters/Associated Press). These deaths resulted not only from the extreme daily heat, but also from the frequency of extremely hot and dry days in areas not accustomed to such conditions. These conditions were part of a prolonged warm and dry spell that began in April in

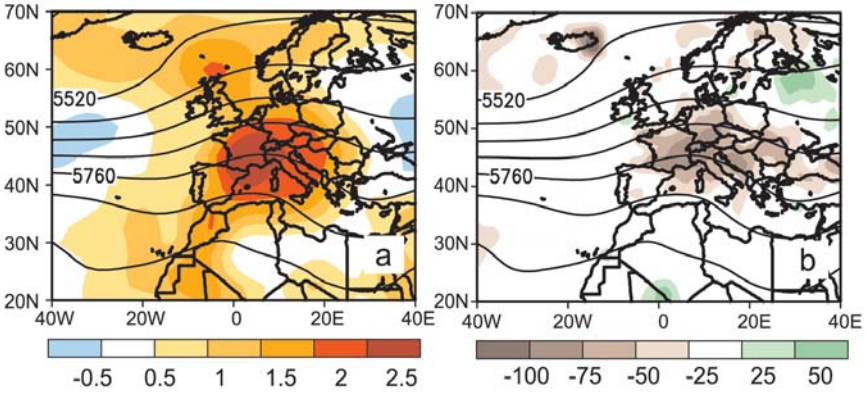

Fig. 6.19. Mean 500-hPa heights (contours, 60 m interval) overlaid with (a) surface temperatures anomalies (°C) and (b) precipitation anomalies (mm) for Apr–Aug 2003. Anomalies are departures from the 1971–2000 base period monthly means.

response to a persistent upper-level ridge of high pressure centered over the continent. The extreme persistence of this ridge was partly related to a prolonged positive phase of the eastern Atlantic (EA) teleconnection pattern.

Most of Europe, from southern Spain to central France, experienced daily maximum temperatures exceeding 34°C on 30–50 days during JJA, which was 20 days more than average (Fig. 6.17). In central and northern France there were 10–30 days with maximum temperatures above 34°C, which was well above the mean of 5 days or less. Two distinct periods of exceptional heat occurred during the season—the first in June and the second during the first half of August. The August heat wave was the more serious of the two, because it coincided with the normal peak in summer temperatures and was accompanied by an almost complete absence of rainfall. Daily maximum temperatures during this period averaged more than 40°C across most of interior Spain, 36°–38°C across southern and central France, and 32°–36°C across northern France (Fig. 6.18, contours). In general, these temperatures were 7.5°–12.5°C above average (Fig. 6.18, shading). For the areal average of Germany, both June and August were the warmest months since the beginning of the twentieth century. Thus, the summer (JJA) became the hottest in Germany since 1901 (average temperature of 19.6°C, which was 3.4°C above the 1961–90 base period), and, with the exception of some stations in northern and northwestern Germany, it was the hottest summer since the beginning of recorded measurements.

Surface temperatures were well above average across Europe throughout April–August, with the largest mean departures exceeding +2.5°C across central Europe and +1.5°C across northern Europe (Fig. 6.19a, shading). Precipitation totals were also well below average during this period, with deficits of 75–100 mm observed throughout central Europe (Fig. 6.19b, shading). The largest temperature and precipitation anomalies coincided with the mean position of a very persistent upper-level ridge (Fig. 6.20a). These regions were also situated south of the axis of an enhanced North Atlantic jet stream (Fig. 6.20b), resulting in a large-scale sinking motion and a reduction in the number and intensity of convective storms, precipitation events, and cold frontal passages.

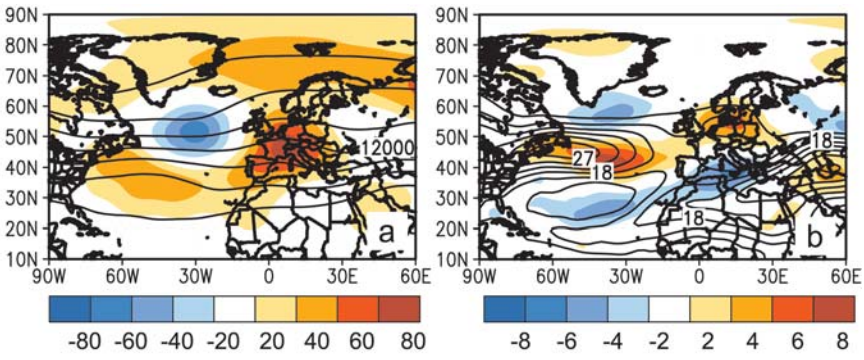

Fig. 6.20. Mean 200-hPa (a) heights and anomalies (m), and (b) wind speeds and anomalies (m s^{-1}) for Apr–Aug 2003. Anomalies (shading) are departures from the 1971–2000 base period monthly means.

These conditions were associated with a larger-scale anomalous circulation characterized by below-average heights at high latitudes from Canada to Great Britain, and above-average heights in the middle latitudes from the northeastern United States to Eastern Europe, as well as in the subtropics (Fig. 6.20). This anomaly pattern (Fig. 6.21) reflected a strong positive phase of the EA teleconnection pattern (Barnston and Livezey 1987). The standardized EA index values for June–August were 2.1, 0.9, and 1.3, respectively. In general, the EA pattern is qualitatively similar to the positive phase of the NAO, but with its anomaly centers shifted south of those associated with the NAO.

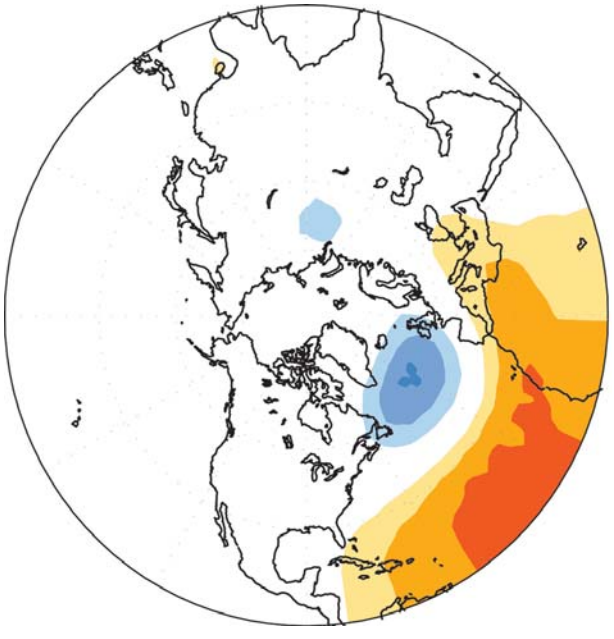

Fig. 6.21. The positive phase of the eastern Atlantic teleconnection pattern, as indicated by 500-hPa height anomalies (positive height anomalies are shaded orange, negative height anomalies are shaded blue).

The southern center of anomalies associated with the NAO also tends to be confined to the anticyclonic flank of the North Atlantic jet stream, whereas the EA pattern exhibits a strong link to the subtropical North Atlantic. During April–August, the positive height anomalies in this region were associated with an amplified subtropical ridge from the eastern United States to northern Africa. This enhanced subtropical ridge was a contributing factor to the above-normal 2003 Atlantic hurricane season (see section 4bi).

e. *Africa*

i) North Africa—M. A. Bell[6] and O. Baddour[3]

The Mediterranean coast of North Africa receives most of its annual rainfall during October–April, largely from midlatitude cyclones and their associated cold frontal incursions into subtropical regions. During most of 1980s and 1990s there were severe drought episodes across northern Africa. During the last 3-yr a succession of wet autumns has brought more rainfall to the northern part of the region. These above-average rains continued during October 2002–April 2003, with totals exceeding 300 mm across the northern half of Morocco and Tunisia, and northeast Algeria (Fig. 6.22a). These amounts were generally 125 mm or more above the long-term average (Fig. 6.22b).

Especially heavy precipitation occurred during January across northern Algeria and Tunisia. Precipitation totals of 25–100 mm during 22–28 January generated some of the worst flooding in 10-yr in northern and central Tunisia. In Morocco, anomalously wet conditions prevailed during January–May.

With the exception of the high elevations of the Atlas Mountains, summers are generally dry and hot. During July–August 2003, a period that coincided with the record heat wave in Europe (see section 6dii), monthly temperatures in some locations in North Africa averaged 3°–4°C above normal. In Morocco, new monthly temperature records were set in several areas during the period. The heat was most extreme during August when several northern Moroccan cities experienced new all-time maximum temperature records, includ-

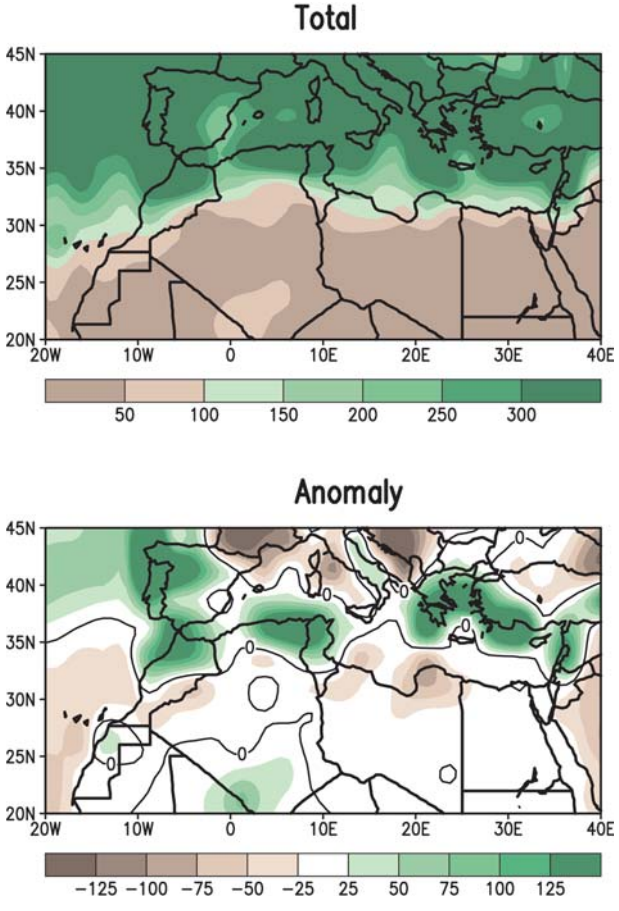

Fig. 6.22. Oct 2002–Apr 2003: (top) total precipitation (mm) and (bottom) anomalies for the northern Africa. Anomalies are departures from the 1979–95 base period monthly means (CAMS–OPI data courtesy of NOAA/CPC).

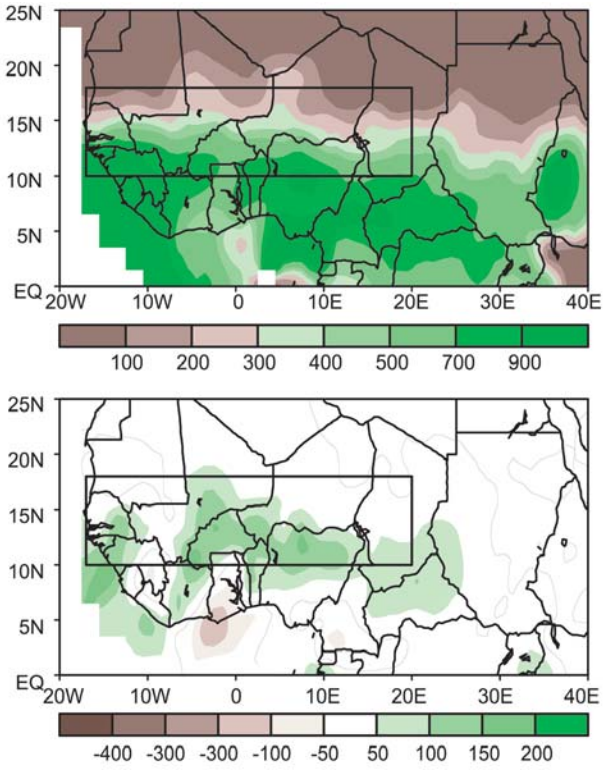

Fig. 6.23. Jun–Sep 2003: (top) total precipitation (mm) and (bottom) anomalies for the African Sahel and Gulf of Guinea regions. The boxed area denotes the approximate boundaries of the Sahel region. Anomalies are departures from the 1979–95 base period monthly means (CAMS–OPI data courtesy of NOAA/CPC).

ing Rabat (44.6°C), Kenitra (47.7°C), and Tangier (43.5°C).

Several locations in North Africa were affected by severe storms and heavy precipitation during the latter part of the year. Much of Morocco and northern Algeria received above-normal rainfall during October. For example, 85 mm of rain fell in less than 24 h during 21–22 October in central Morocco, which was nearly 85% of the annual total of 102 mm. During 17–18 December a second extreme event in northern Morocco produced 127 mm of rain in 24 h. This total was 44% of the average annual rainfall, and 400% of the December monthly average.

ii) West Africa—W. M. Thiaw,[5] G. D. Bell,[5] and M. A. Bell[6]

(i) Rainfall

West African rainfall can be divided into two quasi-homogeneous regions: the African Sahel and the Gulf of Guinea. The African Sahel, defined here as the region between 10°–20°N, 18°W–20°E (Fig. 6.23, boxed region), receives approximately 90% of its mean annual rainfall during June–September. The rainy season is monsoonal in character, and is closely related to the north–south movement of the intertropical convergence zone (ITCZ), which starts its northward progression in March and reaches its northernmost position in August. Seasonal precipitation exhibits a strong meridional gradient, with average totals exceeding 600 mm in the south, and reaching 100–300 mm in the north.

Precipitation totals exceeded 100 mm above average across much of the central Sahel (Fig. 6.23b), which made the 2003 rainy season the second wettest since 1990 (Fig. 6.24). In contrast, rainfall along the Guinea coast was below average during the period, with exceptionally dry conditions observed in July and August. This rainfall pattern reflected an amplified monsoon circulation, with the ITCZ remaining consistently north of its climatological position from May until October [see section 6eii(ii)].

During July–September 2003, when the Sahel was anomalously wet and the Guinea coast anomalously dry, positive SST anomalies in the Atlantic persisted along the equator and southward along the west coast of southern Africa, a configuration more consistent with the opposite pattern (anomalously dry Sahel/wet Guinea coast). However, other conditions, such as slightly above-normal sea level pressures in the equatorial and southern tropical Atlantic and anomalously strong westerly flow at 850 hPa over the Atlantic between 5° and 12°N (Fig. 6.26) were more typical of the wet Sahel/dry Guinea coast rainfall pattern observed during 2003.

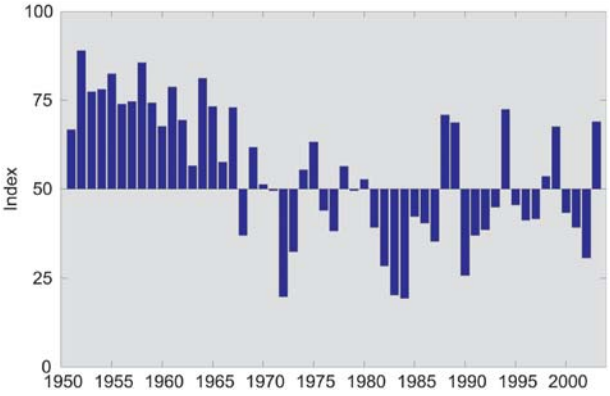

Fig. 6.24. Precipitation index time series for the period 1951–2003 expressed in terms of percentiles. The index was calculated from the 1971–2000 base period seasonal means for the African Sahel during Jun–Sep using a gamma distribution.

The inverse relationship between rainfall anomalies in the Sahel and Guinea coast regions has been a recurring pattern of West African climate variability (Janicot 1992; Ward 1998). During the 1970s–mid-1990s the prevailing pattern was a dry Sahel and a wet Guinea coast. Since 1995, rainfall has returned to near-normal levels across the African Sahel, in association with an overall strengthening of the West African monsoon circulation. Another notable aspect of these stronger monsoon circulations has been a significant increase in Atlantic hurricane activity since 1995 (see section 4bi).

(ii) Atmospheric circulation

Precipitation across the African Sahel is controlled by the depth and northward penetration of the West African monsoon and the associated ITCZ, which in turn is related to the position of the mid- and upper-level jets. These larger-scale circulation features are relatively sensitive to changes in the global monsoon circulation on both interannual and interdecadal time scales (Chelliah and Bell 2004).

The above-average 2003 rainy season resulted from an enhanced West African monsoon circulation and an associated northward shift of the mean ITCZ. At 925 hPa, strong southwesterly winds averaging 6–9 m s^{-1} extended well northward into the Sahel region (Fig. 6.25). This enhanced monsoonal inflow was also evident at 850 hPa (Fig. 6.26), and contributed to a deep penetration of moist, unstable air well into the Sahel region (see Fig. 4.13). The enhanced monsoon was also associated with an anomalous low-level cyclonic circulation across the northern and central Sahel, which contributed to an above-average strength of many African easterly waves and resulted in larger convective rainfall totals throughout the region. This anomalous

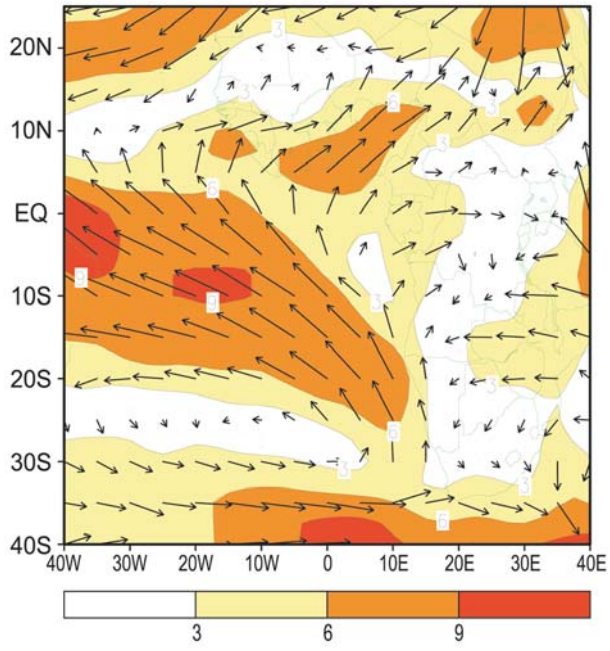

Fig. 6.25. Aug–Sep 2003 mean 925-hPa wind speeds (m s^{-1}) and vector winds over tropical and subtropical Africa.

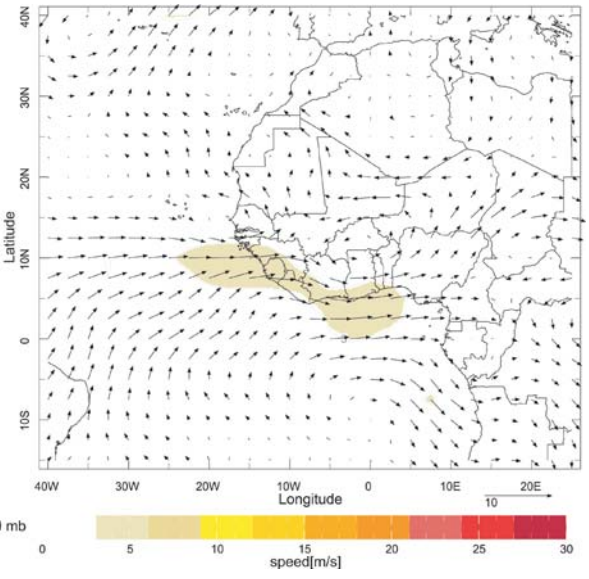

Fig. 6.26. Jul–Sep 2003 anomalous 850-hPa wind speed (shading; m s^{-1}) and wind vectors winds over tropical and subtropical Africa. Anomalies are departures from the 1971–2000 base period monthly means.

cyclonic circulation reflected enhanced cyclonic shear along the equatorward flank of the AEJ, and a northward shift of the mean position of the AEJ to 17.5°N across the western Sahel (Fig. 6.27).

At upper levels, the enhanced monsoon circulation was associated with a strengthening of the subtropical ridges across both hemispheres (see Fig. 4.7), and with a corresponding amplification of the tropical easterly jet. These same conditions contributed to the above-normal 2003 Atlantic hurricane season (see section 4b1).

iii) East Africa and the Greater Horn—P. Ambenje[2] and M. Bell[6]

The 10 Greater Horn of Africa (GHA) countries include Burundi, Djibouti, Eritrea, Ethiopia, Kenya, Rwanda, Somalia, Sudan, Tanzania, and Uganda. Of all of the climate elements, rainfall is the most critical due to the heavy dependence on agricultural activities. However, rainfall varies both temporally and spatially, and extreme rainfall conditions, such as floods and droughts, impact negatively on subsistence activities in the GHA region.

Rainfall in the GHA was examined for each of its three distinct climate regimes. The southern sector (central and southern Tanzania) experiences a climatological rainfall maximum during December–March. The equatorial sector (Uganda, Rwanda, Burundi, Kenya, southern Somalia, northern Tanzania, southern Sudan, and southern Ethiopia) experiences its first rainy season (termed "long rains") during March–May as the rainbelt shifts northward from the Southern Hemisphere. It then experiences its second rainy season (termed "short rains") during October–December as the rainbelt shifts southward from the African Sahel and Sudan regions. In the northern sector (comprising the rest of Sudan and Ethiopia, northern Somalia, Djibouti, and Eritrea), rainfall normally occurs from May–June to September–October. However, areas close to large water bodies, such as Lake Victoria and parts of the coastal strip, receive substantial rainfall throughout the year.

(i) Southern sector

Widespread dry conditions during January–March 2003 (Fig. 6.28) exacerbated the rainfall deficits that had accumulated during the previous April–September period. Generally dry conditions also characterized the

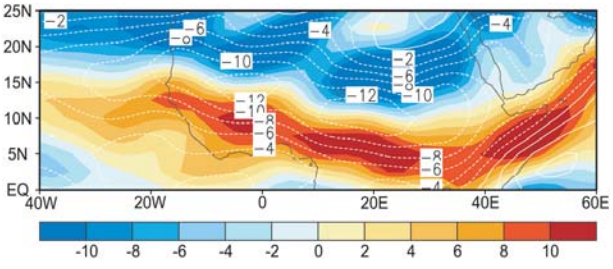

Fig. 6.27. Aug–Sep 2003 mean 600-hPa zonal wind (contours, m s^{-1}) and relative vorticity (shaded, 2 × 10^{-6} s^{-1}) over West Africa.

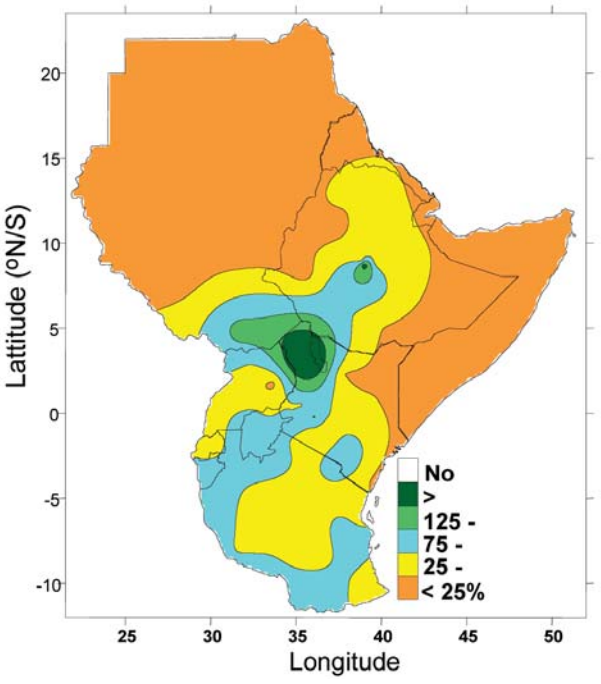

Fig. 6.28. Jan–Mar 2003 percent of normal precipitation over GHA.

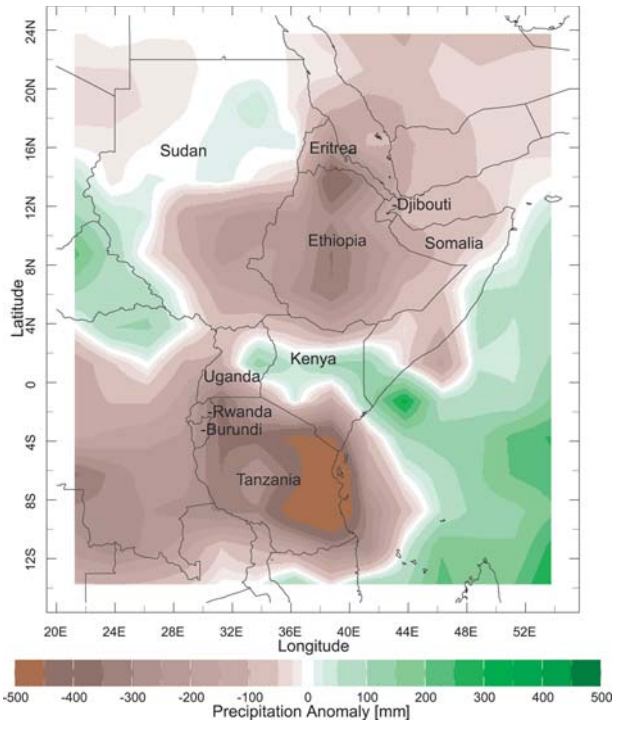

Fig. 6.29. Annual precipitation anomalies for 2003 across the GHA region. Anomalies are departures from the 1979–95 base period (CAMS–OPI data courtesy of NOAA/CPC).

southern sector during the months of April–September 2003. In Tanzania, the annual total rainfall averaged 300–500 mm below average (Fig. 6.29), which led to drought conditions and food shortages for close to 2 million people. Some drought relief occurred during October–November, because above-average rains fell over large portions of the Southern sector.

(ii) Equatorial sector

The equatorial sector experienced generally dry conditions in January and February, with significant rainfall observed across the sector in late April. However, some locations in the marginal areas were characterized by short-lived, intense precipitation events (Fig. 6.29). The wet anomalies over southern Ethiopia, central Tanzania, and parts of western and central Kenya resulted in some locations experiencing their wettest conditions on record (since 1961).

The equatorial sector experienced significant rainfall from late April into May 2003, which produced near-record rains and flooding in northern Kenya, southern Ethiopia, and southern Somalia (Fig. 6.30). Enhanced precipitation was observed over most locations of the western highlands of Kenya from June–August. During October–December below-normal rains were observed in southern Ethiopia, Kenya, and southern Somalia.

(iii) Northern sector

Much of the GHA has suffered from persistent drought conditions for several consecutive years. This has been particularly true in the northern sector, where rainfall deficits during 2002 created food shortages for nearly 14 million people in Ethiopia and Eritrea by early 2003.

The onset of the rainfall season in 2003 occurred during the month of June, which was somewhat later

Fig. 6.30. Cumulative rainfall at Wajir, Kenya (located in northeastern Kenya), during 2003 (red), compared with the long-term annual mean (blue).

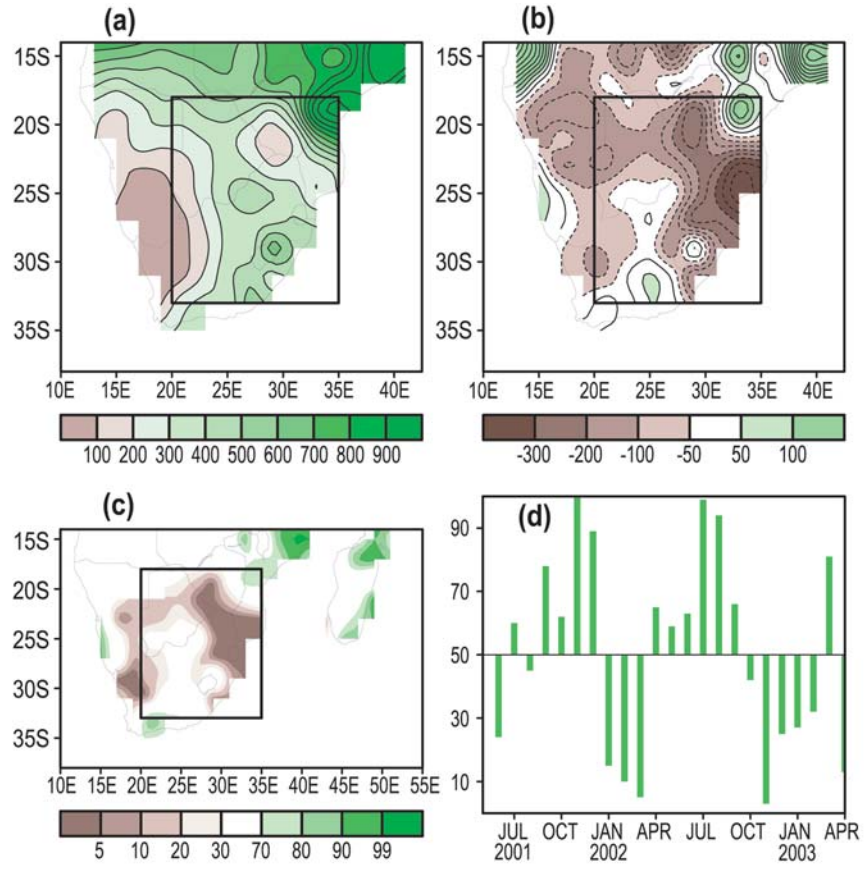

Fig. 6.31. Nov 2002–Apr 2003 southern African precipitation (a) totals (mm), (b) anomalies (mm), and (c) percentiles, based on a gamma distribution fit to the 1971–2000 base period. (d) Monthly time series of precipitation percentiles, based on precipitation totals averaged over the boxed region in southern Africa depicted in panels (a)–(c).

than normal for the sector. Rainfall totals were near normal in June, but declined in July and August over the southern parts of the sector, while the central and western parts of the sector received near-normal rainfall during this period. Rainfall in excess of 200 mm over three consecutive months (June–August) resulted in normal to above-normal conditions. Parts of central Ethiopia, as well as eastern and southern Sudan, continued to receive above-average rainfall in September, which led to some of their largest harvests in 5 yr. However, severe drought conditions continued in northern Somalia and areas of southern and eastern Ethiopia (Fig. 6.31).

iv) Southern Africa—W. M. Thiaw,[5] B. Garanganga,[15] and C. McBride[19]

(i) Rainfall

The rainy season over much of southern Africa extends from October to April, with the largest amounts typically observed between December and March. Exceptions to this unimodal rainfall distribution are found 1) in northern areas where rainfall occurs during October–December and March–May in response to the north–south movement of the ITCZ, 2) in the southwestern Cape region of South Africa where rainfall occurs during both October–April and June–August, and 3) along the southern coast of South Africa and extreme northern Tanzania bordering Lake Victoria, where rainfall is typically observed throughout the year.

October–April rainfall in southern Africa has been generally below average during El Niño years and above average during La Niña years (Ropelewski and Halpert 1987, 1989, and 1996; Hastenrath et al. 1995; Dai et al. 1997; and Thiaw et al. 1999). The October–April 2002–03 rainy season was below average, with rainfall deficits observed throughout the region (Fig. 6.31b). Precipitation was consistently below average from October 2002 to February 2003, and again in April, with March being the only month with above-average totals for the region as a whole (Fig. 6.31d). This indicated a significant delay in the onset of the October rains and an early withdrawal in April. These below-average rainfall anomalies were consistent with moderate El Niño conditions during the period.

The most significant rainfall deficits were found in the East across the normally heavy precipitation areas of eastern South Africa, Botswana, Zimbabwe, and the southern half of Mozambique. Precipitation totals in these areas (Fig. 6.31a) averaged only in the 5th to 20th percentile of occurrences (Fig. 6.31c), which led to a continuation of drought conditions from eastern and northern Botswana into western Zimbabwe, northern South Africa, southern Mozambique, and Swaziland.

The southwestern Cape region of South Africa also recorded below-average rains during October 2002–April 2003, which followed a drier-than-average winter rainy season during June–August 2003. These con-

tinuing rainfall deficits were devastating to agricultural activities in this area.

(ii) Atmospheric circulation

The low-level atmospheric circulation during the below-average October–April 2002–2003 southern Africa rainy season featured easterly winds along the equatorward flank of the Mascarene Islands high pressure system (located over the southern Indian Ocean) averaging 4–8 m s^{-1} from the east central Indian Ocean westward into Madagascar and portions of interior southern Africa (Fig. 6.32). The Mascarene high was notably weaker than average over Madagascar, which resulted in a reduction in the amount of deep tropical moisture penetrating inland from the Indian Ocean. In contrast, the above-average March rains were associated with a broad low-level anomalous cyclonic circulation over southern Africa (Fig. 6.33), which favored the advection of low-level Atlantic moisture into the southern regions of the continent.

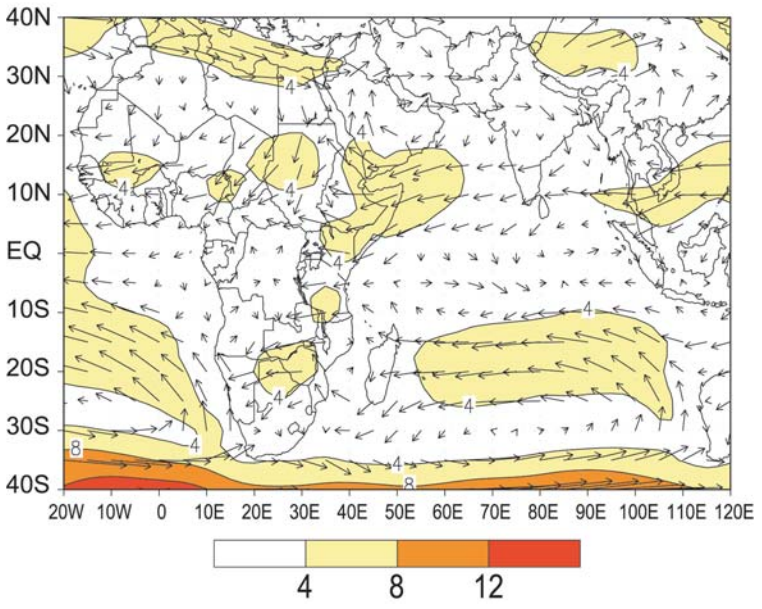

Fig. 6.32. Oct 2002–Apr 2003 mean 850-hPa wind speeds (m s^{-1}) and vector winds over Africa and the Indian Ocean region.

f. Asia

i) China—E. K. Grover-Kopec[6]

Similar to recent years, precipitation extremes were an important feature of China's climate during 2003. Much of the Yellow River basin experienced above-normal precipitation and flooding, while southeastern China was impacted by precipitation deficits that persisted most of the year (Fig. 6.34). This was in stark contrast to the precipitation patterns of 2002, which brought a dry spell to the northeast and abundant rainfall and flooding to the southeast (Waple and Lawrimore 2003).

Climatologically, annual precipitation totals are generally greatest in southeastern China and decrease toward the northwest. The contribution of summer precipitation to annual totals is greatest in the north, with the majority of precipitation occurring during the spring in portions of the interior southeast. In addition, southeastern China and Taiwan often receive abundant rainfall from typhoons and tropical storms between July and October.

Above-average amounts of precipitation fell in a band stretching nearly 2000 km from central coastal China to the eastern extent of the Tibetan Plateau during 2003 (Fig. 6.34). While rainfall throughout the year contributed to these anomalies, locally heavy rainfall in the east during the first half of the region's rainy season was the primary contributor. These rains coincided with weaker-than-average high pressure along

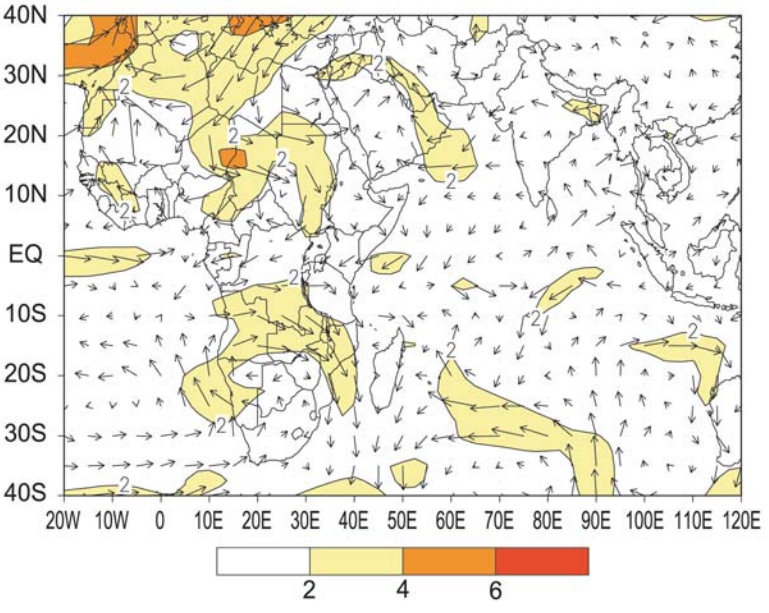

Fig. 6.33. Mar 2003: anomalous 850-hPa wind speeds (m s^{-1}) and vector winds over Africa and the Indian Ocean region. Anomalies are departures from the 1979–95 base period monthly means.

the coast and, subsequently, a persistent low-level boundary that was both stronger and farther east than normal, when compared with climatology. Rainfall in March and April eased soil moisture deficits in the provinces of Hebei, Shandong, and Henan, where some areas began the first 2 months of the year with only 20% of their normal precipitation. The eastern province of Anhui received twice its normal amount of precipitation during June, with over 400 mm falling in some locations. These rains brought severe flooding to the region, particularly in the Huai River valley. According to government statistics, this and other flooding during the first half of the year affected ~100 million people.

Over 70% of the annual precipitation surpluses in the region (Fig. 6.34, black box) came during an above-normal second-half of the rainy season (Fig. 6.35). In areas across the region, precipitation amounts between August and November exceeded the 90th percentile of the climatological distribution. August and September rains caused the worst flooding in 20 yr along the Wei River, a tributary of the Yellow River. These heavy rains continued until the end of the rainy season, because some areas in the Wei River valley received 4 times their climatological precipitation during September, October, and November. Severe rain and flooding across China claimed over 1900 lives during 2003 (source: Chinese Ministry of Civil Affairs).

In contrast to the north, southeastern China and Taiwan experienced an extended dry spell in 2003. Precipitation deficits across the southeast were first observed in the extreme south, and these dry anomalies steadily expanded north and eastward as the year progressed. Coastal southeastern China and northern Taiwan received only 65% and 50% of their normal amount of annual precipitation, respectively. In particular, Taipei received approximately 1 m less than its normal 2325 mm of annual precipitation. The dry spell in southeastern China also coincided with a July heat wave that affected the provinces of Zhejiang, Jiangxi, and Hunan. The heat, drought, and resulting fires in these three provinces reportedly killed 30 people and destroyed 1 million ha of arable land, mostly in Hunan, where 2000 streams and rivers dried up during 2003.

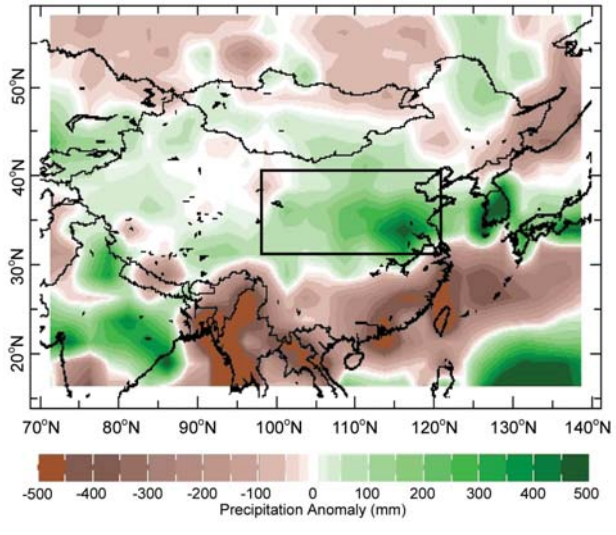

Fig. 6.34. (a) Annual precipitation anomalies (mm) for 2003. Data are from the CAMS–OPI analysis for 2003 (courtesy of NOAA/CPC), with anomalies determined from the 1979–95 base period.

ii) Southwest Asia—E. K. Grover-Kopec[6]

Portions of southwest Asia, centered on Afghanistan, endured a 4-yr drought during the period 1999–2002 (Waple and Lawrimore 2003). Climatologically, the drought-affected areas generally receive most of their precipitation between November and April via extratropical disturbances traveling eastward from the Mediterranean Sea. These winter and spring storms produce snowpack in the mountains, which provides most of the region's annual water supply. Some areas in the arid west receive no precipitation during the summer months, although the South Asian monsoon generally brings precipitation to eastern Afghanistan during the summer.

Precipitation totals continued to be below normal across most of Afghanistan and Iran during 2003 (Fig. 6.36). Southern Afghanistan and northwestern Iran received only about 50% of their average annual precipitation, with deficits exceeding 200 mm in some areas. However, the drought elsewhere in Afghanistan dissipated, because annual precipitation was generally higher than in 2002 (Fig. 6.37). Mountain snow and locally heavy rainfall in the central, east, and northeast

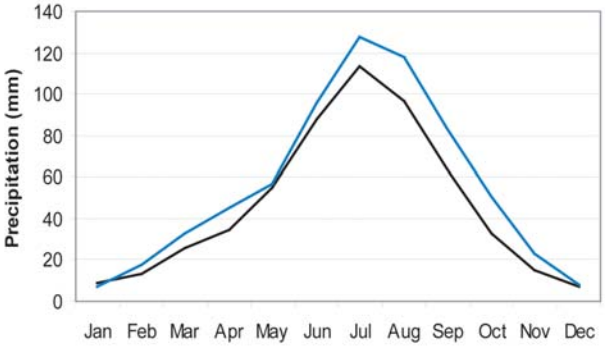

Fig. 6.35. Monthly time series of climatological (black) and observed (blue) precipitation averaged over the region in China within the black box in Fig. 6.34. Data are from the CAMS–OPI analysis for 2003 (courtesy of NOAA/CPC), with anomalies determined from the 1979–95 base period.

of the country during January and February contributed to a record wheat harvest in some of these areas. Although seasonal totals remained below average, parts of southern Afghanistan received 80% more precipitation during January and February 2003 than during all of 2002. Spring rains also brought localized flooding to the northern province of Kunduz, while monsoon rains during August ruptured dams and killed at least 24 people in the southeast.

In contrast to the relatively dry conditions across the south, the northern half of southwest Asia received above-normal amounts of precipitation during 2003 (Fig. 6.36). South-central Kazakhstan received nearly three times, or over 200 mm more, than its annual average. This has been typically one of the only areas in southwest Asia that receives a significant portion of its annual rainfall during the summer months. Above-normal precipitation was also observed in eastern Turkmenistan, eastern and northern Uzbekistan, northern and central Kyrgyzstan, and northeastern Tajikistan. Similar to northern Afghanistan, this was in stark contrast to precipitation totals of 2002. Annual precipitation totals were 100–180 mm higher during 2003 over large areas across these countries (Fig. 6.37). Above-normal precipitation during the spring and early summer, and heavy mountain snows in November, all contributed to the above-average annual totals in northern southwest Asia. In fact, the November rain and snow accumulations accounted for approximately 70% of these annual precipitation surpluses. Heavy rains and snowmelt in April brought flooding and landslides to areas in Kyrgyzstan and Tajikistan, which contributed to Kyrgyzstan recording 8 times as many landslides during the entire year as in 2002.

iii) Russia—O. N. Bulygina[8]

The climate and weather conditions during 2003 were analyzed for both the entire territory and seven quasi-homogeneous climatic regions within Russia (Fig. 6.38). Anomalously warm temperatures were observed across the country as a whole in 2003, with an annual average surface temperature of 1.2°C above the long-term mean, which continued a trend of above-average annual temperature. Russian temperatures have increased at a rate approaching 0.3°C decade^{-1} since 1950. The following is a seasonal breakdown of regional temperature and precipitation anomalies observed during 2003.

(i) Winter

During January 2003, positive air temperature anomalies prevailed over the entire country, with the exception of the northern and northwestern parts of European Russia. February was anomalously warm as well, with above-average temperatures in Siberia

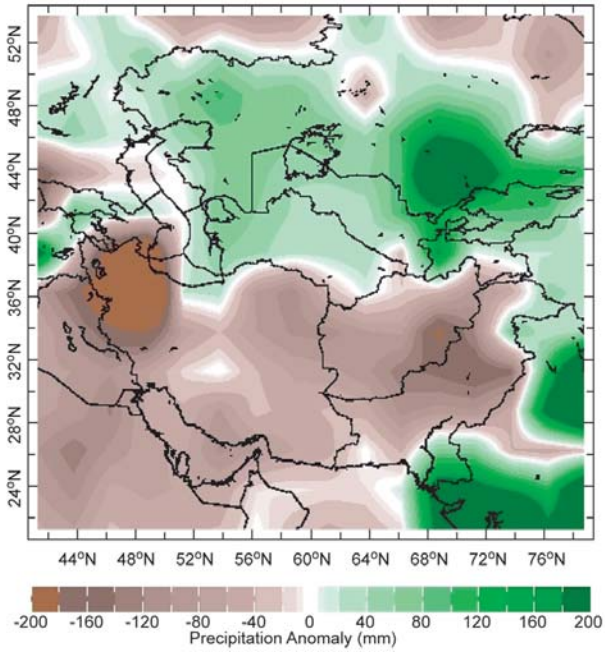

Fig. 6.36. Annual precipitation anomalies (in mm) for 2003. Data are from the CAMS–OPI analysis for 2003 (courtesy of NOAA/CPC), with anomalies determined from the 1979–95 base period.

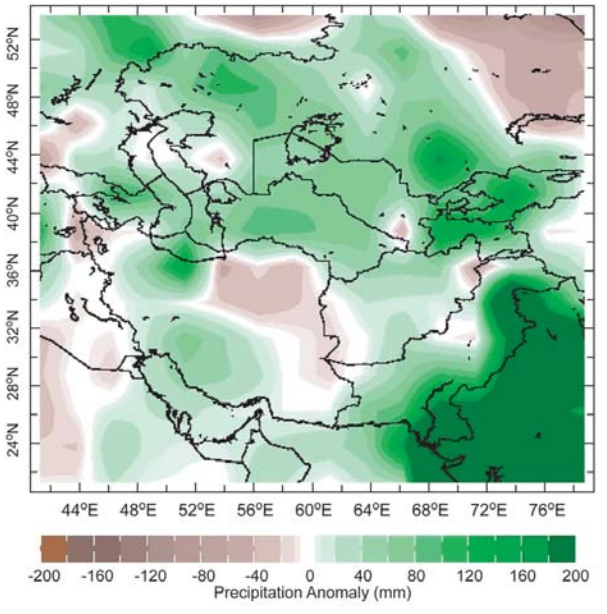

Fig. 6.37. Difference between the 2003 and 2002 annual precipitation anomalies (mm). Positive values indicate greater precipitation totals during 2003. Data are from CAMS–OPI (courtesy of NOAA/CPC), with anomalies determined from the 1979–95 base period.

and in the northwestern part of European Russia. In the Cola Peninsula, the monthly averaged air temperature anomaly exceeded the long-term mean by 6°–7°C.

(ii) Spring

In March, the synoptic weather pattern was dominated by extratropical cyclones in the northern areas of European Russia. These storms generated abundant precipitation, as well as gale-force winds. The coast of Murmansk experienced sustained wind speeds of 26–34 m s^{-1} during the last the third of the month. In the central and southern parts of European Russia, anomalously cold weather affected the region, with temperature anomalies 1°–2°C below average for the month. In April, cooler-than-normal weather persisted across European Russia, with mean monthly temperatures in the North Caucasus and the lower Volga River regions 2°–3°C below normal. Despite precipitation deficits (12%–28% of the monthly mean), ice jams formed on rivers in the Volgograd region due to a sharp temperature rise that occurred during the middle of the month. Vigorous spring flooding swelled small rivers and tributaries in the Rostov region as well.

In late spring, the majority of Russia was warmer than average. Above-normal air temperatures, in conjunction with below-normal rainfall, produced an increased threat of wildfires in the Irkutsk region and Transbaikalia. Smoke from wildfires reduced visibility in Chita to 300 m in mid-May. Precipitation deficits increased the risk of wildfires in the Maritime Territory and the south of Sakhalin Island also. Extremely dry conditions were found on the upper and middle Amur River, with the lowest water levels in these basins in the 100-yr instrumental record.

(iii) Summer

Summer was exceptionally cold in European Russia, and included one of the coldest months of June experienced in the last 100 yr. Monthly mean temperatures in June were 3°–4°C below normal across the region (Fig. 6.38). Several stations (i.e., Arkhangelsk and Volgograd) recorded their all-time lowest temperature

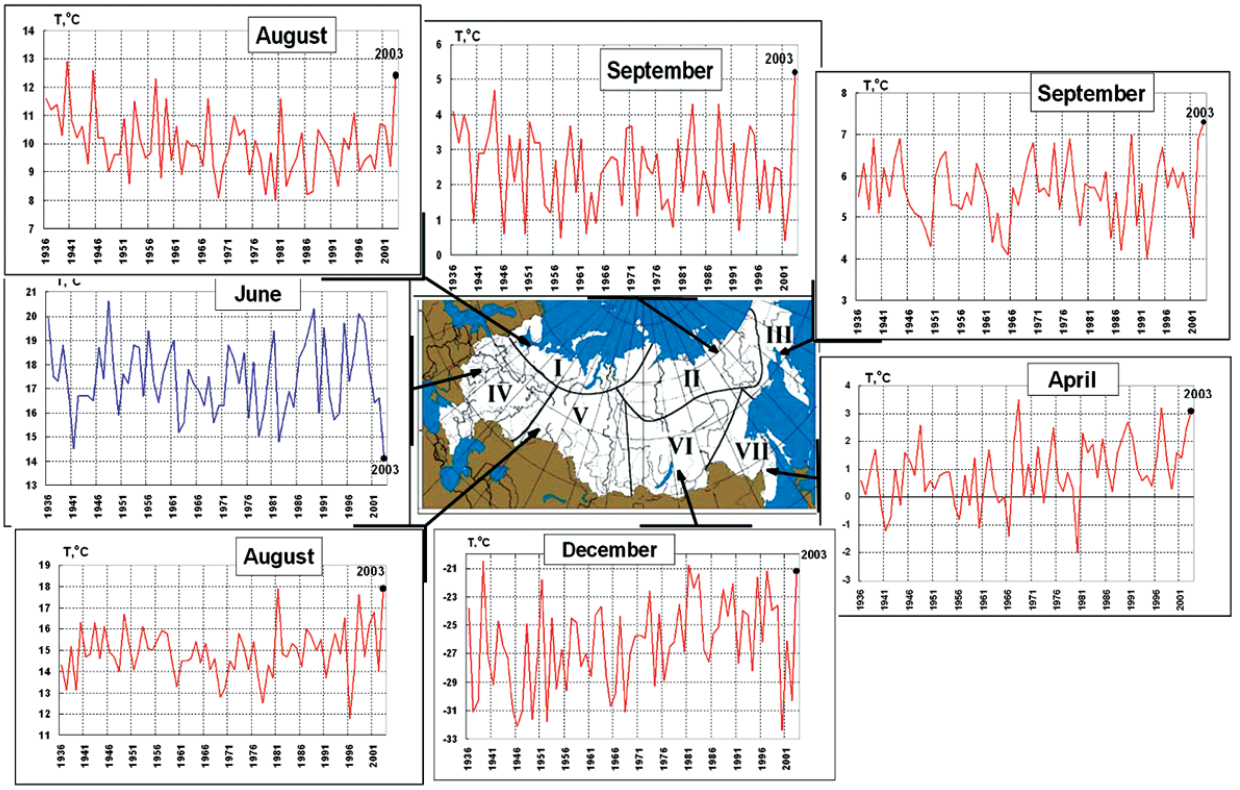

Fig. 6.38. Map of seven quasi-homogeneous climatic regions within Russia (I—the northern part of European Russia and western Siberia, II—the northern part of eastern Siberia and Yakutia, III—Chukotka and Kamchatka, IV—the central and southern parts of European Russia, V—the central and southern parts of western Siberia, VI—the central and southern parts of eastern Siberia, and VII—the Far East). Also shown are time series of the monthly mean temperature averaged over each territory. For each region, an example month in 2003 illustrates the above-average monthly temperature anomalies (except for the time series for June, which was a record cold month across European Russia).

for June. In addition, the cold weather was accompanied by above-normal precipitation. The Ural, Volga–Vyatka, and Volga regions, as well as the northern part of the central region, accumulated over 200% of their mean monthly precipitation. In contrast, western Siberia was anomalously warm in June, with average monthly temperature anomalies exceeding 5°C. During July, above-normal monthly temperatures were recorded across most of Russia. The anomalously warm and dry conditions led to extreme fire danger in the continental areas of the Magadan region, primarily in the republics of Tuva and Kamchatka.

August 2003 was one of the warmest over Russia in the last 100 yr. In the European region, the above-normal temperatures were centered in the northwest. The republic of Komi and the Nenets Autonomous Okrug area reported mean monthly temperature anomalies of 4°–5°C above normal (Fig. 6.39). August 2003 was also one of the wettest months on record in European Russia. At many stations, not only monthly, but also daily precipitation records were broken. For example, on 13 August Moscow had a record-breaking daily amount of precipitation of 59 mm, compared to the August average of 77 mm.

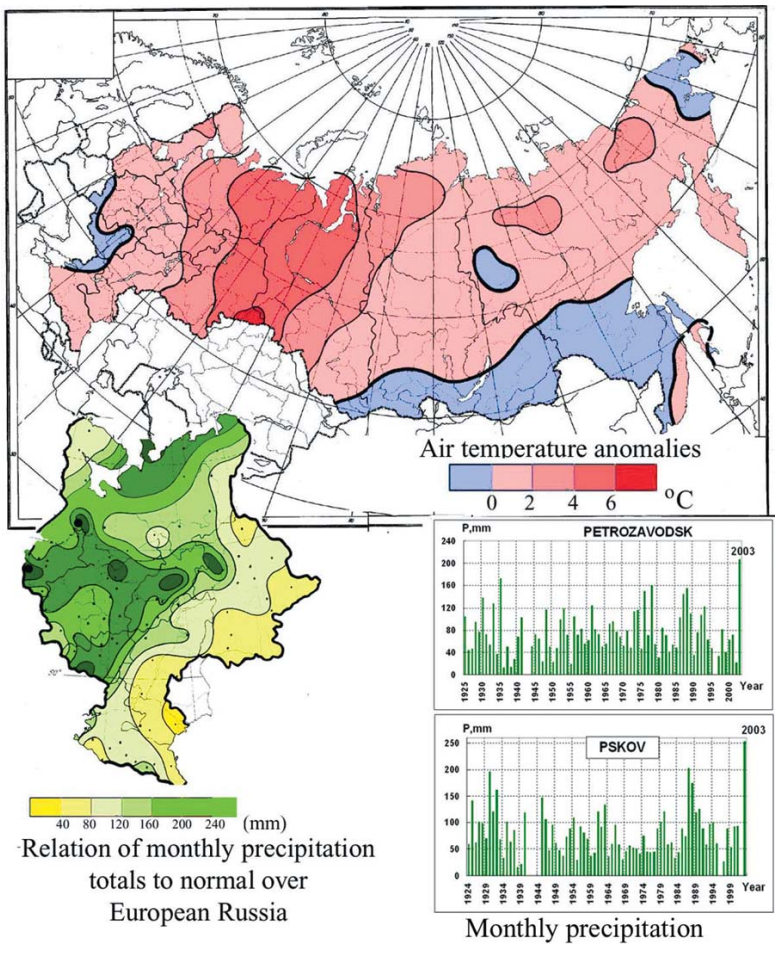

Fig. 6.39. Map: surface temperature anomalies (°C) during Aug 2003 across Russia. Inset: precipitation anomalies over European Russia, with two example graphs illustrating the record wet conditions at two sites (Petrozavodsk and Pskov).

(iv) Autumn

In September, temperature anomalies across most of Russia were near normal, and only in the northern areas of the Far East were monthly mean temperatures above normal (Fig. 6.38). In October, average monthly temperatures across Russia were once again above the long-term mean. Record monthly temperature anomalies were observed in the north of the Magadan region (greater than 8°C) and in the middle Ural (3°–4.5°C). In addition, October was anomalously wet in the southern part of European Russia. Areas of the Volgograd region, the Astrakhan region, and the Stavropol Territory received over 300% of their mean monthly precipitation. In November, cold anomalies were recorded in Siberia (temperature anomalies were –6°C in the Krasnoyarsk Territory). However, in the European and eastern parts of the country (Yakutia, Chukotka, Kamchatka), mean monthly temperatures were above the long-term average. In December, record warmth was again recorded throughout Russia (Fig. 6.40), with several stations measuring their highest monthly averaged surface temperatures since instrumental records began.

iv) South Asian monsoon—R. K. Kolli[18]

While the past 150 yr of instrumental records show no long-term trend in the summer (i.e., southwest) monsoon, interannual fluctuations, such as those associated with ENSO, dominate its observed variability (Fig. 6.41). Having experienced one of the most severe drought years during 2002, brought about by a record low rainfall in July 2002, the countries of South Asia were in need of abundant rainfall during the summer monsoon of 2003. A below-normal seasonal forecast and a delayed onset of the monsoon escalated concerns of continued drought conditions. However, as the season

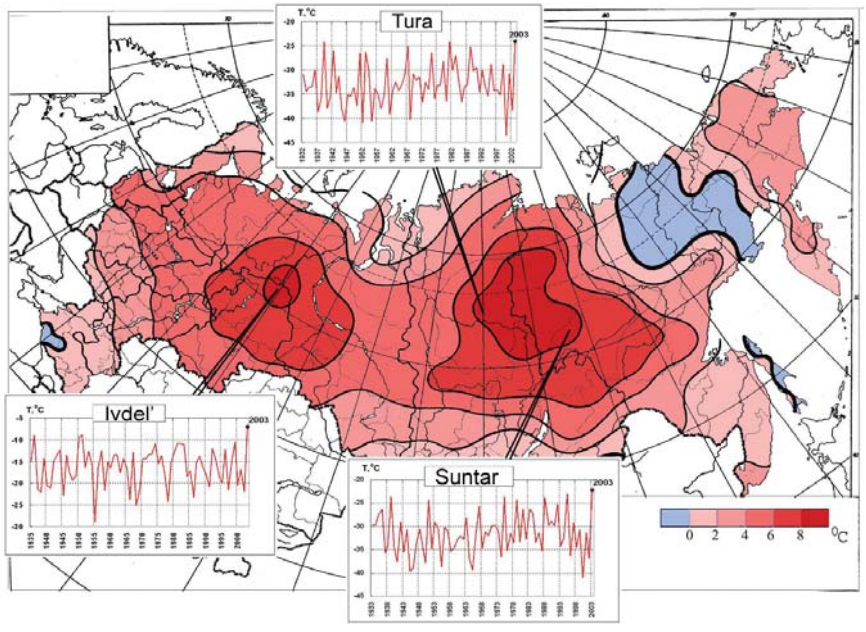

Fig. 6.40. Map of monthly average temperature anomalies (°C) during Dec 2003. The graphs shown illustrate the mean monthly temperature time series in Dec at Tura, Ivdel, and Suntar.

progressed the monsoon brought relief, with rainfall well distributed over time on a subcontinental scale. There were, however, some localized precipitation deficits.

The summer monsoon arrived over Kerala on 8 June, 7 days after the normal date. However, the monsoon quickly made up for the delay in its onset, and covered all of South Asia by 5 July, ~10 days ahead of the normal date (Fig. 6.42). A peculiar aspect of the onset phase during 2003 was that it occurred in northeast India (5 June) prior to Kerala. While this was an atypical feature of the year's monsoon onset, there had been similar instances in the recent past (e.g., 1972, 1995, 1996, 1998, and 2000). Comparing the onset phase in 2003 with the previous year, when the monsoon progressed slowly, a difference of about 40 days was observed in the time taken by the monsoon advance to cover the entire Indian subcontinent.

The leading edge of the southwest monsoon current reached the South Andaman Sea by 16 May, prior to the normal onset date, in association with the formation of a tropical storm over the Bay of Bengal. The unusual and prolonged trajectory of the system likely caused the observed delay in the further progress of the current over the Bay of Bengal. In addition, the modified flow pattern due to the tropical storm caused prolonged heat wave conditions, which extended more than 20 days over many parts of the country (e.g., coastal Andhra Pradesh, Orissa, northern parts of Tamil Nadu, etc.) during late May and early June. Maximum temperatures in several locations soared to above 50°C, and more than 1500 people were reported to have died due to heat stress. In Pakistan, the city of Jacobabad recorded a maximum temperature of 52°C. The extremely hot conditions, coupled with late onset over peninsular India, exacerbated the drought conditions in this area.

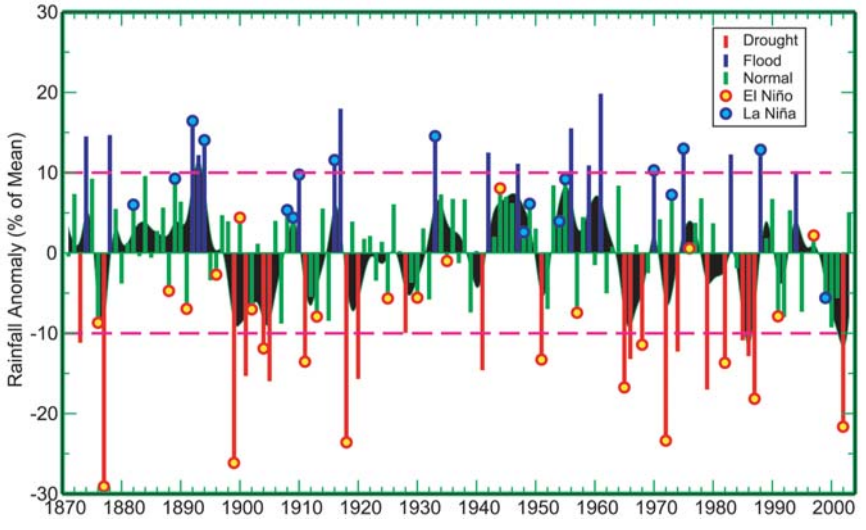

Fig. 6.41. The 1871–2003 summer monsoon seasonal rainfall anomalies (% of long-term mean) over the Indian subcontinent. Bar colors denote years with normal precipitation (green), floods (blue), and droughts (red), while the circles denote years with El Niño (yellow) or La Niña (blue) events in the equatorial Pacific Ocean.

Breaking the recent spell in the declining number of monsoon depressions (the number of depressions was 3, 4, 2, 1, and 0 in the years 1998,

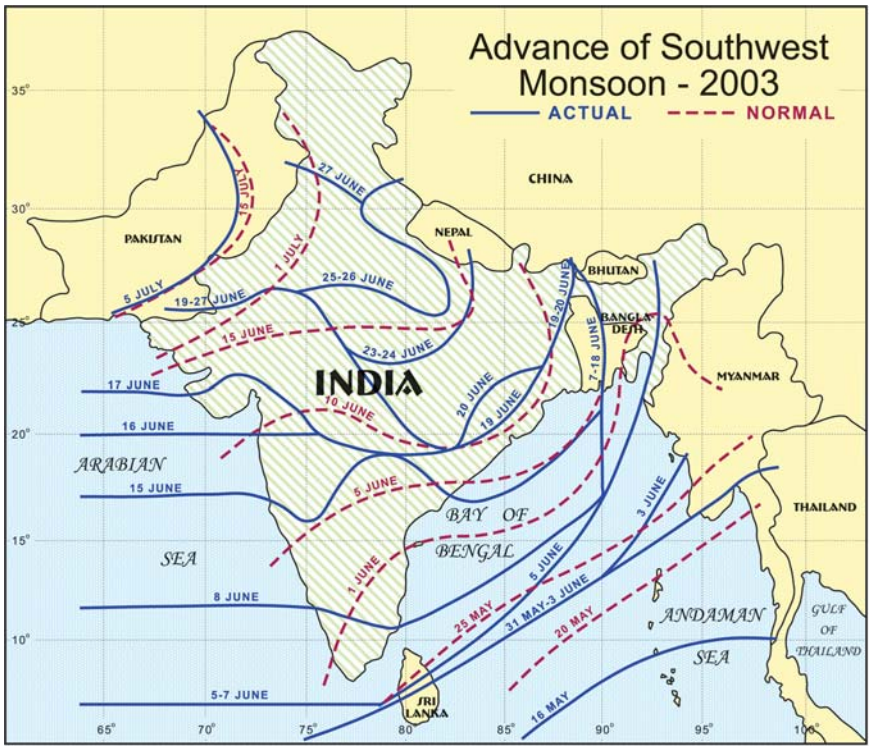

FIG. 6.42. Isochrones of the onset and advance of the summer monsoon in 2003 (solid), compared with the long-term mean dates of advance (dashed).

1999, 2000, 2001, and 2002, respectively), two depressions formed during the monsoon season of 2003 (25–28 July and 27–28 August), both in the Bay of Bengal. The July depression followed a westerly track and was active for about 1 week after crossing the West Bengal coast, and was associated with widespread and heavy rainfall over the central parts of the country. Conversely, the August depression over the northwest Bay of Bengal rapidly weakened into a broad low pressure area after crossing the coast. In addition to these two depressions, 12 low-pressure areas (one in June, four in July, three in August, and four in September) formed during the season, most of which originated as upper-tropospheric cyclonic disturbances, and these upper-level systems contributed to active monsoon conditions over the country. No tropical cyclones (category 1 or higher on the Saffir–Simpson scale) formed during the season; indeed, this added to the declining trend observed in the number of tropical cyclones in the north Indian Ocean during the monsoon season over the past two decades.

A notable feature of the summer monsoon rainfall in 2003 was its equitable distribution in space and time; devoid of any prolonged dry spell (see Fig. 6.43). Monthly as well as seasonal rainfall was within one standard deviation of the respective long-term average. During the first half of June, rainfall activity over peninsular India was quite subdued, primarily due to the late monsoon onset. However, rainfall activity increased during the latter half of the month, and was normal or above normal until the third week of August, with the exception of Karnataka and Kerala. In its final phase, the monsoon was relatively quiescent over the peninsula until the end of the season.

Overall, the first half of the monsoon season was associated with slightly above-average rainfall (109% in June, and 107% in July), while the second half was associated with slightly below-average rainfall (95% in August and 96% in September). Rainfall during the 2003 summer monsoon season was in excess (> 20% of normal) in 8 meteorological subdivisions, normal (−20% to +20%) in 23, and deficient (< 20%) in 5 subdivisions. The seasonal rainfall over the country as a whole was about 105% of its long-term mean. As mentioned above, the states of Karnataka and Kerala bore the brunt of maximum rainfall deficiency (see Fig. 6.44). The seasonal rainfall anomalies were −34% and −32% over the meteorological subdivisions of north interior Karnataka and Kerala, respectively. In fact, Kerala remained under rainfall deficits through-

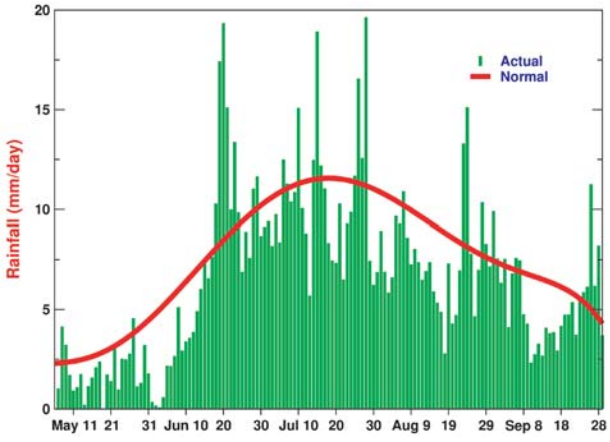

FIG. 6.43. The observed daily rainfall (mm day^{-1}) during the 2003 monsoon season, and the long-term daily mean precipitation (red line) over India.

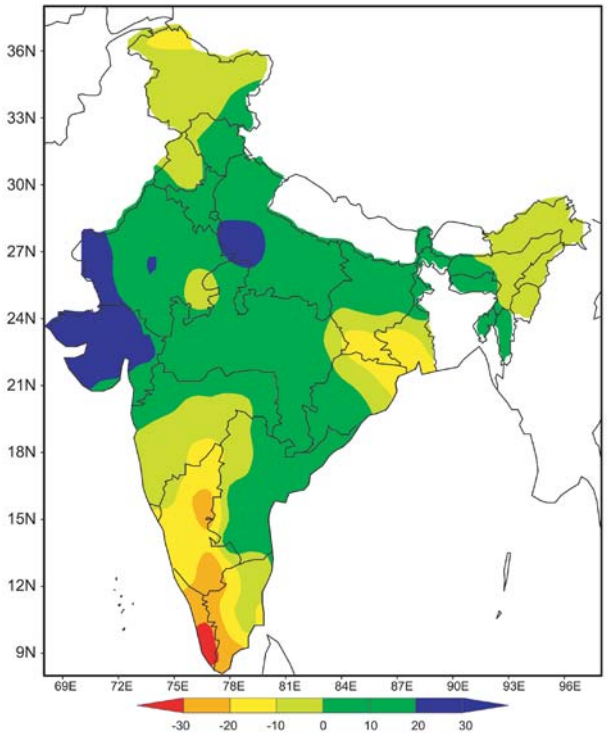

Fig. 6.44. Spatial patterns of the seasonal mean rainfall anomalies (% of long-term mean) over India during the monsoon season of 2003.

out the monsoon season. Coupled with the fact that these regions have received deficient rainfall over the past 3–4 yr, severe water shortages were reported not only in the respective areas, but also in the downstream regions due to reduced river levels.

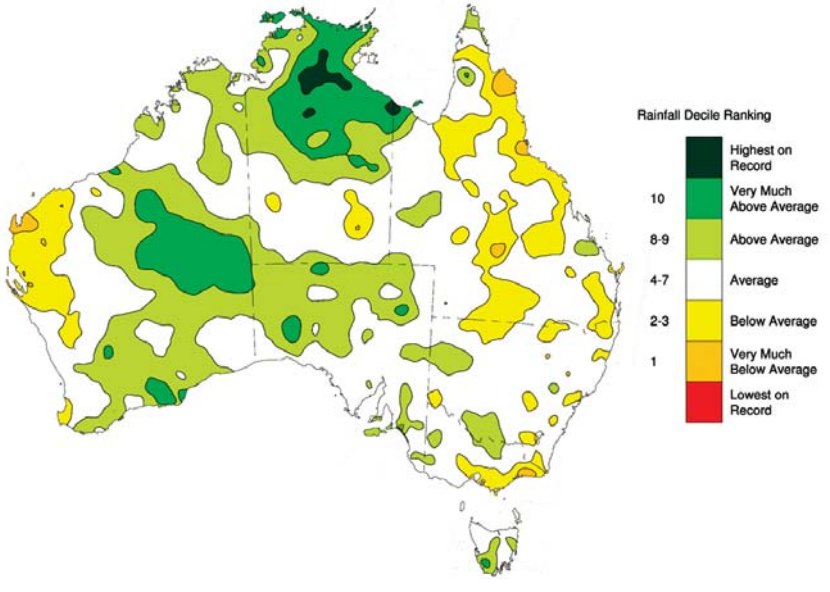

Fig. 6.45. Rainfall deciles determined for the period 1 Jan through 31 Dec 2003.

The summer monsoon began its withdrawal over Pakistan and western Rajasthan around 17 September, with a delay of ~2 weeks from the normal date. However, the withdrawal progressed briskly and coincided with the normal dates in most other parts of the country. It withdrew from the entire country by 15 October, which coincided with the normal date of withdrawal of the summer monsoon.

g. Australasia and the Southwest Pacific—A. Watkins[24] and J. Salinger[22]

i) Australia

The Australian climate of 2003 was largely influenced by the cessation of the El Niño warm event in the equatorial Pacific Ocean during the first half of the year, and a subsequent return to near-neutral ENSO conditions. A La Niña cold event failed to materialize, despite signs of its development during late May and early June, and the recovery from severe rainfall deficiencies that had accumulated during the 2002–03 Australian drought was slow to develop and spatially inhomogeneous. While a general return to near-normal rainfall patterns commenced during February, the hydrological, agricultural and societal impacts of one of Australia's worst droughts in its recorded meteorological history remained for much, if not all, of 2003.

(i) Rainfall

The Australian El Niño–related dry event lasted from March 2002 through January 2003. Analysis of rainfall records collected by the Australian Bureau of Meteorology for this 11-month period showed that 90% of the country received rainfall below that of the long-term median, with 56% of the country receiving rainfall in the lowest 10% (i.e., decile 1) of recorded totals (Australia-wide rainfall records commenced in 1900). This was the sixth greatest extent of decile-1 rainfall for any 11-month period on record. The extent of the drought, and the rainfall deficit recovery in 2003, was highlighted by the difference between the 2003 and 2002 rainfall totals for the period from February to December (not shown). Most regions in southern and eastern Australia received between 100 and 400 mm more rainfall during this period in 2003 than during the same period in 2002.

The general return to near-normal rainfall conditions for Australia during 2003 (Fig. 6.45) was highlighted by the mean Australia-wide rainfall total (476 mm) being almost equal to the 1961–90 normal base period (472 mm). Compared to the long-term record (Fig. 6.46), however, 2003 was the 37th wettest year for Australia out of 104 yr of observations, some 38 mm above the long-term median rainfall of 438 mm. Overall, 61% of the country experienced rainfall that was above the long-term median, which was significantly different than 2002 when only 18% of the country experienced wetter-than-normal conditions. Similarly, only 1.2% of the country experienced rainfall in the lowest 10% of recorded totals (decile 1) during 2003, compared to 36% the year before.

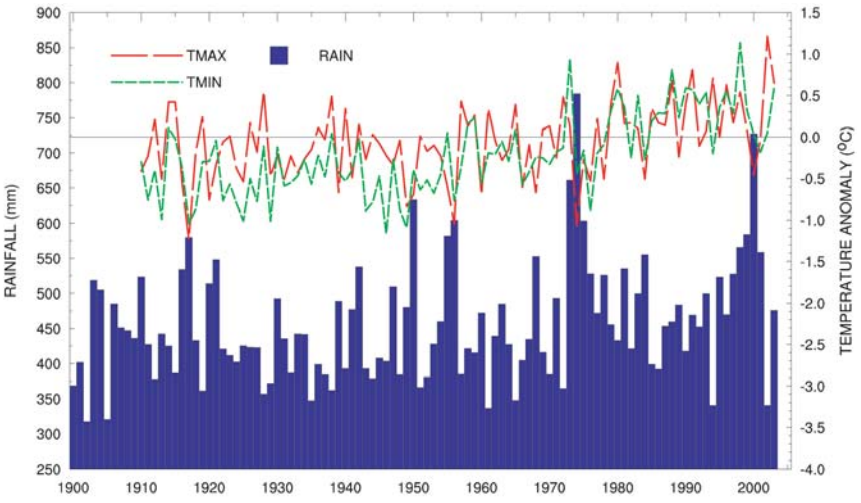

Fig. 6.46. Australia-wide annual mean precipitation (blue bars), along with the maximum (red line) and minimum (green line) temperature anomalies (°C) plotted with respect to the 1961–90 base period. The 1961–90 climatological normal rainfall for Australia is 472 mm.

Although the 2002/03 Australian meteorological drought subsided in mid-2003, the gradual return to near-normal conditions meant that the hydrological drought remained, with subsequent and severe impacts upon reservoirs. In Australia's second largest city, Melbourne, the period from March 2002 to February 2003 was the driest 12-month period since records commenced in 1855, with only 317 mm of accumulated precipitation. The low-water storages led to the establishment of fairly stringent water restrictions for the greater Melbourne area, Sydney, and Canberra. Ongoing dry conditions in southeastern Queensland saw storage dam levels fall to extremely low levels (generally just 20%–30% of capacity, with some less than 10%). Irrigation allowances were reduced or suspended in many major catchments in eastern Australia, impacting heavily on agricultural activities.

(ii) Temperatures

The slow return toward normal meteorological, agricultural, and hydrological conditions was likely impacted by the higher-than-normal daytime and nighttime temperatures, and the resulting increase in broad-scale evaporation rates. The Australia-wide maximum temperature anomaly for 2003 was the 6th highest on record (records commenced in 1910), with a value 0.65°C above the 1961–90 mean. Anomalies for the full year of up to +2.5°C were recorded in eastern Queensland (Fig. 6.47), while large parts of Queensland experienced anomalies of +1.5°C. Similarly, the minimum temperature anomaly was the fourth highest on record at +0.59°C, and again the largest deviations from normal were recorded in Queensland, with anomalies of over +1.5°C in the central and eastern parts of the state

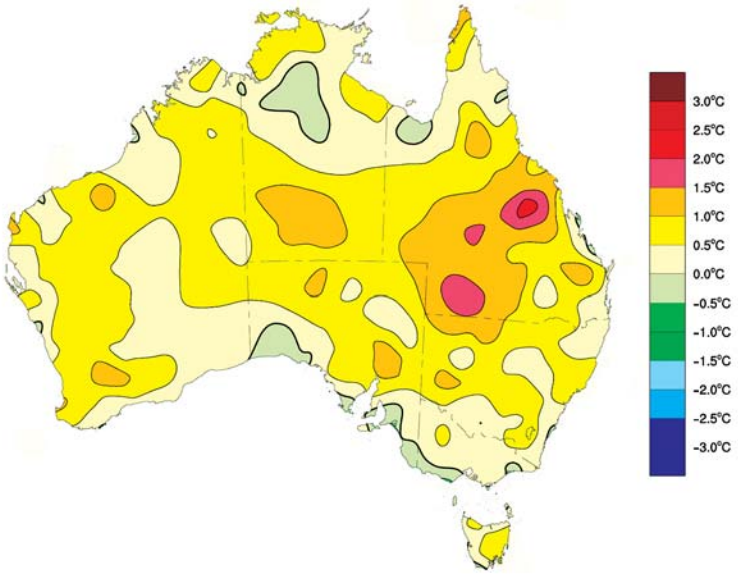

Fig. 6.47. Maximum temperature anomalies across Australia during 2003, with respect to the 1961–90 base period.

(not shown). Combined, the Australia-wide mean temperature anomaly of +0.62°C was the 6th highest on record, only 0.01°C less than the mean temperature anomaly for 2002. The significantly above-normal Australian temperatures of 2003 were the result of a fairly typical post–El Niño warm period, as heat from the November–December 2002 peak of the event dissipated over the following months, overlaid on the longer-term warming trend.

The latter half of 2003 was exemplified by a record-breaking heat wave during September in New South Wales, South Australia, and Victoria, as well as very high temperatures in the Northern Territory and Queensland. In New South Wales, White Cliffs and Menindee experienced maximum temperatures of 39.5°C, breaking the previous New South Wales September record of 38.8°C. Nine other locations in northern and western New South Wales also exceeded 38.8°C. In Victoria, Mildura's maximum temperature of 37.4°C broke the previous Victorian September record of 35.6°C. In South Australia, Moomba had a maximum of 41.4°C, breaking the previous South Australian September record of 40.5°C. Birdsville, Queensland, reached 42.4°C, and this new record fell just short of the all-time Queensland temperature record of 42.6°C. Another heat wave in northwest Western Australia late in the month broke the all-time Australian September record, when West Roebuck, near Broome, Western Australia, recorded 43.1°C on 27 September. In addition, Fitzroy Crossing Aerodrome reached 42.9°C, which exceeded the old mark of 42.8°C.

(iii) Bushfires

One of the major environmental impacts of the hot and dry conditions, both early in the year and as a result of residual conditions from 2002, was wildfire, particularly late in the Australian summer (early 2003). Major bushfires burned in New South Wales, Victoria, the Australian Capital Territory, Western Australia, and Tasmania during 2003. Fires ignited by lightning strikes in the alpine areas of southeast Australia affected New South Wales, the Australian Capital Territory and Victoria. These fires joined together to form a massive complex that burned for 59 days during January and February. Smoke and haze not only affected regions close to the fires themselves, but also spread over 200 km southwest to Melbourne, where on 20 January visibility was reduced to less than 3 km (Fig. 6.48). This fire, which burned over 1.1 million ha in Victoria alone, was the third largest fire in southeastern Australian history, after the "Black Friday" fires of January 1939, and the "Black Thursday" fires of February 1851.

Fig. 6.48. Smoke from the southeast Australian alpine fires of Jan/Feb 2003, which reached Melbourne, ~200 km to the southwest, on (left) 20 Jan 2003, and (right) the normal view 24 h later after the winds shifted to the south. (Photos taken from the Australian BOM Head Office, Melbourne.)

ii) Southwest Pacific

The 2002/03 El Niño event, although decaying, had a significant impact upon the southwest Pacific during the first 4 months of 2003. The event had a noticeable impact on the region's precipitation anomalies at the beginning of the year, with above-average rainfall over Kiribati and below-average rainfall over much of New Caledonia and Fiji. Fluctuations in the southwest Pacific climate continued for some months after the El Niño had dissipated. The final one-third to one-half of the year brought a more consistent climatic pattern to the southwest Pacific, because the equatorial Pacific Ocean settled into a near-neutral ENSO state.

SSTs, and, hence, mean air temperatures, were at least 0.5°C above average throughout much of the tropical southwest Pacific in 2003 (Fig. 6.49). The largest positive anomalies occurred along the equator, from Nauru, to the north of Rawaki Island, and eastward toward eastern Kiribati, with SSTs ~1.0°C above average. The year was also one of the warmest years on record for mean air temperatures in the Marquesas (0.9°C above average at Hiva Hoa) and the Tuamotu Islands (0.7°C above average at Takaroa) of French Polynesia. However, Fiji was fairly typical of the western half of the basin, with an annual mean air temperature 0.3°C above normal, which reflected the warmer-than-normal SSTs for much the southwest Pacific during 2003.

Above-average surface atmospheric pressures in the Coral Sea were observed in every month except March, leading to suppressed convection over the southern parts of the Solomon Islands, northern Vanuatu, and areas toward the date line. Suppressed convective activity was also observed in an extensive region along the equator from the date line eastward toward South America, including Eastern Kiribati and the Marquesas

Islands (Fig. 6.50). These two regions of decreased convection and high clouds led to prolonged dry periods for both Fiji and eastern Kiribati. The 2003 rainfall total at Willis Island was extremely low (358 mm)—only 32% of average. Likewise, Ono-i-lau in Fiji recorded 1068 mm (65% of average), with Hiva Hoa in the Marquesas Islands receiving 751 mm of rainfall (62% of average)—one of the lowest annual rainfall totals on record.

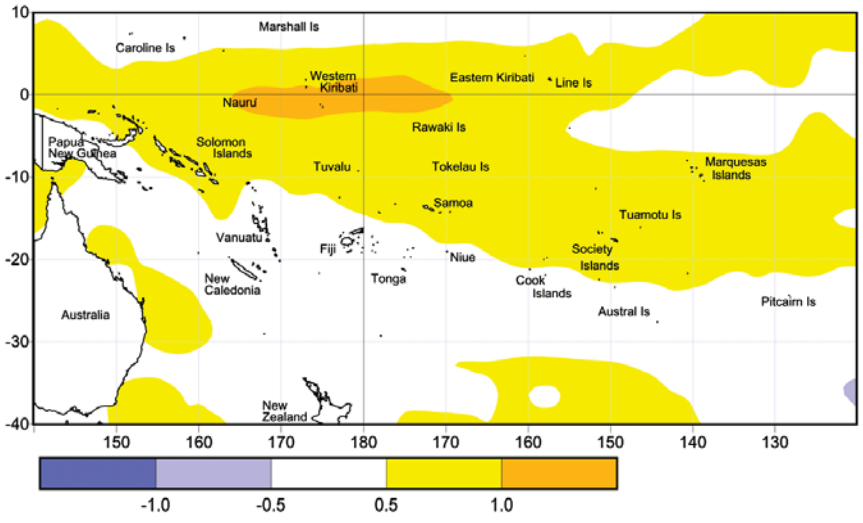

Fig. 6.49. Annually averaged SST anomalies (°C) for 2003 across the southwest Pacific basin (yellow/orange shading denotes warmer-than-average SSTs, and light-blue/blue shading denotes cooler-than-average SSTs).

Areas of enhanced convection affected the region north of Papua New Guinea, the Marshall Islands, and parts of southern French Polynesia during 2003. For the year, the SPCZ was generally farther north and east than usual. However, its main region of convective activity was concentrated in areas east of the date line from February to May, moving to areas west of the date line from September to November. This anomalous position of the SPCZ generated above-average annual precipitation in parts of New Caledonia, Tonga, and the southern Cook Islands.

In total, the 2002–03 tropical cyclone season brought 11 cyclones to the southwest Pacific, comparable to the long-term average of 10. Tropical Cyclone Erica in March was one of the strongest to hit New Caledonia in 50 yr, with gusts to 234 km h^{-1}. Unusually, two tropical cyclones developed very late in the season during June—Gina and Epi, both of which were relatively weak tropical storms. In this case, a Madden–Julian Oscillation event had just previously propagated over or near a relatively small region of warm SST anomalies in the western South Pacific, creating a set of antecedent conditions that were uniquely primed for such late tropical cyclogenesis events.

iii) New Zealand

Anticyclones were more prevalent during the entire year across New Zealand (Fig. 6.51), resulting in the driest year on record in some areas of southern New Zealand, with precipitation totals of only about 60% of normal. Rainfall was also well below average in north Canterbury and central Marlborough, with totals less than 75% of normal. For the year, there were at least 20 heavy rainfall events, of which 9 produced floods, mainly in the North Island. The year was also exceptionally sunny over much of the South Is-

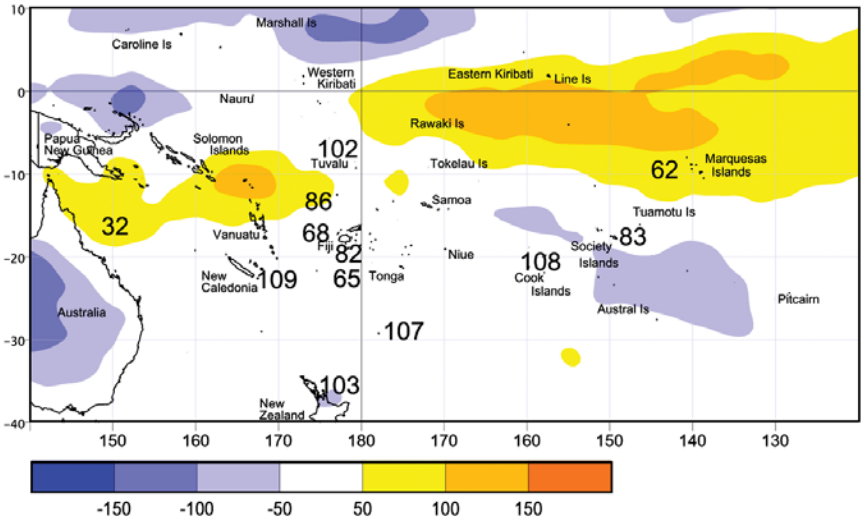

Fig. 6.50. Annually averaged OLR anomalies (W m^{-2}) for 2003, represented by shaded areas, and annual precipitation percentage of average, shown by numbers. Higher OLR values (yellow or orange) were associated with clearer skies and lower rainfall, while lower the OLR values (blue) were associated with cloudy conditions and typically higher average precipitation.

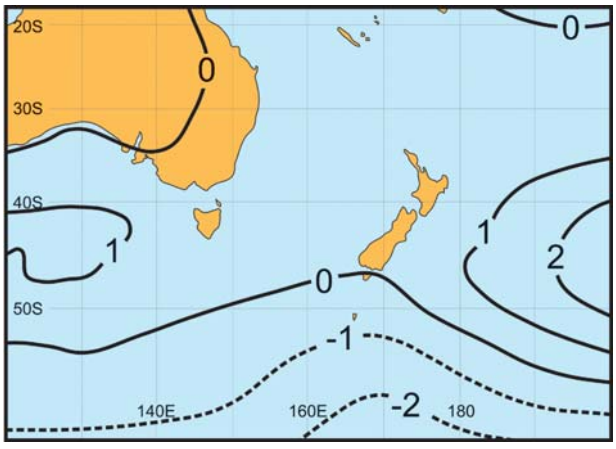

Fig. 6.51. Mean Sea Level Pressure (MSLP) anomaly map for 2003 over the New Zealand region (hPa).

land, with totals close to, or more than, 115% of normal in Nelson (which recorded 2707 sunshine hours, its second highest annual total on record), Westland, Canterbury, Otago, and Southland. Wellington, on the southern end of the North Island, also recorded its sunniest year on record. The anomalously sunny conditions generated above-average temperatures across New Zealand, with an average annual temperature during 2003 of 12.7°C, which was 0.1°C above the 1971–2000 mean.

The year began with more frequent easterlies over the North Island, with anticyclones to the southwest from January through April. As a result, January through the early part of May was very dry in the southwest of the North Island, as well as in eastern regions of both islands, and these anomalously dry conditions spread eastward toward the end of the year. In contrast, New Zealand experienced more frequent northwesterly flow in mid-May through August, with near-normal precipitation during this period.

Winter in New Zealand had a remarkably mild start, with the warmest June on record (records date back over 150 yr), with nationwide temperatures 2.0°C above average. However this was followed by an anomalously cold July. There were five significant snowfall events during the winter that affected low-lying areas. Cold and snowy weather struck New Zealand during the first week of July, where locally up to 30 cm (~12 in) of snow fell in the eastern South Island and the North Island high country. This snowstorm was described as one of the worst in 50 yr, causing thousands of power outages to homes and businesses, closing airports, and stranding hundreds of motorists.

The latter part of the year was dominated by variable west-to-southwesterly flow, which produced anomalously dry conditions along with soil moisture deficits that became quite severe throughout Otago, Canterbury, and central Marlborough, and significant in Wairarapa, Nelson, and parts of Northland. However, severe northwesterly gales (up to 176 km h^{-1} at South West Cape) affected central and eastern New Zealand in September, along with several destructive tornadoes on the West Coast on 18 September. October brought late frosts and snowfalls to the South Island hill country, which resulted in thousands of newborn lambs lost to exposure.

At the end of the year, a heat wave affected the South Island, with temperatures reaching 36.0°C at Middlemarch in eastern Otago on the 31 December—the highest December temperature on record in the Middlemarch area, and equal to the highest for December for the Otago region (36.0°C at Alexandra in December 1988).

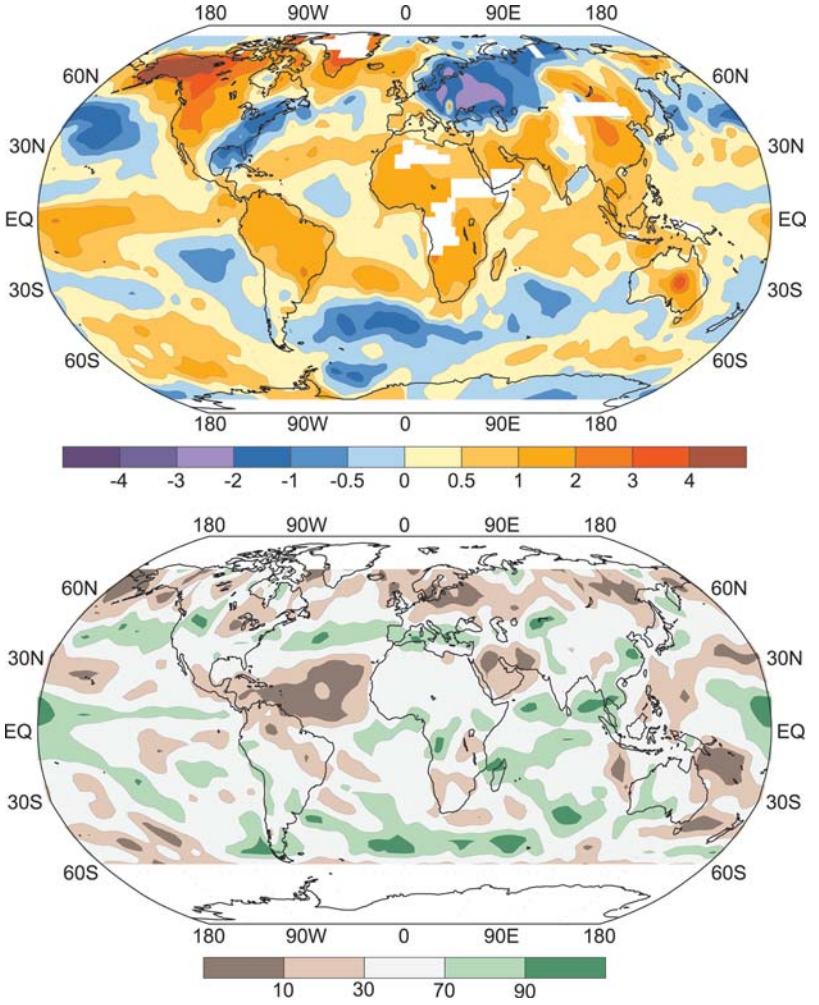

Fig. 7.1. Dec 2002–Feb 2003 (top, °C) surface temperature anomalies and (bottom) precipitation percentiles based on a gamma distribution fit to the 1979–2000 base period. Temperature anomalies (1971–2000 base period) were based on station data over land and sea surface temperature over water. Precipitation data were obtained from a combination of rain gauge observations and satellite-derived precipitation estimates (Janowiak and Xie 1999). The analysis was omitted in data-sparse regions (white areas).

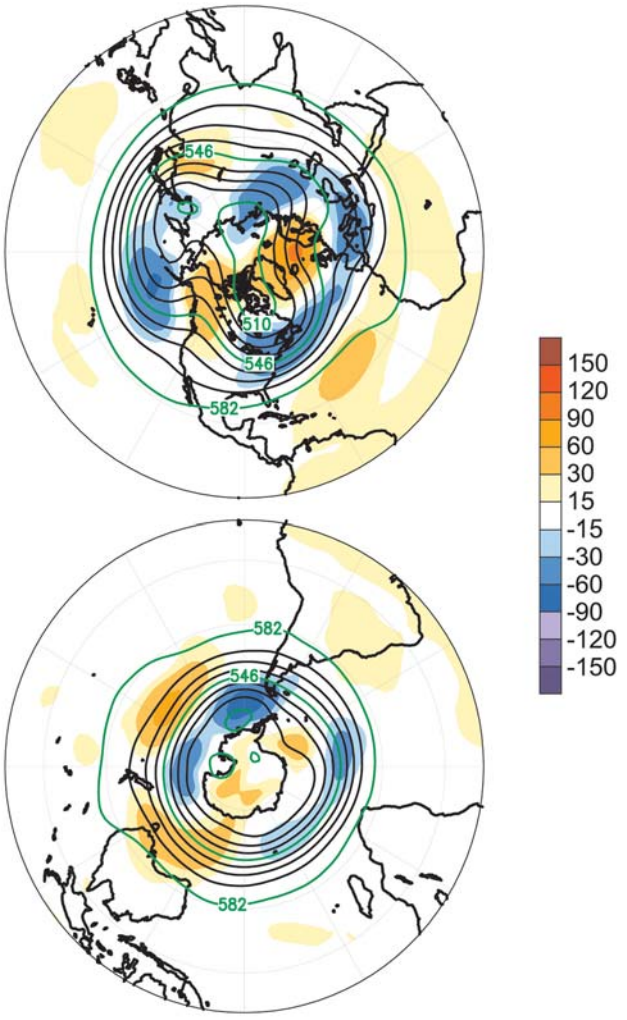

Fig. 7.2. Dec 2002–Feb 2003 (top) Northern Hemisphere and (bottom) Southern Hemisphere 500-hPa geopotential heights (contour interval is 9 dam) and anomalies (shading). Anomalies are departures from the 1979–2000 base period means.

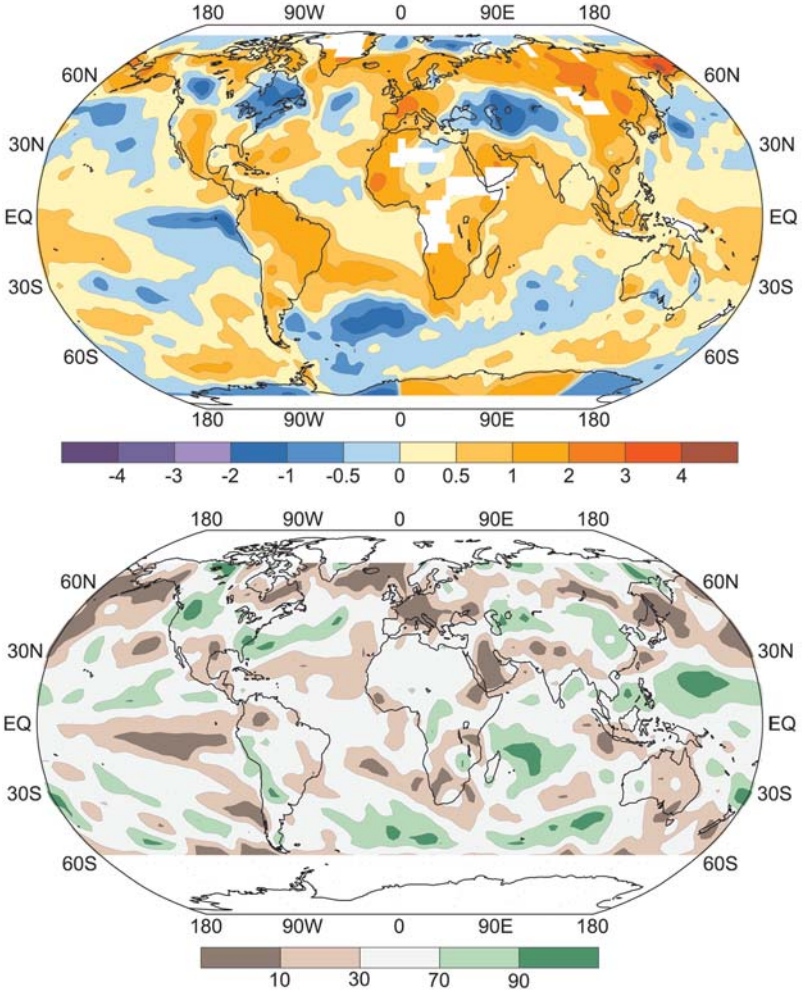

FIG. 7.3. Mar–May 2003 (top, °C) surface temperature anomalies and (bottom) precipitation percentiles based on a gamma distribution fit to the 1979–2000 base period. Temperature anomalies (1971–2000 base period) were based on station data over land and sea surface temperature over water. Precipitation data were obtained from a combination of rain gauge observations and satellite-derived precipitation estimates (Janowiak and Xie 1999). The analysis was omitted in data-sparse regions (white areas).

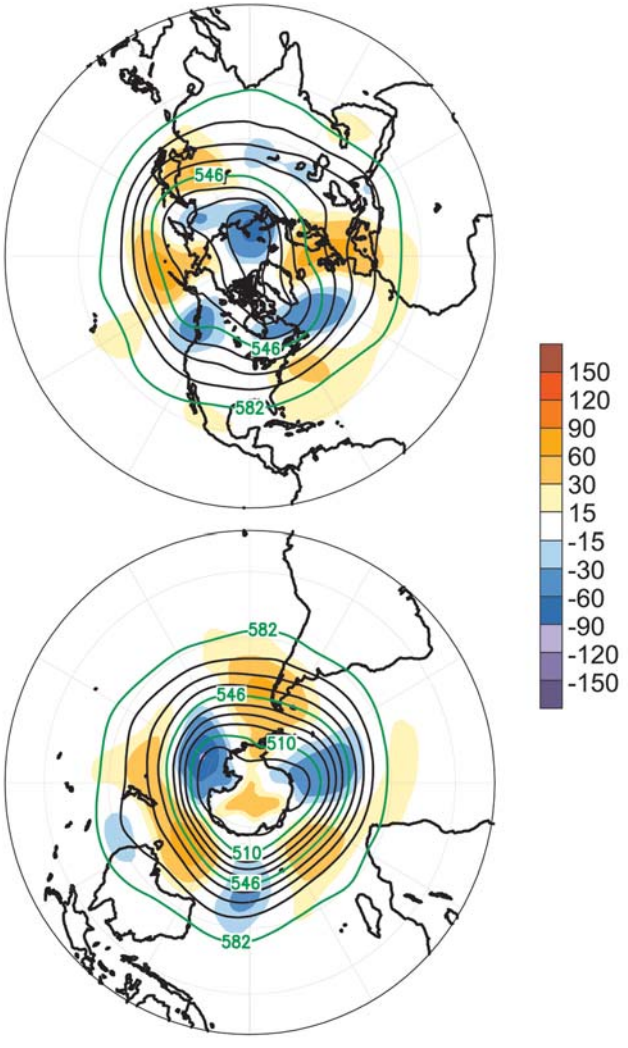

FIG. 7.4. Mar–May 2003 (top) Northern Hemisphere and (bottom) Southern Hemisphere 500-hPa geopotential heights (contour interval is 9 dam) and anomalies (shading). Anomalies are departures from the 1979–2000 base period means.

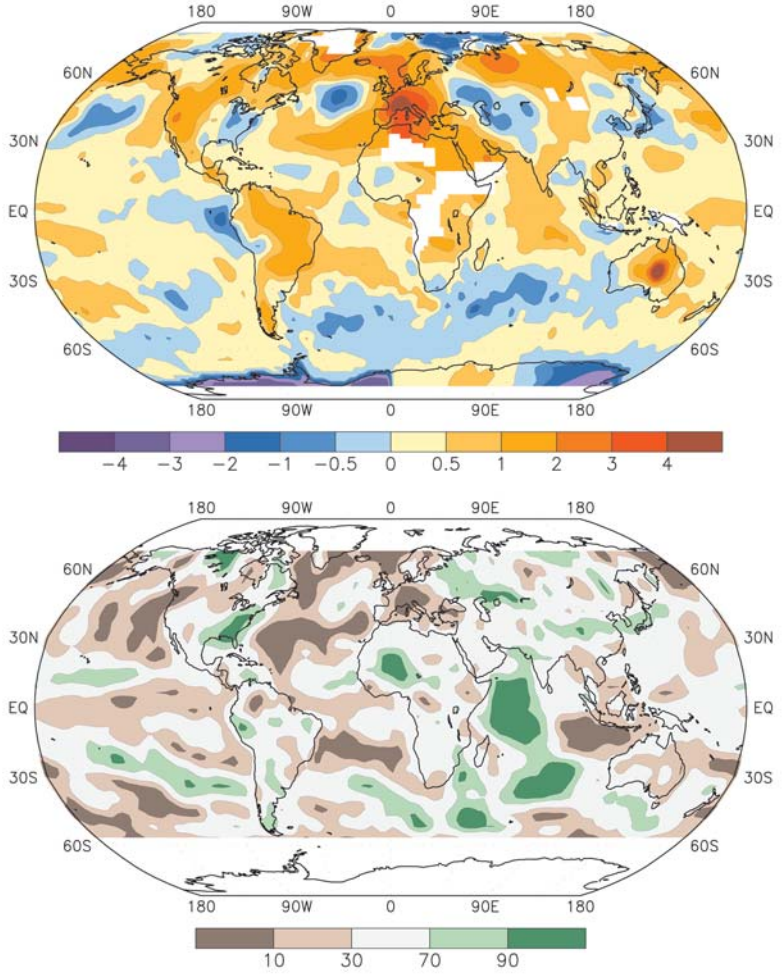

FIG. 7.5 Jun–Aug 2003 (top, °C) surface temperature anomalies and (bottom) precipitation percentiles based on a gamma distribution fit to the 1979–2000 base period. Temperature anomalies (1971–2000 base period) were based on station data over land and sea surface temperature over water. Precipitation data were obtained from a combination of rain gauge observations and satellite-derived precipitation estimates (Janowiak and Xie 1999). The analysis was omitted in data-sparse regions (white areas).

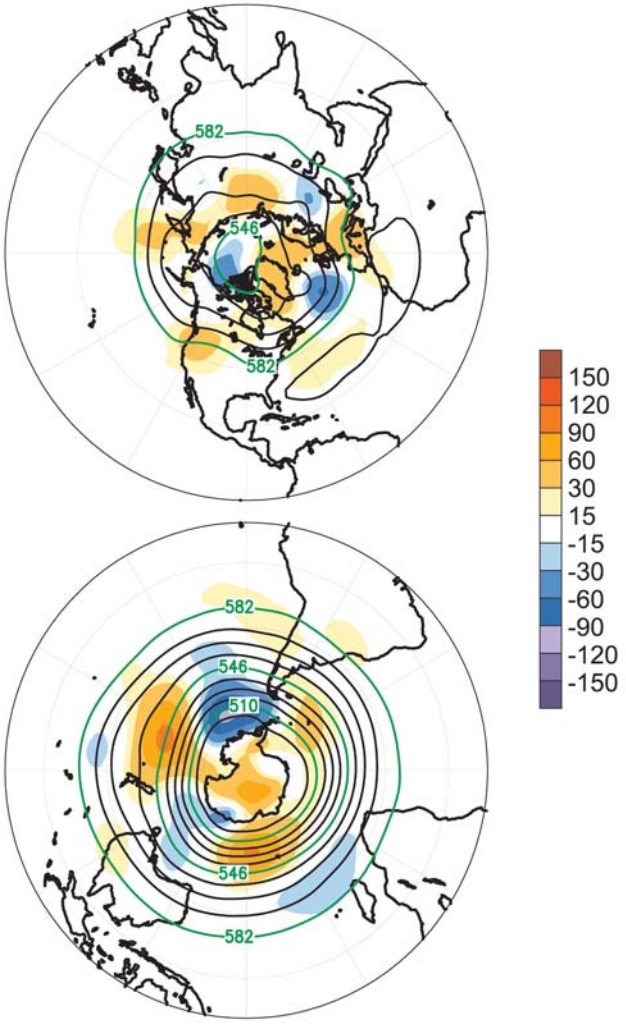

FIG. 7.6. Jun–Aug 2003 (top) Northern Hemisphere and (bottom) Southern Hemisphere 500-hPa geopotential heights (contour interval is 9 dam) and anomalies (shading). Anomalies are departures from the 1979–2000 base period means.

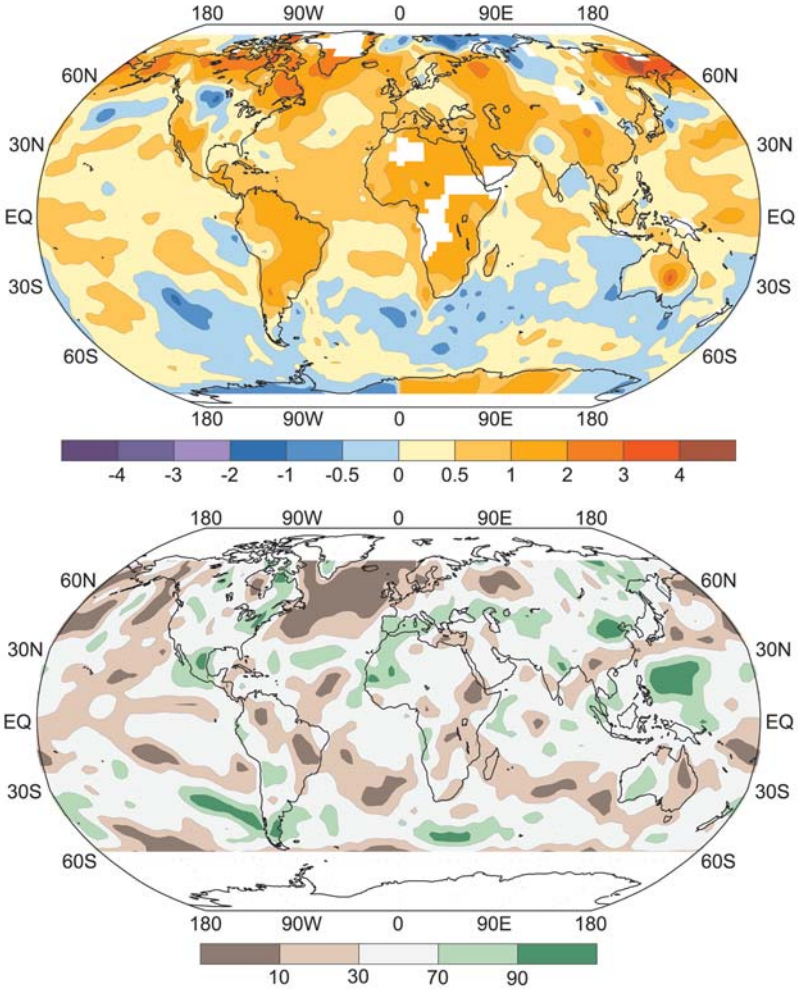

FIG. 7.7. Sep–Nov 2003 (top, °C) surface temperature anomalies and (bottom) precipitation percentiles based on a gamma distribution fit to the 1979–2000 base period. Temperature anomalies (1971–2000 base period) were based on station data over land and sea surface temperature over water. Precipitation data were obtained from a combination of rain gauge observations and satellite-derived precipitation estimates (Janowiak and Xie 1999). The analysis was omitted in data-sparse regions (white areas).

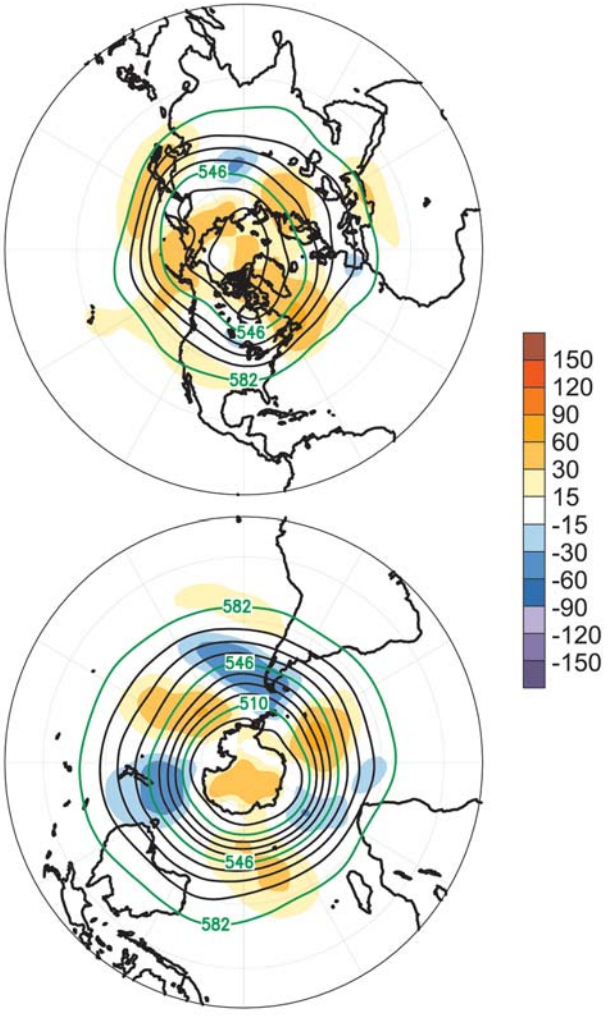

FIG. 7.8. Sep–Nov 2003 (top) Northern Hemisphere and (bottom) Southern Hemisphere 500-hPa geopotential heights (contour interval is 9 dam) and anomalies (shading). Anomalies are departures from the 1979–2000 base period means.

ACKNOWLEDGMENTS. This assessment would not have been possible without assistance and contributions from many scientists around the world. These scientists are named in the appendix and include a broad cross section of expertise from within the NOAA community, various federal laboratories, universities, and other institutions across the globe. We would like to thank them all for their timely and valuable input. We would also like to thank the anonymous reviewers whose comments and suggestions improved this article. Other reviews from Sharon LeDuc, David Easterling, Gerry Bell, and Wassila Thiaw were also unquestioningly helpful. Acknowledgement must also be given to Paul Llanso of the WMO for his invaluable suggestions, editing assistance, and liaison with the WMO. Special acknowledgement must be given to Sara Veasey at NCDC for the extensive time and graphical expertise she used in preparing this document. This assessment was supported by a grant from the NOAA Office of Global Program's Climate Change Data and Detection Program, with additional funding provided by the WMO's World Climate Research Programme.

APPENDIX: CONTRIBUTORS

National Climatic Data Center
- Scott Stephens
- Candace Tankersley
- Trevor Wallis
- Richard Heim
- Stuart Hinson

Hadley Centre for Climate Prediction and Research
- Nick Rayner

British Antarctic Survey
- Gareth Marshall

University of Illinois at Urbana–Champaign
- Bill Chapman

NOAA/Climate Monitoring and Diagnostics Laboratory/OAR
- C. D. Keeling
- K. Thoning
- S. A. Montzka
- J. H. Butler
- T. Thompson
- D. Mondeel
- J. Elkins
- P. C. Novelli
- E. J. Dlugokencky

Rutgers University
- Thomas Estilow

REFERENCES

Bailey, C., and Coauthors, 2003: An objective climatology, classification scheme, and assessment of sensible weather impacts for Appalachian cold-air damming. *Wea. Forecasting*, **18**, 641–661.

Barnston, A. G., and R. E. Livezey, 1987: Classification, seasonality and persistence of low-frequency atmospheric circulation patterns. *Mon. Wea. Rev.*, **115**, 1083–1126.

Behringer, D. W., M. Ji, and A. Leetmaa, 1998: An improved coupled model for ENSO prediction and implications for ocean initialization. Part I: The ocean data assimilation system. *Mon. Wea. Rev.*, **126**, 1013–1021.

Belchansky, G. I., D. C. Douglas, and N. G. Platonov, 2004: Duration of the Arctic sea ice melt season: Regional and interannual variability, 1979–2001. *J. Climate*, **17**, 67–80.

Bell, G. D., 2003: The 2002 Atlantic hurricane season. *State of the Climate in 2002,* A. M. Waple and J. H. Lawrimore, Eds., *Bull. Amer. Meteor. Soc.*, **84**, S1–S68.

——, and L. F. Bosart, 1988: Appalachian cold-air damming. *Mon. Wea. Rev.*, **116**, 137–161.

——, and Coauthors, 1999: Climate Assessment for 1998. *Bull. Amer. Meteor. Soc.*, **80**, S1–S48.

——, and Coauthors, 2000: Climate Assessment for 1999. *Bull. Amer. Meteor. Soc.*, **81**, S1–S50.

Beniston, M., 2004: The 2003 heat wave in Europe: A shape of things to come? An analysis based on Swiss climatological data and model simulations. *Geophys. Res. Lett.*, **31**, L02204, doi:10.1029/2003GL01885.

Bruhwiler, L. M., E. S. Kasischke, E. J. Dlugokencky, and P. Tans, 2000: Boreal biomass burning during 1998 and anomalous northern hemispheric CO. *EOS, Trans. Amer. Geophys. Union*, **81**, 260.

Chapman, W. L. and J. E. Walsh, 1993: Recent variations of sea ice and air temperature in high latitudes. *Bull. Amer. Meteor. Soc.*, **74**, 2–16.

Chelliah, M., and G. D. Bell, 2004: Tropical multidecadal and interannual climate variations in the NCEP–NCAR Reanalysis. *J. Climate*, **17,** 1777–1803.

Christy, J. R., R. W. Spencer, W. B. Norris, W. D. Braswell, and D. E. Parker, 2003: Error estimates of version 5.0 of MSU/AMSU bulk atmospheric temperatures. *J. Atmos. Oceanic Technol.*, **20**, 613–629.

Ciais, P., P. P. Tans, M. Trolier, J. W. C. White, and R. J. Francey, 1995: A large Northern Hemisphere terrestrial CO_2 sink indicated by the $^{13}C/^{12}C$ ratio of atmospheric CO_2. *Science*, **269**, 1098–1102.

Conway, T. J., P. P. Tans, L. S. Waterman, K. W. Thoning, D. R. Kitzis, K. A. Masarie, and N. Zhang, 1994: Evidence for interannual variability of the carbon cycle from the NOAA CMDL global air sampling network. *J. Geophys. Res*., **99**, 22 831–22 855.

Cook, E. R., 2000. *Niño-3 Index Reconstruction.* IGBP PAGES/WDCA Contribution Series 2000-052, World Data Center for Paleoclimatology. [Available online at ftp://ftp.ngdc.noaa.gov/paleo/treering/reconstructions/nino3_recon.txt.]

——, D. M. Meko, D. W. Stahle, and M. K. Cleaveland, 1999: Drought reconstructions for the continental United States. *J. Climate*, **12**, 1145–1162.

Dai, A., I. Y. Fung, and A. D. Del Genio, 1997: Surface observed global land precipitation variations during 1900–88. *J. Climate*, **10**, 2943–2961.

Daniel, J. S., and S. Solomon, 1998: On the climate forcing of carbon monoxide. *J. Geophys. Res.,* **103**, 13 249–13 260.

——, ——, R. W. Portmann, and R. R. Garcia, 1999: Stratospheric ozone destruction: The importance of bromine relative to chlorine. *J. Geophys. Res.*, **104**, 23 871–23 880.

Dlugokencky, E. J., S. Houweling, L. Bruhwiler, K. A. Masarie, P. M. Lang, J. B. Miller, and P. P. Tans, 2003: Atmospheric methane levels off: Temporary pause or new steady state? *Geophys. Res. Lett.,* **30**, 1992, doi:10.1029/2003GL018126.

Drobot, S. D., and M. R. Anderson, 2001: An improved method for determining snowmelt onset dates over Arctic sea ice using Scanning Multi-channel Microwave Radiometer and Special Sensor Microwave/Imager data. *J. Geophys. Res.,* **104**, 24 033–24 049.

——, and J. A. Maslanik, 2003: Interannual variability in summer Beaufort Sea ice conditions: Relationship to spring and summer surface and atmospheric variability. *J. Geophys. Res.*, **108**, 3233, doi:10.1029/2002JC001537.

Folland, C. K., and Coauthors, 2001a: Observed climate variability and change. *Climate Change 2001: The Scientific Basis*, J. T. Houghton et al., Eds., Cambridge University Press, 99–181.

——, and Coauthors, 2001b: Global temperature change and its uncertainties since 1861. *Geophys. Res. Lett*., **28**, 2621–2624.

Forbes, G. S., D. W. Thomson, and R. A. Anthes, 1987: Synoptic and mesoscale aspects of an Appalachian ice storm associated with cold-air damming. *Mon. Wea. Rev*., **115**, 564–591.

Fujita, T. T., 1971: Proposed characterization of tornadoes and hurricanes by area and intensity. SMRP No. 91, University of Chicago.

Gadgil, S. J., P. V. Joseph, and N. V. Joshi, 1984: Ocean-atmosphere coupling over monsoon regions. *Nature*, **312**, 141–143.

Goldenberg, S. B., and L. J. Shapiro, 1996: Physical mechanisms for the association of El Niño and West African rainfall with Atlantic major hurricanes. *J. Climate*, **9**, 1169–1187.

——, C. W. Landsea, A. M. Mestas-Nuñez, and W. M. Gray, 2001: The recent increase in Atlantic hurricane activity: Causes and implications. *Science*, **293**, 474–479.

GPCC, 1998: The Global Precipitation Climatology Centre. [Available online at http://gpcc.dwd.de.]

Gray, W. M., 1984: Atlantic seasonal hurricane frequency. Part 1: El Niño and 30 mb quasi-biennial oscillation influences. *Mon. Wea. Rev.*, **112**, 1649–1668.

Hall, B. D., and Coauthors, 2002: Halocarbons and other atmospheric trace species. *Climate Monitoring and Diagnostics Laboratory Summary Report No. 25, 1998–1999*, NOAA Oceanic and Atmospheric Research, D. B. King, R. C. Schnell, and R. M. Rosson, Eds., 154 pp.

Halpert, M. S., and G. D. Bell, 1997: Climate Assessment for 1996. *Bull. Amer. Meteor. Soc*., **78**, S1–S49.

——, and ——, 2003: ENSO and the tropical Pacific. *State of the Climate in 2002*, A. M. Waple and J. H. Lawrimore, Eds., *Bull. Amer. Meteor. Soc*., **84**, S1–S68.

Hare, S. R., and N. J. Mantua, 2000: Empirical evidence for North Pacific regime shifts in 1977 and 1989, *Progress in Oceanogr*aphy, Vol. 47, Pergamon, 103–145.

Hastenrath, S., 1990: Decadal-scale changes of the circulation in the tropical Atlantic sector associated with Sahel drought. *Int. J. Climatol*., **10**, 459–472.

——, L. Greischar, and J. Van Heerden, 1995: Prediction of the summer rainfall over South Africa. *J. Climate*, **8**, 1511–1518.

Heim, R. R, Jr., 2002: A review of 20th century drought indices used in the United States. *Bull. Amer. Meteor. Soc.,* **83**, 1149–1165.

Horel, J. D., and J. M. Wallace, 1981: Planetary-scale phenomena associated with the Southern Oscillation. *Mon. Wea. Rev.,* **109**, 813–829.

Horton, E. B., C. K. Folland, and D. E. Parker, 2001: The changing incidence of extremes in worldwide and Central England temperatures to the end of the twentieth century. *Climatic Change*, **50**, 267–295.

Hurrell, J. W., 1995: Decadal trends in the North Atlantic Oscillation and relationships to regional temperature and precipitation. *Science*, **269**, 676–679.

Jacka, T. H and W. F. Budd, 1998: Detection of temperature and sea ice extent changes in the Antarctic and Southern Ocean. *Ann. Glaciol.,* **27**, 553–559.

Janicot, S., 1992: Spatiotemporal variability of West African rainfall. Part II: Associated surface and airmass characteristics. *J. Climate*, **5**, 499–511.

Janowiak, J. E., and P. Xie, 1999: CAMS–OPI: A global satellite–rain gauge merged product for real-time precipitation monitoring applications. *J. Climate*, **12**, 3335–3342.

Jauregui, E., 2003: Climatology of landfalling hurricanes and tropical storms in Mexico. *Atmosfera*, **16**, 193–204.

Johannessen, O. M., and Coauthors, 2004: Arctic climate change—Observed and modeled temperature and sea ice variability. *Tellus,* in press.

Jones, P. D., 1994: Hemispheric surface air temperature variations: A reanalysis and an update to 1993. *J. Climate*, **7**, 1794–1802.

——, and A. Moberg, 2003: Hemispheric and large-scale surface air temperature variations: An extensive revision and an update to 2001. *J. Climate*, **16**, 206–223.

——,T. J. Osborn, K. R. Briffa, C. K. Folland, B. Horton, L. V. Alexander, D. E. Parker, and N. A. Rayner, 2001: Adjusting for sampling density in grid-box land and ocean surface temperature time series. *J. Geophys. Res.,* **106,** 3371–3380.

JTWC, 2004: Joint Typhoon Warning Center best track dataset. [Available online at https://metoc.npmoc.navy.mil/jtwc/best tracks/.]

Karl, T. R., C. N. Williams, F. T. Quinlan, and T. A. Boden, 1990: *United States Historical Climatology Network.* Carbon Dioxide Information and Analysis Center, Environmental Science Division Publication 3404.

Kasischke, E. S., and Coauthors, 2000: Contributions of 1998 fires in the boreal forest to atmospheric concentrations of carbon monoxide and methane. *EOS, Trans. Amer. Geophys. Union*, **81**, 260.

Keeling, C. D., T. P. Whorf, M. Wahlen, and J. Vanderplicht, 1995: Interannual extremes in the rate of rise of atmospheric carbon dioxide since 1980. *Nature*, **375**, 666–670.

Landsea, C. W., 1993: A climatology of intense (or major) Atlantic hurricanes. *Mon. Wea. Rev.*, **121**, 1703–1713.

——, and W. M. Gray, 1992: The strong association between Western Sahelian monsoon rainfall and intense Atlantic hurricanes. *J. Climate*, **5**, 435–453.

——, R. A. Pielke, A. M. Mestas-Nuñez, and J. A. Knaff, 1999: Atlantic basin hurricanes: Indices of climatic changes. *Climatic Change*, **42**, 89–129.

Langenfelds, R. L., R. J. Francey, B. C. Pak, L. P. Steele, J. Lloyd, C. M. Trudinger, and C. E. Allison, 2002: Interannual growth rate variations of atmospheric CO_2 and its $d^{13}C$, H_2, CH_4, and CO between 1992 and 1999 linked to biomass burning. *Global Biogeochem. Cyc.*, **16**, 1048, doi:10.1029/2001GB001466.

Lawrimore, J. H., and Coauthors, 2001: Climate Assessment for 2000. *Bull. Amer. Meteor. Soc.*, **82** (June), S1–S55.

Marland, G. and Coauthors, 2003: The climatic impacts of land surface change and carbon management, and the implications for climate-change mitigation policy. *Climate Policy*, **3**, 149–157

Maslanik, J. A., M. C. Serreze, and T. Agnew, 1999: On the record reduction in 1998 western Arctic sea ice cover. *Geophys. Res. Lett.*, **26**, 1905–1908.

Mears, C. A., M. C. Schabel, and F. J. Wentz, 2003: A reanalysis of the MSU channel 2 tropospheric temperature record. *J. Climate*, **16**, 3650–3664.

Mestas-Nuñez, A. M., and D. B. Enfield, 1999: Rotated global modes of non-ENSO sea surface temperature variability. *J. Climate*, **12**, 2734–2746.

Mo, K. C., and V. E. Kousky, 1993: Further analysis of the relationship between circulation anomaly patterns and tropical convection. *J. Geophys. Res.*, **98**, 5103–5113.

Montzka, S. A., and P. J. Fraser, 2003: Controlled substances and other source gases. *Scientific Assessment of Ozone Depletion: 2002 Global Ozone Research and Monitoring Project*, WMO Report No. 47.

——, J. H. Butler, J. W. Elkins, T. M. Thompson, A. D. Clarke, and L. T. Lock, 1999: Present and future trends in the atmospheric burden of ozone-depleting halogens. *Nature,* **398**, 690–694.

——, ——, J. H. Butler, B. D. Hall, D. J. Mondeel, and J. W. Elkins, 2003: A decline in tropospheric organic bromine, *Geophys. Res. Lett.,* **30**, 1826, doi:10.1029/2003GL017745.

Nakicenovic, N., and Coauthors, 2000: *IPCC Special Report on Emissions Scenarios*. Cambridge University Press, 599 pp.

Novelli, P. C., K. A. Masarie, P. M. Lang, B. D. Hall, R. C. Myers, and J. C. Elkins, 2003: Reanalysis of tropospheric CO trends: Effects of the 1997–1998 wildfires. *J. Geophys. Res.* **108**, 4464, doi:10.1029/2002JD003031.

Parker, D. E., C. K. Folland, and M. Jackson, 1995: Marine surface temperature: Observed variations and data requirements. *Climatic Change*, **31**, 559–600.

Peterson, T. C., and R. S. Vose, 1997: An overview of the Global Historical Climatology Network temperature database. *Bull. Amer. Meteor. Soc.*, **78**, 2837–2849.

Prather, M. J., 1996: Natural modes and time scales in atmospheric chemistry: Theory, GWPs for CH_4 and CO, and runaway growth. *Geophys. Res. Lett.,* **23**, 2597–2600.

Quayle, R. G., T. C. Peterson, A. N. Basist, and C. S. Godfrey, 1999: An operational near-real-time global temperature index. *Geophys. Res. Lett.*, **26**, 333–335.

Reed, R. J., D. C. Norquist, and E. E. Recker, 1977: The structure and properties of African wave disturbances as observed during Phase III of GATE. *Mon. Wea. Rev.*, **105**, 317–333.

Ropelewski, C. F., and M. S. Halpert, 1987: Global and regional scale precipitation patterns associated with the El Niño/Southern Oscillation. *Mon. Wea. Rev.*, **115**, 1606–1626.

——, and ——, 1989: Precipitation patterns associated with the high index phase of the Southern Oscillation. *J. Climate*, **2**, 268–284.

——, and ——, 1996: Quantifying Southern Oscillation–precipitation relationships. *J. Climate*, **9**, 1043–1059.

Rudolf, B., H. Hauschild, W. Rueth, and U. Schneider, 1994: Terrestrial precipitation analysis: Operational method and required density of point measurements. *Global Precipitation and Climate Change*, M. Desbois and F. Desalmond, Eds., NATO ASI Series I, Vol. 26, Springer-Verlag, 173–186.

Serreze, M. C., and Coauthors, 2003: A record minimum arctic sea ice extent and area in 2002. *Geophys. Res. Lett.*, **30**, 1110, doi:10.1029/2002GL016406.

Shapiro, L. J., 1989: The relationship of the quasi-biennial oscillation to Atlantic tropical storm activity. *Mon. Wea. Rev.*, **117**, 1545–1552.

Simpson, R. H., 1974: The hurricane disaster potential scale. *Weatherwise*, **27**, 169–186.

Smith, T. M., and R. W. Reynolds, 1998: A high-resolution global sea surface temperature climatology for the 1961–90 base period. *J. Climate*, **11**, 3320–3323.

Stammerjohn, S. E., and R. C. Smith, 1997: Opposing Southern Ocean climate patterns as revealed by trends in regional sea ice coverage. *Climatic Change*, **37**, 617–639.

Stone, R. S, E. G. Dutton, J. M. Harris, and D. Longenecker, 2002: Earlier spring snowmelt in northern Alaska as an indicator of climate change. *J. Geophys. Res.,* **107**, 4089, 10.1029/2000JD000286.

Swetnam, T. W., and J. L. Betancourt, 1990: Fire-Southern Oscillation relations in the southwestern United States. *Science*, **249**, 1017–1020.

Thiaw, W. M., A. B. Barnston, and V. Kumar, 1999: Predictions of African rainfall on the seasonal time scale. *J. Geophys. Res.*, **104**, 31 589–31 597.

Thompson, D. W. J., and J. M. Wallace, 1998: The Arctic Oscillation signature in the wintertime geopotential height and temperature fields. *Geophys. Res. Lett.*, **25**, 1297–1300.

Vaughan, D. G., and C. S. M. Doake, 1996: Recent atmospheric warming and retreat of ice shelves on the Antarctic Peninsula. *Nature*, **379**, 328–331.

Vinnikov, K. Y., and N. C. Grody, 2003: Global warming trend of mean tropospheric temperature observed by satellites. *Science*, **302**, 269–272.

——, and Coauthors, 1999: Global warming and Northern Hemisphere sea ice extent. *Science*, **286**, 1934–1937.

Vose, R. S., R. L. Schmoyer, P. M. Steurer, T. C. Peterson, R. Heim, T. R. Karl, and J. Eischeid, 1992: *The Global Historical Climatology Network: Long-Term Monthly Temperature, Precipitation, Sea Level Pressure, and Station Pressure Data.* Carbon Dioxide Information Analysis Center, Oak Ridge National Laboratory, Rep. ORNL/CDIAC-53, NDP-041, 189 pp.

Waple, A. M., and Coauthors, 2002: Climate Assessment for 2001. *Bull. Amer. Meteor. Soc.*, **83** (June), S1–S62.

——, and J. H. Lawrimore, 2003: State of the climate in 2002. *Bull. Amer. Meteor. Soc.*, **84** (June), S1–S68.

Ward, M. N., 1998: Diagnosis and short-lead time prediction of summer rainfall in tropical North Africa at interannual and multidecadal timescales. *J. Climate*, **11**, 3167–3191.

Westerling, A. L., and T. W. Swetnam, 2003: Interannual to decadal drought and wildfire in the western United States. *EOS, Trans. Amer. Geophys. Union*, **84**, 554–555.

Whitney, L. D., and J. S. Hobgood, 1997: The relationship between sea surface temperatures and maximum intensities of tropical cyclones in the Eastern North Pacific Ocean. *J. Climate*, **10**, 2921–2930.